TÉCNICO LISBOA

Wideband Wearable Antenna

Pedro Guilherme Moreira Falcão

Thesis to obtain the Master of Science Degree in

Electrical and Computer Engineering

Supervisor: Prof. Custódio José de Oliveira Peixeiro

Examination Committee:

Chairperson: Prof. José Eduardo Charters Ribeiro da Cunha Sanguino

Supervisor: Prof. Custódio José de Oliveira Peixeiro

Member of the Committee:

Prof. Carlos Alberto Barreiro Mendes

September 2021

Declaration

I declare that this document is an original work of my own authorship and that it fulfills all the requirements of the Code of Conduct and Good Practices.

To my family and friends…

Acknowledgments

The author would like to express his sincere gratitude to Professor Custódio Peixeiro for the continuous support during this thesis, for his patience, dedication, knowledge and guidance.

To Mr. Carlos Brito and Professor Carlos Fernandes, for their knowledge, experience and participation in the fabrication and test of the prototypes.

A special thanks to the author´s parents, brother and friends, for their unconditional encouragement and support during this journey.

To Instituto Superior Técnico (IST), a school filled with science and knowledge, where the author completed his studies.

Finally, a very special thanks to Instituto de Telecomunicações (IT), the institution that sponsored and hosted this thesis.

Resumo

As antenas possuem um papel fundamental no funcionamento e evolução da sociedade, pois são componentes essenciais dos sistemas que possibilitam a transmissão de informação sem fios, a curta e longa distância. O tráfego de dados tem aumentado exponencialmente nos últimos anos e é esperado que continue a aumentar a um ritmo acelerado. Com inúmeras aplicações, novas antenas são estudadas e desenvolvidas todos os anos.

O tema da dissertação foi sugerido pelo Center for Nanotechnology and Technical, Functional and Intelligent Materials, CeNTI, no âmbito do projeto iP Vest. Este projeto consiste no desenvolvimento de vestuário de proteção inteligente com duas funções especificas: a primeira proteger o utilizador de condições atmosféricas agressivas como vento, chuva, calor e frio, e a segunda atuará de forma ativa contendo toda a sensorização e comunicação para a proteção de alerta do utilizador. O sistema de antenas proposto destina-se a ser integrado nesse vestuário possibilitando a estimativa da intensidade do campo eletromagnético incidente.

As antenas impressas são uma classe de antenas que apresentam vantagens importantes, possuem uma configuração planar de baixo perfil, são leves e relativamente baratas e fáceis de fabricar e integrar com dispositivos eletrónicos. São versáteis em termos da frequência de ressonância, polarização e impedância, mas normalmente possuem uma largura de banda estreita e uma eficiência de radiação baixa.

Esta dissertação descreve a análise, o projeto (com otimização), o fabrico e o teste de um conjunto de monopolos impressos, projetados para funcionar na banda de 700 MHz a 3.5 GHz, com uma impedância de entrada de 50 Ω, com coeficiente de reflexão inferior a -10 dB para toda a banda de trabalho e polarização linear ortogonal dupla.

O procedimento de projeto consistiu em várias simulações no software CST de diferentes configurações do monopolo impresso de modo a aumentar a sua largura de banda.

As antenas desenvolvidas possuem uma espuma absorvente destinada a mitigar os efeitos do escudo condutor que protege o corpo do utilizador.

Os resultados experimentais que foi possível obter (coeficiente de reflexão de entrada) mostram uma boa concordância com os resultados da simulação numérica (CST), validando o procedimento de projeto seguido e provando o conceito de antena proposto.

Keywords:

Antena Monopolo, Antenas Impressas, Antena de Banda Larga, Antenas Integradas no Utilizador, Sistema de Antenas, CeNTI, iP Vest

Abstract

Antennas have a fundamental role in the functioning and evolution of society, as they are essential components of systems that enable the wireless transmission of information, over short and long distances. Data traffic has increased exponentially in recent years and is expected to continue to increase at an accelerated pace. With countless applications, new antennas are studied and developed every year.

The theme of the dissertation was suggested by the Center for Nanotechnology and Technical, Functional and Intelligent Materials, CeNTI, within the scope of the iP Vest project. This project consists in the development of intelligent protective clothing with two specific functions: the first to protect the user from aggressive weather conditions such as wind, rain, heat and cold, and the second will act in an active way containing all the sensing and communication for the protection and alert of the user. The proposed antenna system is intended to be integrated into this garment, making it possible to estimate the intensity of the incident electromagnetic field.

Printed antennas are a class of antennas that have important advantages, have a low-profile planar configuration, are light and relatively inexpensive to manufacture, and are easy to integrate with electronic devices. They are versatile in terms of resonance frequency, polarization and impedance but typically have a narrow bandwidth and low radiation efficiency.

This dissertation describes the analysis, design (with optimization), fabrication and testing of a set of printed monopoles, designed to work in the 700 MHz to 3.5 GHz band, with an input impedance of 50 Ω, with a reflection coefficient less than -10 dB for the entire working band and dual orthogonal linear polarization.

The design procedure consisted of several simulations in the CST software of different configurations of the printed monopole in order to increase its bandwidth.

The developed antennas have an absorber foam to mitigate the effects of the conductive shield that protects the user's body.

The experimental results that it was possible to obtain (input reflection coefficient) show a good agreement with the numerical simulation results (CST), validating the design procedure followed and proving the concept of the proposed antenna.

Keywords:

Antenna Monopole, Printed Antennas, Broadband Antenna, Wearable Antennas, System of Antennas, CeNTI, iP Vest

Contents

List of Figures

List of Tables

Glossary

2D	Bi-dimensional
3D	Tri-dimensional
AUT	Antenna Under Test
BW	Bandwidth
CEiia	Center of Engineering and Product Devolvement
CEM	Computer Electromagnetic
CeNTI	Center for Nanotechnology and Technical, Functional and Intelligent Materials
CF	Carvalho Fernandes
CITEVE	Centro Tecnológico Têxtil e Vestuário
CPW	Coplanar Waveguide
CST	Computer Simulation Technology
CTIC	Communications an Information Technology by Commission
DUT	Device Under Test
DXF	Drawing Exchange Format File
EM	Electromagnetic
EMF	Electromagnetic Fields
FR4	Flame Retardant 4
HARPSENS	Head Mounted AR Platform with Plug and Play Sensor Functionality
IST	Instituto Superior Técnico
IT	Instituto de Telecomunicações
PC	Personal Computer
PCB	Printed Circuit Board
PDF	Portable Document Format
R&D	Research and Development

SAR Specific Absorption Rate

SMA SubMiniature A

UV Ultraviolet Radiation

VNA Vector Network Analyser

WBAN Wireless Body Area Networks

1. Introduction

1.1 Motivation

Nowadays, wireless communications are an essential part of civilization. Sharing data is now faster, cheaper and more efficient. The traffic of information is growing fast over the years as the population and the number of internet users grow. With this growth, there is a need of improved coverage and better signal quality, resulting in more base stations and more electromagnetic radiation exposure. There is a considerable concern about the possible consequences to a human being exposed to electromagnetic fields over a long period. These high intensity fields are present in professional scenarios such as base stations since the intensity of electromagnetic fields is stronger in the emission and decays with distance. In that specific scenario, it is important to know the amplitude of the electromagnetic wave incident on the workers who maintain or install new antennas. The estimation of the intensity of such electromagnetic waves is the main objective of this thesis.

With the development of integrated circuit and printed circuit board (PCB) technology, printed antennas have drawn a lot of attention in the antenna R&D community. They are lightweight, low cost, robust, easy to fabricate and install. These antennas have a planar low profile and are versatile in terms of resonance frequency, radiation pattern, polarization and impedance. With so many advantages, printed antennas are a good candidate to be used in the proposed problem.

To develop this type of antennas, the antenna research and development community has many computational electromagnetic (CEM) tools at their disposal, these tools simulate a virtual environment in order to minimize financial resources and optimize the antenna. Although the available software is accurate to the point that the simulated results are close to the measured results it is essential to measure the radiation pattern, gain, reflection factor and other parameters in real conditions. These measurements are made in a radio frequency anechoic chamber.

The idea for the theme of this masters thesis was initially suggested by CeNTI, following the project iP Vest. The iP Vest project aims to investigate and develop innovative solutions for technical and functional clothing with smart multi-risk protection, using new textile materials with advanced performance and new directly integrated sensor systems, thus promoting individual protection and user information.

CeNTI, Center for Nanotechnology and Technical, Functional and Intelligent Materials, is the result of a partnership between three universities (Aveiro, Minho and Porto) and three technological entities (CITEVE, CTIC and CEiia). The promoters of iP Vest are also part of the European consortium HARPSENS (Head Mounted AR Platform with Plug and Play Sensor Functionality) witch aims to develop a smart helmet with augmented reality (Cyclops) and a smart vest with sensors integrated into the textile structure. Both should reach the market in 2022. [1-3]

There is currently commercial equipment for measuring the electric field (applications designed to avoid high exposures) developed by eNGN Technologies, a FieldFox handheld analyser embedded with an EMF measurement app, along with and EMF triaxial isotropic antenna. Both tools are ideal to verify the exposure levels in the field set by the government and regulatory agents. [4] In this thesis, a similar solution integrated in the user's clothing is proposed.

1.2 Objectives

The general goal of the thesis is the development of an expertise in the antenna field. This thesis specific main goal is to design, fabricate and test a system of wearable wideband antennas with the purpose of measuring the amplitude of the electric field received by the user in a professional unknown work environment. The direction of the incident electric field into the user is undefined just like its polarization, therefore the system will work with space sectorization and probing of orthogonal polarizations. For each antenna it is requested dual linear polarization, an input impedance of 50 Ω and a reflection coefficient below -10 dB for the working bandwidth from 0,7 GHz to 3,5 GHz. The gain of the antenna is not a critical requirement since it is small or moderate, that is, as far as it reflects an adequate coverage of all sectors.

1.3 Thesis Structure

This thesis is organized into six chapters. Chapter 1 presents the motivation, the objectives, the original contributions and the structure of the thesis. Initially, an overview of the global traffic path followed by the context of application of this thesis is presented, highlighting the requirements and the description of the proposed project.

Chapter 2 contains the state of the art, starting with a brief introduction and contains a detailed analysis and description concerning the printed monopole antenna, including its design rules, its feeding techniques and some general miniaturization procedures.

Chapter 3 presents the design and optimization procedure. It starts with a description of the software used and then with a study and analysis of each parameters influence in the antenna performance. This is where the study and optimization is carried out for the printed monopole in FR4 with absorbent foam and the outcome configuration is presented along with its simulated results.

Chapter 4 explores the fabrication and testing processes in detail to later compare the experimental results with the simulated results. The chapter ends with a detailed explanation of the test procedure regarding the input reflection coefficient measurement, the radiation pattern and also the gain measurement, including the experimental results of the antenna prototype.

Chapter 5 describes the development of the system of antennas. From voltage monitors at the terminals of each monopole, it is possible to estimate the amplitude of the incident electric field in a certain direction.

At last, chapter 6 is devoted to draw the main conclusions of the thesis, summing up the main achievements of the work developed throughout this project and indicating some interesting future work enhancements that can be realized.

1.4 Original Contributions

As mentioned before, the general purpose of this thesis is the development of an expertise in the antenna field. The work carried out goes through all the important stages of an EM engineering process, namely, analysis, design (with optimization), fabrication and test.

Initially it has been necessary to obtain know-how on the printed monopole antenna working principles and get acquainted with the software simulation tool (CST). It was then possible to develop a well sustained activity that has allowed the following original contributions:

- Detailed parametric analysis of printed monopole antennas. All the relevant parameters such as: size and geometry, feeding line, feeding coaxial cable, termination, dipole width and substrate shape, have been studied.
- Design and optimization, fabrication and test of a printed monopole antenna with size restrictions and large bandwidth.
- Design and optimization, fabrication and test of a pair of dual-linear polarized monopoles with weak mutual coupling.
- Design and optimization of the antenna system with five printed monopoles antenna with spatial sectorization.

2. State of the Art

2.1 Introduction

Nowadays, a fast development in the field of wireless communications has been observed and therefore the necessity to develop antennas with compact size, low cost, light weight, planar configuration, and easy to install, increases. Microstrip antennas are most suitable candidates for such applications. In the present, they are used for military and commercial applications, such as mobile radio and wireless communications that have similar specifications.

The concept of microstrip antenna can be traced to 1953 by Deschamps and Sichak, when the authors developed a high resolution X-band antenna with a shaped vertical pattern and horizontal beam width of less than one degree. In order to achieve the operation goals the authors designed a long linear array with a cylindrical reflector weighing the benefits of using a sectoral lens, a slot array, or an array composed of waveguide-fed horns as feed mechanism. Given the bulk of this waveguide system with 300 radiating elements, the authors developed a microstrip feeding system. [5] The microstrip patch we recognize today did not become well known until the 1970's through the work of Byron [6], Munson [7, 8], and Howell [9, 10]. However, the work provided by Deschamps and Sichak presented new ways to think about the antenna structures and subsequent performance benefits and reductions in size, weight, and cost that could be realized through the use of microstrip or stripline transmission lines. In the four decades since, there are literally thousands of papers on this topic.

A microstrip antenna, which is a specific form of printed antenna, is a low-profile antenna that has many advantages: it is lightweight, inexpensive to fabricate, easy to feed, and easily integrated with electronics. Radiation patterns are somewhat hemispherical, with a moderate directivity, usually around 6-8 dB. It is usually flat and that´s why microstrip antennas are referred as planar antennas. When a particular patch shape and mode are selected, they are very versatile in terms of resonance frequency, polarization, pattern, and impedance. Major disadvantages of microstrip antennas are their narrow bandwidth, low power, poor polarization purity, poor scan performance, spurious feed radiation and low efficiency. There are methods to increase the bandwidth and the efficiency, such as increasing the height of the substrate. However, as the height increases, surface waves are introduced which are not desirable as they extract power from the total available for direct radiation. Surface waves can be eliminated, while maintaining large bandwidths, by using cavities. Stacking is another method used to increase the bandwidth of microstrip elements. The bandwidth is inversely proportional to ε_r, meaning a foam substrate can provide a larger bandwidth [11]-[13].

2.2 Printed Antennas

2.2.1 Basic Characteristics

In its most basic form, a microstrip antenna is manufactured with a flat plate over a ground plane. This antenna is built of printed circuit board material and the substrate makes up the patch antenna's dielectric. There are numerous dielectric substrates that can be used for the design of microstrip antennas, and their dielectric constants are usually between 2.2 and 12. The ones that are most desirable for good antenna performance are thick substrates whose dielectric constant is in the lower end of the range because they provide better efficiency and larger bandwidth. Thin substrates with higher dielectric constants are desirable for microwave circuitry because they require tightly bound fields to minimize undesired radiation and coupling, and lead to smaller element sizes. Thicker substrate increases the gain to some extent, but may lead to undesired radiation pattern and coupling. A quite big challenge remains regarding this matter, if on one side antenna performance is important, on the other, circuit design is almost crucial, since printed antennas are regularly combined with other microwave circuits [14]. The microstrip patch is designed so its pattern maximum is normal to the patch, this is accomplished by properly choosing the mode of excitation beneath the patch.

Common microstrip antenna shapes are square, rectangular, thin strip (dipole), circular, elliptical, triangular, disc sector, circular ring and ring sector but any continuous shape is possible. For a rectangular patch the length L of the element is usually $\lambda_0/3 < L < \lambda_0/2$. The patch and the ground plane are separated by a dielectric substrate, as shown in Figure 2.1 [11].

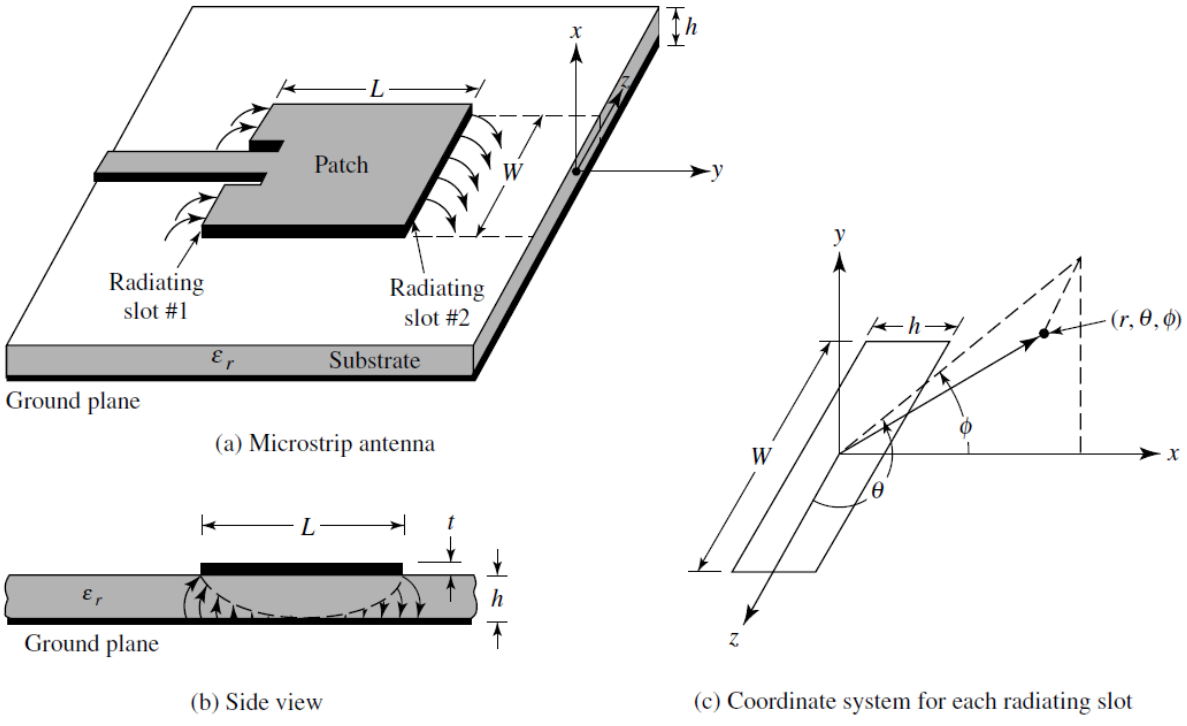

Figure 2.1 - Microstrip antenna and coordinate system (reproduced from [11])

The size of the ground plane is also important, a ground plane that is too small will result in a reduced front to back ratio. Making the ground plane larger increases the gain, but as the ground plane size increases, diffraction near the edges of the patch plays less of a role and increasing the size of an already “large” ground plane has very little effect on gain. Linear and circular polarizations can be achieved with either single elements or arrays of microstrip elements.

2.2.2 Feed Type

There are different configurations available that can be used to feed microstrip antennas. These methods can be contacting and non-contacting. In the contacting method the RF power is fed directly to the radiating patch using a connecting element such as a microstrip line. In the non-contacting method, power is transferred between the microstrip line and the radiating patch through electromagnetic coupling. The most popular feeding techniques are the microstrip line and the coaxial probe for contacting schemes, aperture coupling and proximity coupling for non-contacting schemes. All this examples can be observed in next four figures [15-18].

2.2.2.1 Microstrip Line and Coaxial Probe Feed

A conducting strip is connected directly to the edge of the microstrip patch, it is usually of much smaller width compared to the patch. The microstrip-line feed is easy to fabricate and model. This type of feed arrangement has the advantage that the feed can be etched on the same substrate to provide a planar structure.

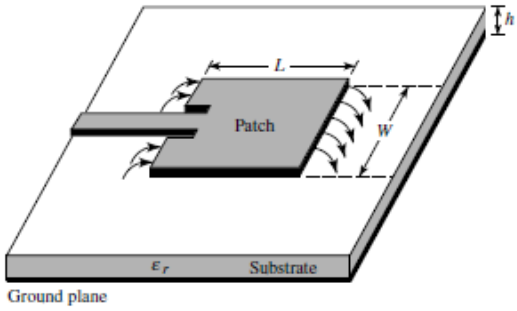

Figure 2.2 - Microstrip line feed (reproduced from [11])

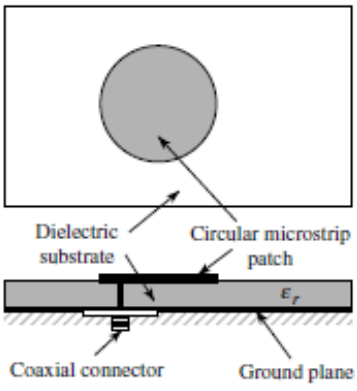

Figure 2.3 - Coaxial probe feed (reproduced from [11])

In the coaxial probe feed type the inner conductor of the coaxial connector extends throughout the dielectric and is attached to the radiation patch while the outer conductor is connected to the ground plane. The coaxial probe feed is also easy to fabricate and match, and it has low spurious radiation, which make it widely used. However, it has narrow bandwidth and it is more difficult to model, especially for thick substrates.

2.2.2.2 Other Feeding Types

Both the feed types, microstrip line and coaxial probe, have inherent asymmetries which generate higher order modes which produce cross-polarized radiation. To overcome some of these problems, non-contacting aperture coupling feeds have been introduced.

The aperture coupling is the most difficult to fabricate due to multiple layers, however, it is somewhat easier to model and has moderate spurious radiation. In the aperture coupling method the radiating patch and the microstrip feed line are separated by the ground plane. On the bottom side of the lower substrate there is a microstrip feed line whose energy is coupled to the patch through a slot on the ground plane separating the two substrates, leading to low cross polarization due to the symmetry of the configuration. Since the ground plane separates the patch and the feed line, spurious radiation is minimized. Typically, a thick low dielectric constant material is used for the top substrate, and a thin dielectric constant material for the bottom substrate.

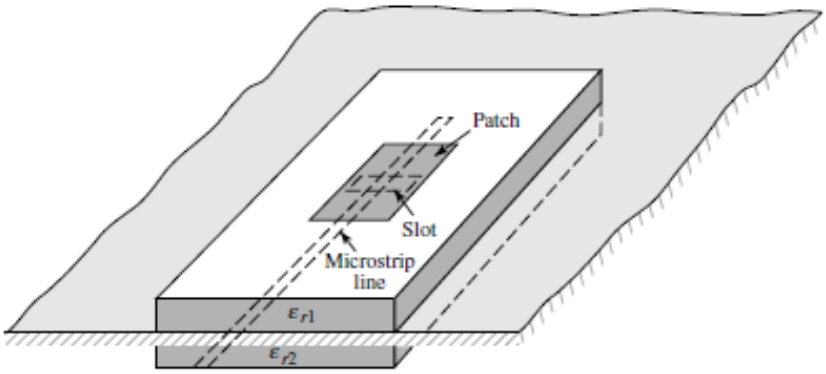

Figure 2.4 - Aperture-coupled feed (reproduced from [11])

Finally, the proximity coupling feed, this type of feed is also based on the electromagnetic coupling scheme. For this method, the microstrip feed line is placed between two dielectric substrates and the radiating patch is on top of the upper substrate. The main advantage of this feed technique is that it has low spurious feed radiation. The major disadvantage of this feed scheme is that it is difficult to fabricate because of the two dielectric layers, that need proper alignment.

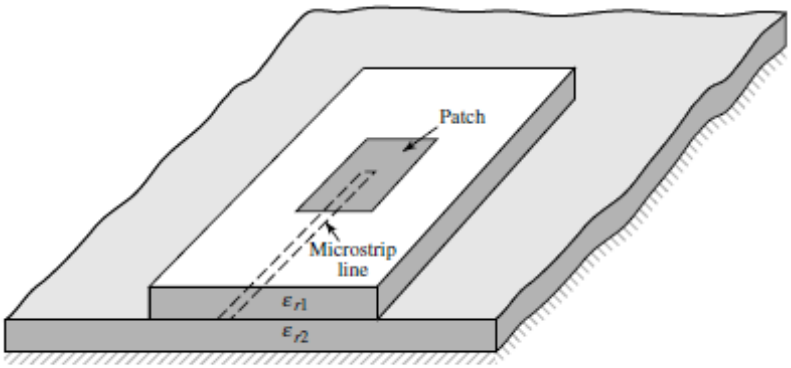

Figure 2.5 - Proximity-coupled feed (reproduced from [11])

2.2.3 Analysis

There are many methods of analysis for microstrip antennas. The most popular are the transmission-line [16] [20], cavity [16] [19] [20], and full wave [21] among others. The transmission-line is the easiest solution and gives good physical insight, but is less accurate and it is more difficult to model coupling. The cavity model compared to the transmission-line model, is more accurate but at the same time more complex. It also gives good physical insight and is rather difficult to model coupling. The full wave models are very accurate and can treat single elements, finite and infite arrays, stacked elements, arbitrary shaped elements, and coupling but they are the most complex models and give less if any physical insight.

Typically the transmission line and the cavity models are used in the pre-design stage to obtain approximate values for the antenna dimensions and later a full wave method is used to optimize the structure.

The transmission model will be used below. For the following study, a rectangular patch will be used, since is the most common configuration. A rectangular microstrip antenna can be represented as an array of two slots, each of width W and height h, separated by a distance L where L and W are the rectangular patch dimensions and h is the substrate thickness. Basically the transmission-line model represents the microstrip antenna by two slots, separated by a low-impedance Z_c transmission line of length L.

2.2.3.1 Fringing Effects

Fringing fields have an important effect on the performance of a microstrip antenna. Due to the fact that the dimensions of the patch are finite along the length and width, the fields at the edges of the patch undergo fringing (principal mode). In microstrip antennas, the electric field in the center of the patch is zero, the radiation is due to the fringing field between the proximity of the patch and the ground plane. This is illustrated along the length in figures 2.6 a and b. The amount of the fringing field is a function of the dimensions of the patch and the height of the substrate. The higher the substrate, the larger the fringing field is.

For the principal E-plane fringing is a function of the ratio of the length of the patch L to the height h of the substrate (L/h) and the dielectric constant ϵ_r of the substrate. In microstrip antennas usually L/h $\gg$ 1 and

W/h ≫ 1 therefore this effect is reduced but it must be taken into account because it influences the resonance frequency of the antenna.

As it can be noticed in figure 2.6 b, the waves travel through both the substrate and the air. As W/h »1 and ϵ_r ≫1 the electric field lines concentrate mostly in the substrate. Due the effect of fringing the microstrip patch antenna behaves as electrically wider compared to its physical dimensions.

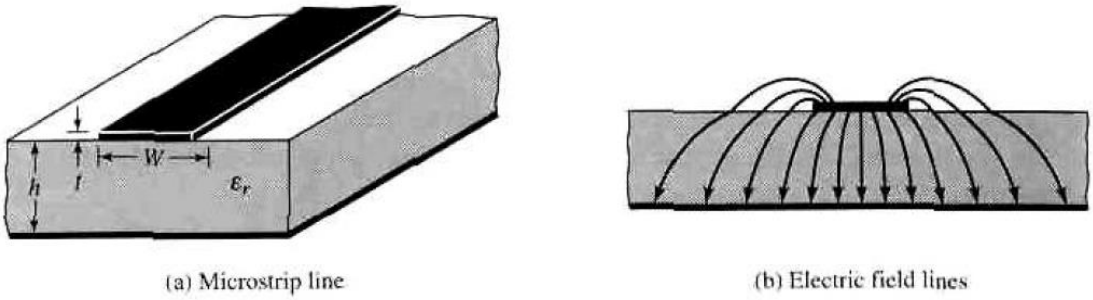

Figure 2.6 - Microstrip antenna - fringing effect (reproduced from [11])

Since some waves travel in the substrate and some in air, an effective dielectric constant ϵ_{reff} is introduced to account for fringing and the wave propagation in the line. For low frequencies, the effective dielectric constant is constant. At intermediate frequencies, its values begin to increase and approach the values of the dielectric constant of the substrate. The expression for the effective dielectric constant can be defined as [11].

$$\epsilon_{reff} = \frac{\epsilon_r+1}{2} + \frac{\epsilon_r-1}{2}\left[1 + 12\frac{h}{W}\right]^{-\frac{1}{2}} \quad (2.1)$$

For W/h>1

2.2.3.2 Effective Length, Resonant Frequency and Effective Width

The fringing effects make the patch looks larger than its physical dimensions. With that said, there are new dimensions when working with this type of antennas, called the effective length and effective width.

In figure 2.7 it is clear that the dimensions of the patch along its length have been extended on each end by a distance ΔL, which is a functions of the effective dielectric constant ϵ_{reff} and the width-to-height ratio (W/h).

A practical approximate relation for the horizontal extension of the length is [11].

$$\frac{\Delta L}{h} = 0.412 \times \frac{(\epsilon_{reff}+0.3)\left(\frac{W}{h}+0.264\right)}{(\epsilon_{reff}+0.258)\left(\frac{W}{h}+0.8\right)} \quad (2.2)$$

Since the length of the patch has been extended by ΔL on each side, the effective length of the patch in now.

$$L_{eff} = L + 2\Delta L \quad (2.3)$$

For the dominant mode TM_{010}, the resonant frequency of the microstrip antenna is a function of its length. As $L = \frac{\lambda}{2}$, it is given by

$$f_{r_{010}} = \frac{1}{2L\sqrt{\epsilon_r}\sqrt{\mu_0\epsilon_0}} = \frac{c_0}{2L\sqrt{\epsilon_r}} \tag{2.4}$$

Where c_0 is the speed of light in free space. Since this resonance frequency does not account for fringing, it must be modified to include edge effects and should be computed using

$$f_{rc_{010}} = \frac{1}{2L_{reff}\sqrt{\epsilon_{reff}}\sqrt{\mu_0\epsilon_0}} = \frac{1}{2(L+2\Delta L)\sqrt{\epsilon_{reff}}\sqrt{\mu_0\epsilon_0}} \tag{2.5}$$

$$f_{rc_{010}} = q\frac{1}{2L\sqrt{\epsilon_r}\sqrt{\mu_0\epsilon_0}} = q\frac{c_0}{2L\sqrt{\epsilon_r}} \tag{2.6}$$

Where

$$q = \frac{f_{rc_{010}}}{f_{r_{010}}} \tag{2.7}$$

The q factor is referred to as the fringing factor. If we increase the substrate height h, the fringe effect also increases and leads to larger separations between the radiating edges, however by increasing the actual length of the patch, the resonance frequency decreases.

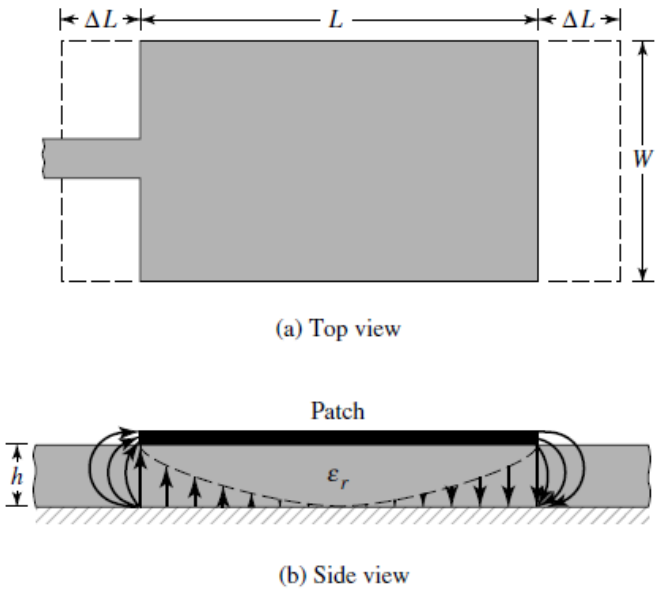

Figure 2.7 - Microstrip patch - effective length due to fringing (reproduced from [11])

2.2.3.3 Design

A design procedure is outlined in [11] which leads to practical designs of rectangular microstrip antennas based on the formulation that has been described. The procedure assumes that the dielectric constant of the substrate (ϵ_r), the resonant frequency (f_r), and the height of the substrate h values are known. The procedure is as follows:

1. Specify $\epsilon_{r,}$ f_r and h
2. For an efficient radiator, a practical width that leads to good radiation efficiencies is:

$$W = \frac{1}{2f_r\sqrt{\mu_0\epsilon_0}}\sqrt{\frac{2}{\epsilon_r+1}} = \frac{c_0}{2f_r}\sqrt{\frac{2}{\epsilon_r+1}} \quad (2.8)$$

   where c_0 is the free-space velocity of light.
3. Determine the effective dielectric constant of the microstrip antenna using equation (2.1)
4. Determine the length ΔL using equation (2.2)
5. The actual length of the patch can now be determined using equation (2.5).

If for instance, a square patch is envisaged, the steps 2 to 5 can be repeated, using in each iteration a value for W equal to the value of L obtained in the previous iteration. This iterative procedure converges very quickly (2 or 3 iterations are usually enough).

2.3 Printed Monopole Antenna

As already stated, microstrip antennas have several advantages over conventional microwave antennas, they are light weight, compact, cheap to fabric and conformable. Choosing the right feed, linear and circular polarization can be achieved. They are also easily integrated with microwave integrated circuits. However, despite its popularity, they have some drawbacks, low gain and efficiency, half space radiation pattern and narrow impedance bandwidth.

In order to avoid some of the drawbacks of microstrip antennas, printed monopoles are introduced. The printed monopole antenna is included in a broad class of microstrip antennas. They have similar configuration but printed monopole antennas have a truncated ground plane providing larger bandwidth and nearly omnidirectional radiation characteristics. For proper matching of the printed monopole with the microstrip feed line, the dielectric constant and thickness of the substrate and the width of the feed need to be chosen carefully.

Figure 2.8 represents the simplest configuration of the printed monopole, a thin microstrip, of width W, placed on top of the dielectric substrate, of height h, with the truncated ground plane on the other side.

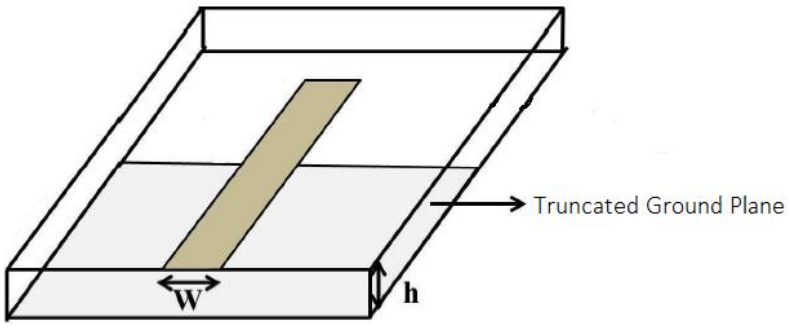

Figure 2.8 - Simplest configuration of printed monopole

Similar to microstrip patch antennas, the printed monopole can take many shapes regarding the patch geometry, for example, rectangular, triangular, circular, elliptical, octagonal, and others [27-32]. Different geometries of the patch or the ground plane result mostly in variations in the return loss but to a lesser extent also of the gain and radiation pattern among the frequency band. Different geometries of the monopole patch, as well as their bandwidth are shown in figure 9 [30].

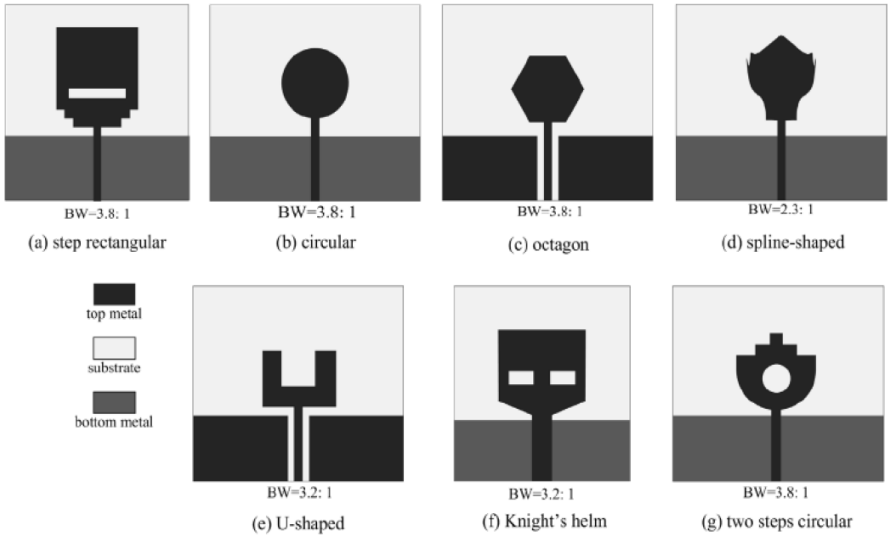

Figure 2.9 - Various printed monopole structures (reproduced from [26])

Printed monopole antennas are categorized in different configurations in terms of theirs excitation and location of the ground plane as shown in figure 2.9. All the configurations except c) and e) are microstrip line fed printed monopoles in which the patch is excited by a microstrip line. The patch and the ground plane are in different faces of the dielectric and the ground plane extends up to feed line only with a little gap to the patch. Finally the configuration c) and e) are coplanar waveguide (CPW) fed printed monopoles in which the ground and the patch are lying on the same face of the dielectric substrate whereas the other side of the dielectric is not metalized [22-26].

2.4 Wearable Antennas

2.4.1 Introduction

In recent years, wearable antennas, have gained much attention due to all the practical applications and possibilities in enabling lightweight, flexible, low cost and portable wireless communication and sensing. A wearable antenna is meant to be a part of the clothing used for communication purposes, which includes tracking and navigation, mobile computing and public safety. The practical use of these antennas present some challenges, since they need to be capable of operating with minimum degradation in close proximity to the human body and need to be implemented using flexible materials and designed in a low profile structure. Size constraints, effects of structural deformation, fabrication complexity and accuracy are aspects that need to be

considered when designing a wearable antenna. Despite slight variations in importance according to applications, most of these issues exist in the context of body-worn implementation [34].

Wearable antennas have an abundant range of applications, major fields are in healthcare, sports, entertainment, military, space and others, as displayed in figure 2.10 [35]. For example, in healthcare these antennas can monitor users giving real time information, heart rate, respiratory rate and temperature of the body, they can track brain and eye movement and also monitor the posture of the user [36-37]. In sports and fitness, there is a high demand for systems to deliver real time information about the user performance. They can help optimizing training sessions by sensing body temperature and tracking the activity of the user. In entertainment applications, wearable antennas are multimedia orientated and require high speed transfer of voice, video and data in real time. Examples of them include the glasses for augmented reality, smartwatches as touchscreen computer. In the military and the space fields there are numerous applications, such as smart suits, battlefield personal care and intelligence to astronaut monitoring [38].

Figure 2.10 - World of wearable technology applications

Textile antennas are a different class of antennas as they are partially or entirely made out of textile material, in comparison with conventional ones, which consist of solid materials. Commonly, wearable antenna

requirements for all modern application require light weight, low cost and almost maintenance-free characteristics.

2.4.2- Wearable Antennas Challenges

The main challenges in the design of a wearable antenna are low cost, lightweight, compactness, desired radiation characteristics and stable performance under varying conditions since it is necessary to consider the shifting in the operational frequency band detuning due to the human body loading effect.

Relatively to radiation characteristics, for on body communications, it is desirable to have wide beam or omnidirectional radiation [39]. It is also necessary to take into account bending or crumpling of the antenna which has a strong impact on its performance, namely resonance frequency, bandwidth and reflection coefficient. Furthermore, it is required to consider the positioning, as bending limitations and scenarios can be determined based on the antenna placement. The sensitivity and specific absorption rate (SAR) are requirements too as the challenge to make the antenna insensitive to the variation of the gap between the antenna and the human body. Finally, wetness is another challenge in wearable antennas as water has a much high dielectric constant than the fabric. When a wearable antenna absorbs water, the performance drops dramatically reducing the resonance frequency.

The fabrication method is also a challenge to take into account when designing wearable textile antennas, since they define how fast and how accurate low cost prototypes are obtained. Most common fabrication techniques are wet-etching and embroidery methods, inkjet printing and screen printing.

Usually, wearable antennas are implemented in a specific part of the clothing for unobtrusive effective on/off body communications [46]. Instead of using the traditional method to fabric these antennas, sewing or printing methods, it is possible to button the antenna on the fabric of the wearer outfit. This method saves the antenna from the risks of degradation due to their physical deformation and enables performance stability due to its rigid substrate. Zippers are also integrated on clothes and other wearable accessories, they are effective radiators due to their metallic structure [46]

2.4.3- Effects of the Human Body

As the human body is made of 65% to 80% of water and lossy body tissues, when a wearable antenna is placed close to the human body, its resonance frequency, impedance bandwidth, and radiation pattern will be potentially changed. The distinct permittivity and conductivity values of the different types of human tissue influence the reflection coefficient and affect the power absorbed by the body, decreasing the radiation efficiency of the antenna.

Wearable antennas need to be designed to operate properly in the vicinity of human body [46]. In addition, special attention must be paid to the Specific Absorption Rate (SAR), which aids in the quantitative study of power absorption issues required to meet the standards in order to avoid harming the human body. SAR quantifies the amount of EM radiation a human body can withstand without any health problems and is defined

as the ratio between the transferred power and the mass (kg/lb) of the body where the values are being evaluated [42].

2.4.4- Effect of Bending

In real life applications, bending occurs when the antenna is applied to rounded parts of the body. Physical deformation is one of the main concerns in ensuring the effective operation of wearable antennas because it can shift the resonance frequency and it affects its polarization due to change in the current density on the radiating elements. Moreover, this also potentially increases the SAR values on the wearer's body.

The resonance frequency has a different behaviour depending on whether the antenna is bent around its width or around its length. Special consideration should be given when designing wearable antennas for WBAN applications, since the resonance frequency offset with respect to antenna curvature angle could significantly limit the antenna performance. The RF performance of wearable antennas is most significantly affected by bending in the E-plane [41].

There are several methods to overcome this problem such as increasing the bandwidth, so that if the frequency shifts, the antenna will still be able to operate in the required bandwidth. The antennas can be designed to be as symmetric and small as possible so that they are minimally affected in the effective length despite being bent in different directions [34].

3. Antenna Design and Optimization

3.1 Introduction

The development of an antenna is a difficult process and can be resumed in five steps: design, simulation, optimization, fabrication and test. With the help of a software tool like CST (Computer Simulation Technology) Studio the design and optimization procedure is done through several simulations adjusting parameters values and components dimensions that influence the performance of the antenna. A brief description of CST software tool is done in Appendix A.

The printed monopole consists in three main components, a metallic printed element placed on a dielectric substrate with a ground plane. All the components can take different configurations of its shape and dimensions. In this chapter, we consider different geometries for the patch and some configurations and associated modifications for the ground plane.

3.2 Design Specifications

3.2.1 Input Reflection Coefficient

The input reflection coefficient, S_{11}, is one of the parameters that best shows the performance of the antenna as it compares the power of the reflected electromagnetic wave with the power of the incident wave. The lower the power of the reflected wave, the better is the matching between the coaxial feeding cable and the antenna. The level allowed for the input reflection coefficient defines the working bandwidth. The very common -10 dB level is used in this work.

3.2.2 Frequency Band

This project is required to cover a frequency band from 700 MHz to 3500 MHz, which translates into an impedance bandwidth of 5:1 for an input impedance of 50 Ω. For such broadband antenna, unlike single resonance monopole antennas, some special design considerations have to be taken into account. Instead of resonance or operating frequency, the lower band-edge frequency and the total bandwidth are the most relevant design parameters for these printed monopole antennas. The lower band-edge frequency depends primarily on the maximum height of the monopole, whereas bandwidth depends on how impedance of the various modes is matched with the microstrip or coplanar feed line.

3.2.3 Directivity and Efficiency

As explained in chapter 5, several identical antennas will be used to form an antenna system capable of estimating the amplitude of the electric field of the incident electromagnetic wave. The use of a small number of antenna elements requires individual small/moderate directivity. A quarter-wavelength monopole presents

as omnidirectional radiation pattern with a (ideal) directivity of 5,15 dB which is adequate for the envisaged application. In this case efficiency is not a critical parameter as it can be verified in section 5.4.

3.2.4 Antenna Size

The antenna size, is very important because several antennas need to be integrated into the user garment. If size was not a constraint, then this project would be of much less importance. It is the small size of these antennas that allow this integration with acceptable interaction between them. One of the outcomes of this project is the good trade-off between size and performance.

3.3 Optimization Procedure for the Free Space Monopole

In this chapter different antenna configurations are simulated, studying the influence of each parameter on their performance. In order to understand the influence of each parameter, a scan of values of the parameter under study is carried out keeping all others constant. The simulation process started by designing one conventional printed monopole not only to understand how the software works but also to validate it. After learning how to design the printed monopole antenna and learning to manage the CST software, the author started the design and optimization simulating a printed monopole.

The chosen material for the dielectric substrate was FR4, this being relatively cheap and easy to access despite introducing some losses. Since the antenna has to operate mainly at low frequencies this substrate is a good option because it performs poorly with increasing frequency. The FR4 substrate has a dielectric constant ε_r = 4,3 and loss tangent tan δ = 0,025. For all simulations, a thickness of h=1,6 mm was chosen for the substrate.

Different configurations were simulated for the printed monopole, starting with the simplest of all, a straight strip. After obtaining some information about the line width, a microstrip patch antenna was also simulated. Looking for larger bandwidth and better performance new patch configurations were tested, namely a square patch, a triangular patch, an inverted triangular patch and finally an octagonal patch. For some configurations, changes to the ground plane and patch were simulated. Regarding the ground plane, these changes consisted of coplanar configurations or changes in the geometry of the conventional ground plane. For the patch, the changes consisted on inserting slots or adding triangular plates.

3.3.1 Simple Monopole

The simulation process started by designing the simple microstrip monopole described in figure 3.1. One of the design requirements is an input impedance of 50 Ω, therefore one important part of the optimization process is to reach an impedance matching between the antenna and the coaxial cable. In order to transfer the maximum power from a source to a load, the load impedance should match the source impedance.

The monopole has a total length L_f = 75 mm printed on a 150 x 150 mm dielectric substrate FR4 backed by a 150 x 50 mm ground plane. The aim of this study was to understand how different values for the microstrip width (W_f) would affect the input reflection coefficient for a specific substrate thickness h. A variation of 0.5 mm to 3 mm in width was made with 0.5 mm intervals. The monopole dimensions are summarized in table 3.1.

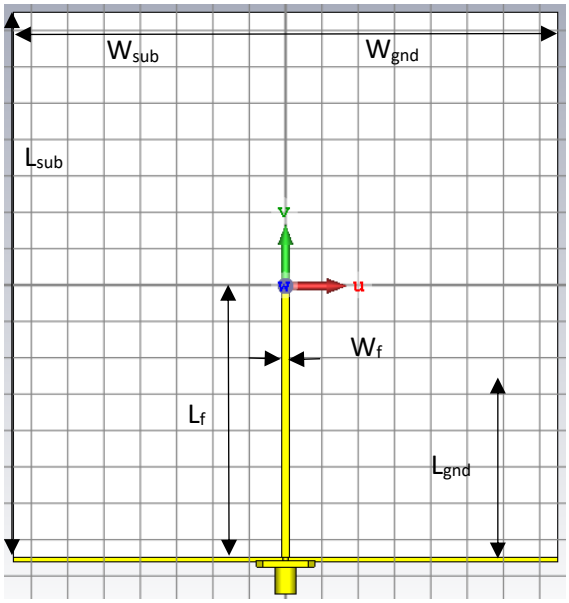

Figure 3.1 – Simple printed monopole configuration

Table 3.1 – Simple monopole dimensions

Substrate width (W_{sub})	150 mm
Substrate length (L_{sub})	150 mm
Substrate thickness (h)	1.6 mm
Ground plane width (W_{gnd})	150 mm
Ground plane length (L_{gnd})	50 mm
Monopole total length (L_f)	75 mm
Microstrip width (W_f)	0.1 – 3 mm

The input reflection coefficient result S_{11} are presented in figure 3.2.

As expected the width of the microstrip line deeply affects the antenna´s reflection coefficient behaviour approximately between 1.2 GHz and 3 GHz. It is observed that increasing the width W_f from 0.5 mm to 3 mm shifts both the lowest and the highest frequency for witch the reflection coefficient is bellow – 10 dB narrowing the working bandwidth. On the other hand, for W_f = 0.5 mm, the S_{11} curve takes values above -10 dB at intermediate frequencies. The microstrip line was fed by a coaxial cable through a 50 Ω SMA port. In this case, a W_f of 2 mm clearly provides the best impedance matching. The radiation pattern is presented in figure 3.3 for different operation frequencies. It is observed in the three cutting planes, as expected from a conventional monopole, an approximately omnidirectional radiation diagram.

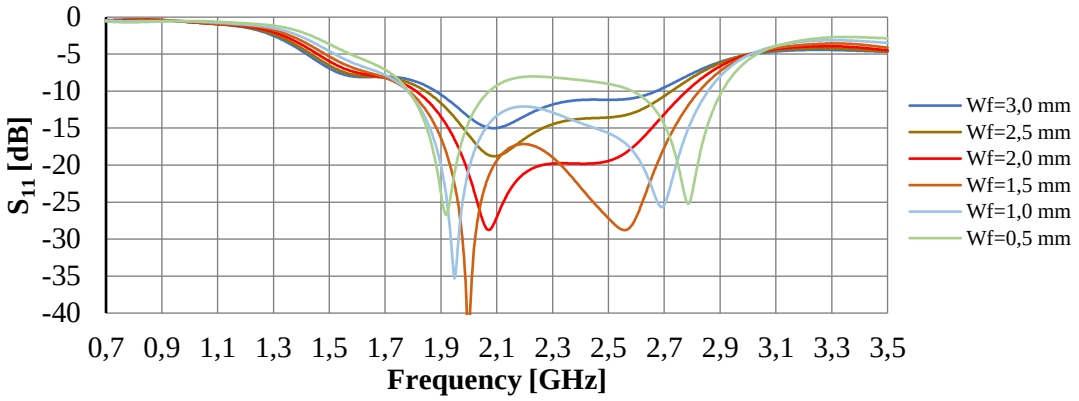

Figure 3.2 – Simple monopole reflection coefficient for width variation

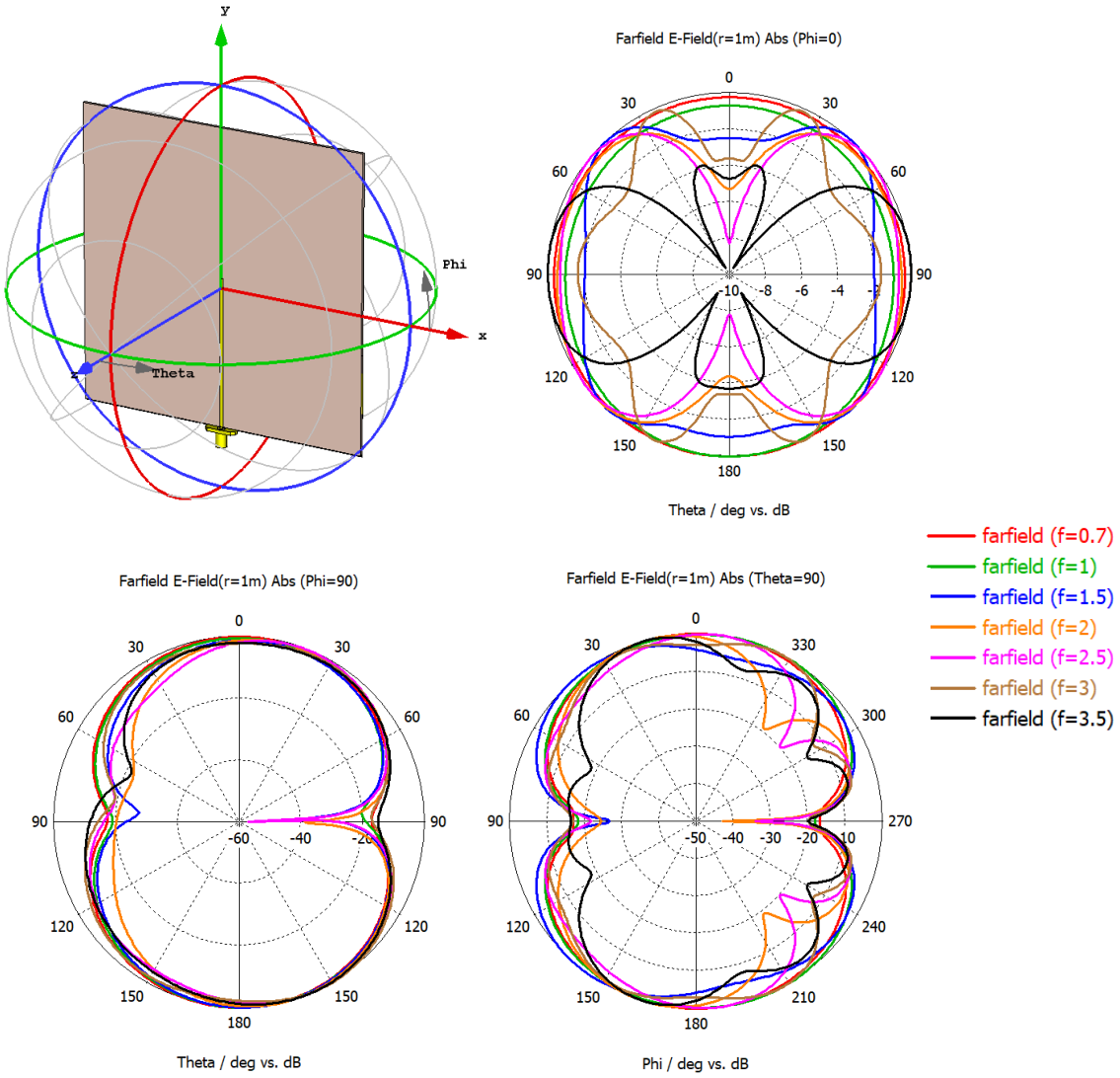

Figure 3.3 - Radiation patterns of the simple monopole

3.3.2 Square Patch Monopole

In order to increase the bandwidth, the monopole is modified with the addition of a square patch maintaining the total length (figure 3.4). The square patch is simulated by increasing the width of the line from the ground plane with a gap g between them. The simulated monopole has the parameters with the same values from the one before, the substrate has 150 x 150 mm, the ground plane has 150 x 50 mm and the microstrip line plus the patch have height of 75 mm. Now, with the widening of the microstrip line, a new parameter g is added. This parameter g represents the distance between the lower limit of the patch and the upper limit of the ground plane and for the next simulations takes the value g = 5 mm.

A variation of 2 mm to 20 mm in width is made with 2 mm intervals. The designed antenna had the dimensions indicated in table 3.2.

Table 3.2 – Square monopole dimensions

Substrate width (W_{sub})	150 mm
Substrate length (L_{sub})	150 mm
Substrate thickness (h)	1.6 mm
Ground Plane width (W_{gnd})	150 mm
Ground Plane length (L_{gnd})	50 mm
Microstrip + Patch length (L_f)	75 mm
Microstrip width (W_f)	2 mm
Patch width (W_{patch})	2 – 20 mm
Patch length (L_{pacth})	20 mm
Gap (g)	5 mm

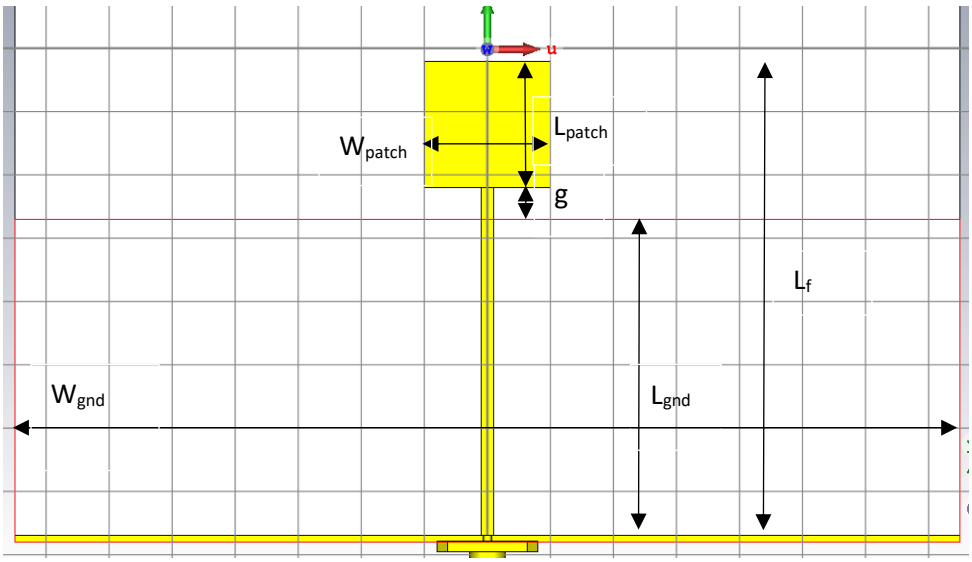

Figure 3.4 – Square patch monopole configuration

A representation of how the antenna reflection coefficient changes with different values of W_{patch} is presented in figure 3.5.

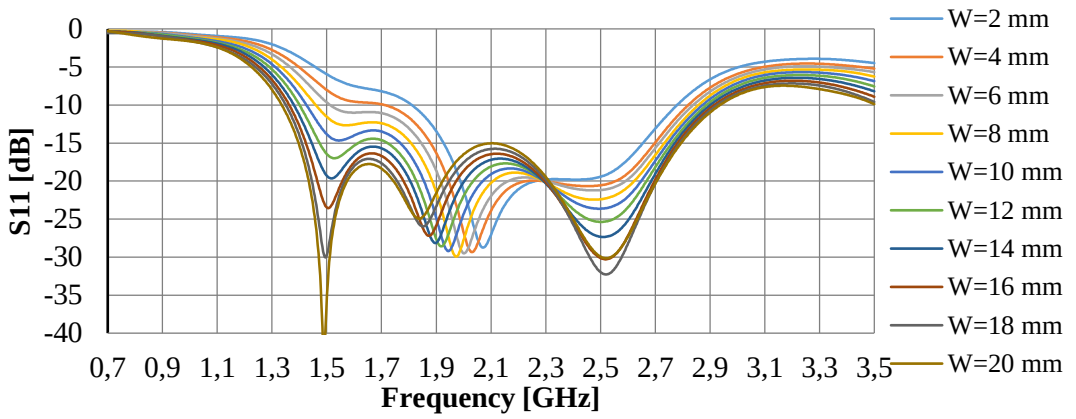

Figure 3.5 – Square patch monopole reflection coefficient for width variation

From figure 3.5, it can be verified that increasing the width of the microstrip keeping a distance g from the ground plane, creating a rectangular patch, clearly improves the working bandwidth, especially at the lower limit of the frequency band. In this particular case the value W_{patch} = 20 mm provides the best impedance matching while W_{patch} = 2 mm as the worst S_{11} behaviour.

- Study of Gap g

Keeping the parameters of the previous simulations for the rectangular patch antenna, $W_{sub} = L_{sub} = W_{gnd}$ = 150 mm, L_{gnd} = 50 mm e L_f = 75 mm, W_f = 2 mm e W_{patch} = 20 mm, the parameter g is varied between the values 0 mm and 4 mm . In this way, since the total length of the monopole is kept at 75 mm, the L_{patch} parameter also varies. The results as shown in figure 3.6.

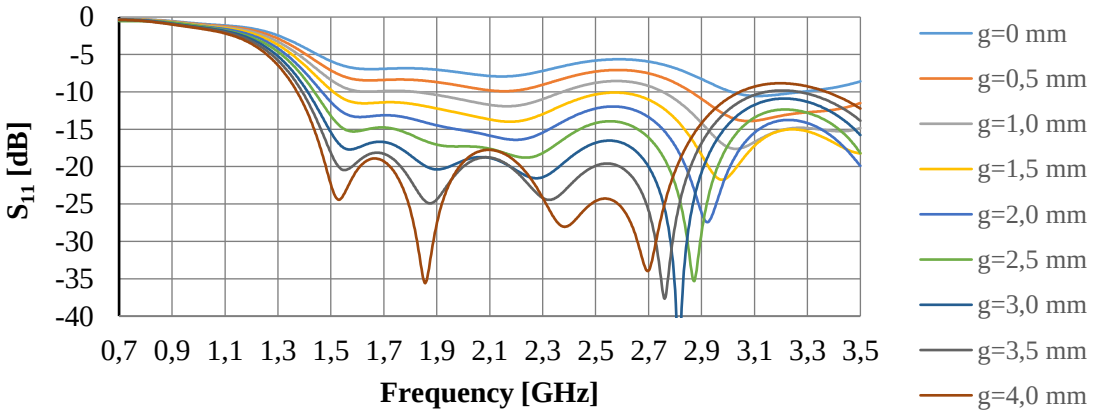

Figure 3.6 - Square patch monopole reflection coefficient for gap g variation

From the analysis of figure 3.6 it is possible to conclude that g is a critical parameter in designing the model. In this case, if the gap g takes values below 1.5 mm the reflection coefficient behaviour is significantly worst due the proximity to the ground plane. For values above 3.5 mm the maximum frequency for which S_{11} is

below -10 dB decreases and changes the working bandwidth. Thus, the next simulations are carried out with a g = 3 mm.

- Square Patch Dimensions

Since the minimum operating frequency is directly related with the patch length and width, in order to obtain a better performance in the lower limit of the frequency band, a variation of the dimensions of the square patch is simulated. Keeping the previous parameters constant W_{sub} = L_{sub} = W_{gnd} = 150 mm, L_{gnd} = 50 mm, g = 3 mm e W_f = 2 mm, a variation of 16 x 16 mm to 32 x 32 mm in the dimensions of the patch is made with 2 mm intervals. The corresponding results are shown in figure 3.7.

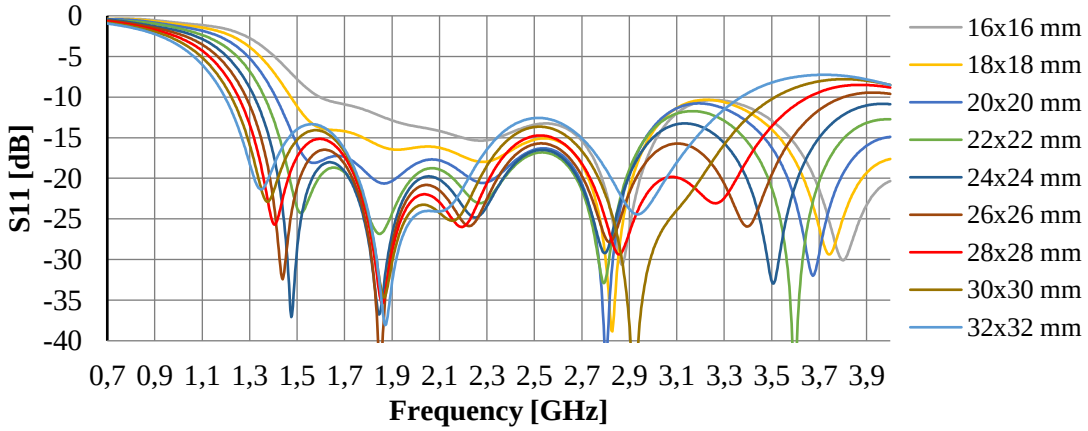

Figure 3.7 – Square patch monopole reflection coefficient for patch dimensions variation

By analysing figure 3.7, it can be verified that decreasing the patch size, the bandwidth decreases as the minimum frequency for which S_{11} <- 10 dB increases. On the other hand, as the patch size increases, the bandwidth increases as the minimum frequency to which S_{11} <- 10 dB decreases. For this case the dimensions W_{patch} = L_{patch} = 28 mm show the best behaviour for the 700 MHz to 3500 MHz band in a compromise between the minimum and maximum frequency in which the condition of the input reflection coefficient is satisfied.

- Square Patch – Ground Plane Dimensions

Keeping the parameters of the previous simulations, W_{sub} = L_{sub} = W_{gnd} = 150 mm, W_f = 2 mm, g = 3 mm e W_{patch} = L_{patch} = 28 mm, the parameter L_{gnd} is varied between the values 25 mm and 75 mm with 5 mm intervals, the results shown in figures 3.8 and 3.9 were obtained.

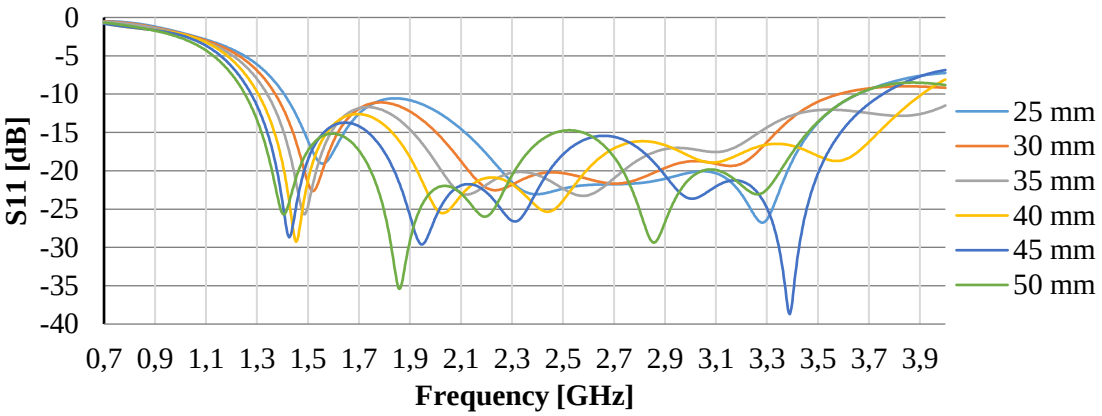

Figure 3.8 – Square patch monopole reflection coefficient for ground dimensions variation (<50 mm)

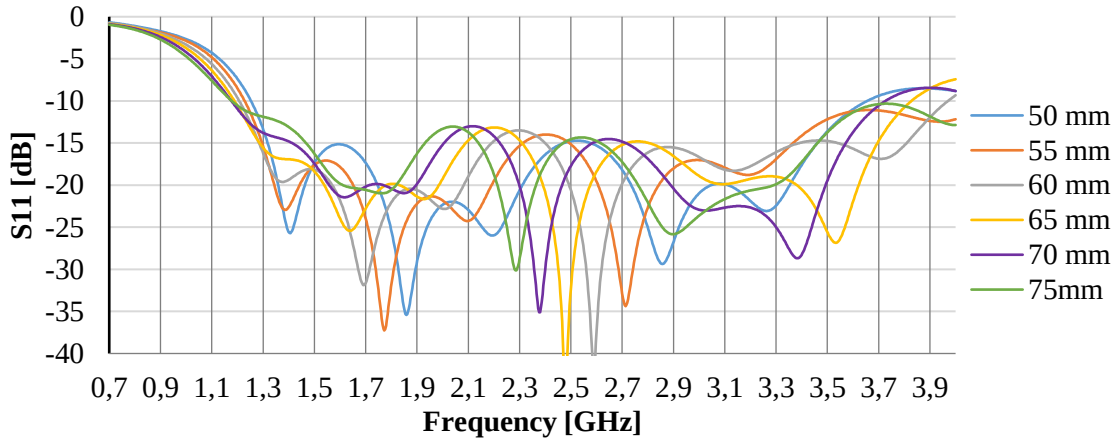

Figure 3.9 – Square patch monopole reflection coefficient for ground dimensions variation (>50 mm)

By analysing the results shown in figures 3.8 and 3.9, it is concluded that for both cases, when decreasing or increasing the length of the ground plane, at the frequency f = 3500 MHz the input reflection coefficient is less than -10 dB for all configurations. It is observed that when decreasing the length of the ground plane, the minimum frequency for which S_{11} <- 10 dB increases. Otherwise, increasing the length of the ground plane decreases this frequency. The length L_{gnd} = 70 mm is chosen for the following simulations.

- Square Patch – Substrate Dimensions

The goal of this section is to understand how the input reflection coefficient varies for different dimensions of the dielectric substrate L_{sub} = W_{sub}. Keeping the parameters of the previous simulations, W_f = 2 mm, g = 3 mm, W_{patch} = L_{patch} = 28 mm e L_{gnd} = 70 mm, the parameters L_{sub} = W_{sub} = W_{gnd} change from 100 mm to 200 mm with 10 mm interval. The corresponding results are shown in figures 3.10 and 3.11.

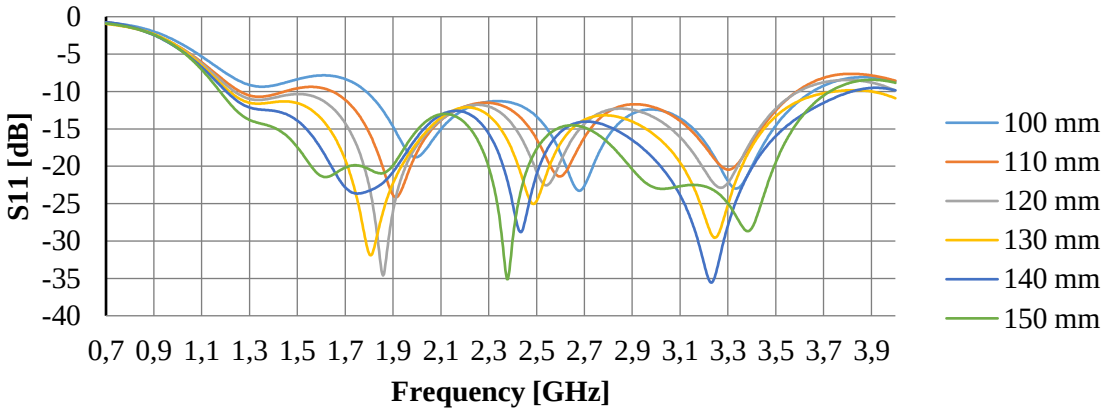

Figure 3.10 – Square patch monopole reflection coefficient for substrate dimensions variation (<150 mm)

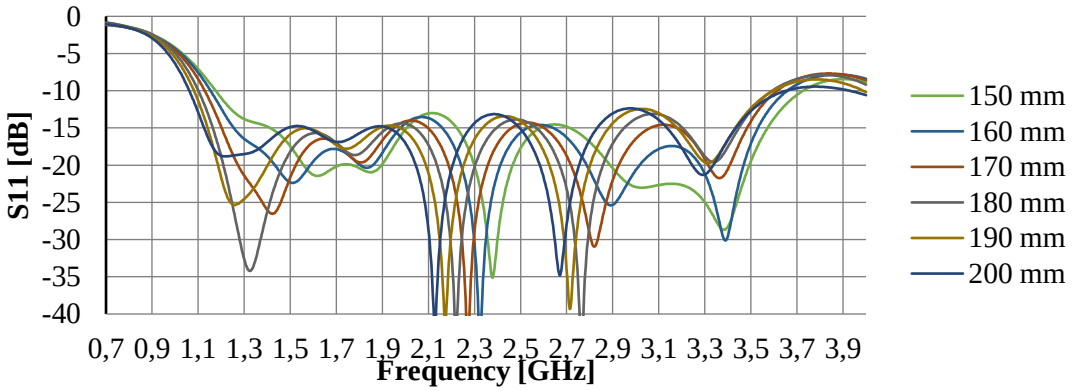

Figure 3.11 - Square patch monopole reflection coefficient for substrate dimensions variation (>150 mm)

From the analysis of results shown in the figures 3.10 and 3.11, it is concluded that for both cases, when decreasing or increasing the dimensions of the substrate, the frequency f = 3500 MHz presents a input reflection coefficient less than -10 dB for all configurations. It is also observed that when decreasing the substrate, the minimum frequency for which S_{11} <- 10 dB increases. Otherwise, increasing the substrate, this frequency decreases. Since the minimum frequency required in the working band f = 700 MHz, the setting $L_{sub} = W_{sub}$ = 200 mm is chosen in future simulations.

- Square Patch – New Patch Dimensions

In order to obtain an S_{11} <-10 dB at frequency f = 700 MHz, new simulations are made for larger patch dimensions with the previously optimized substrate and ground plane dimensions. Keeping the parameters of the previous simulations, W_f = 2 mm, g = 3 mm, $L_{sub} = W_{sub}$ = 200 mm and L_{gnd} = 70 mm the results shown in figure 3.12 were obtained. The reflection coefficient is represented only for a few values of $W_{patch} = L_{patch}$ to make it easier to analyse the results.

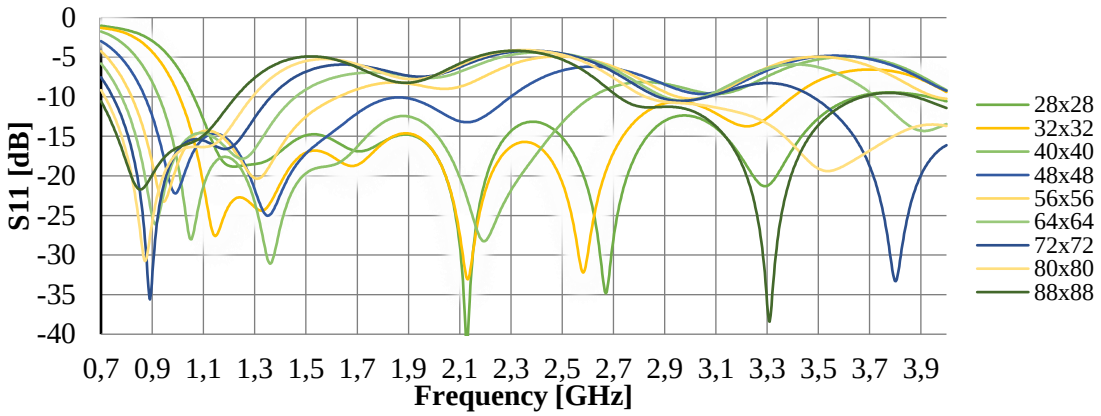

Figure 3.12 – Square patch monopole reflection coefficient for new patch dimensions variation

It is observed that when increasing the dimensions of the patch, the minimum frequency for which S_{11} <- 10 dB decreases as expected and verified in previous simulations. Otherwise, decreasing the dimensions of the patch increases this frequency. For the dimensions W_{patch} = L_{patch} = 88 mm, S_{11} is below - 10 dB at f = 700 MHz. It is concluded that the dimensions of the patch are a compromise between the minimum and maximum frequency in which the condition of the input reflection coefficient is satisfied.

3.3.3 Trapezoidal Patch Monopole

Using the previous model with a square patch as a start point, a new patch configuration based on a trapezoidal patch is simulated in order to increase bandwidth. Keeping the previous parameters, W_f = 2 mm, L_{sub} = W_{sub} = 200 mm, L_{gnd} = 70 mm, W_{patch} = L_{patch} = 88 mm and g = 5 mm, a new parameter is added W_{tri} representing the length of the top side of the trapezoidal patch.

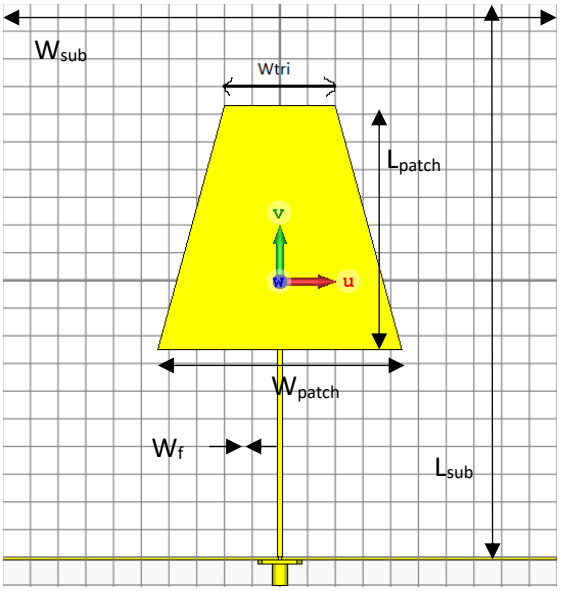

Figure 3.13 – Trapezoidal patch monopole configuration

In the simulation process, the W_{tri} parameter varies between 88 mm which is its initial value, up to 4 mm, removing 2 mm on each side in each iteration. The designed dimensions of the trapezoidal patch monopole are summarized in table 3.3. The input reflection coefficient results are shown in figure 3.14.

Table 3.3 – Dimensions of the trapezoidal patch monopole

Substrate width (W_{sub})	200 mm
Substrate length (L_{sub})	200 mm
Substrate thickness (h)	1.6 mm
Ground plane width (W_{gnd})	200 mm
Ground plane length (L_{gnd})	70 mm
Microstrip width (W_f)	2 mm
Patch width (W_{patch})	88 mm
Patch length (L_{pacth})	20 mm
Gap (g)	5 mm
Trapezoidal patch width (W_{tri})	4 – 88 mm

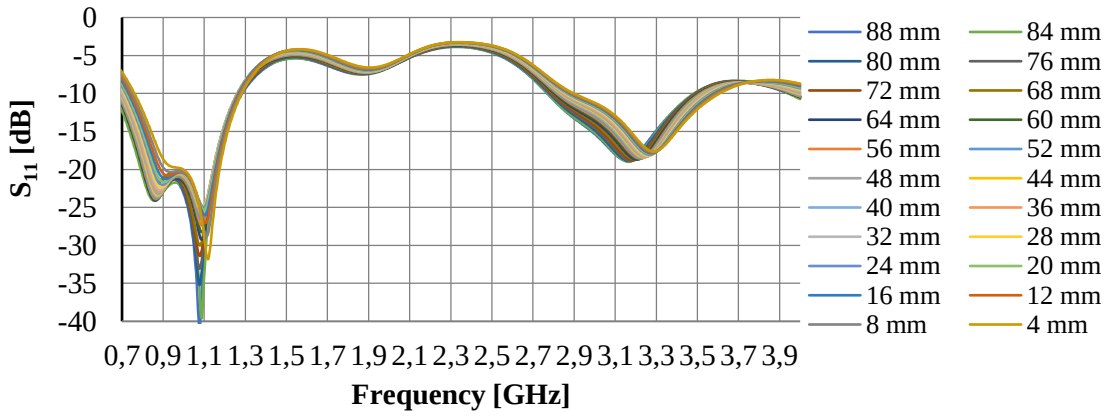

Figure 3.14 – Input reflection coefficient for trapezoidal patch monopole width variation

From the results shown in figure 3.14, it can be concluded that the trapezoidal patch is not an interesting solution since the S_{11} has little change in relation to the previous configuration. It is found that by decreasing W_{tri} the minimum frequency for which S_{11} <- 10 dB increases.

3.3.4 Inverted Trapezoidal Patch Monopole

Inverting the previous monopole configuration we obtain an inverted trapezoidal patch. Keeping the previous parameters, W_f = 2 mm, g = 5 mm, L_{sub} = W_{sub} = 200 mm, L_{gnd} = 70 mm, W_{patch} = L_{patch} = 88 mm, the parameter W_{tri} now represents the length of the bottom side of the patch.

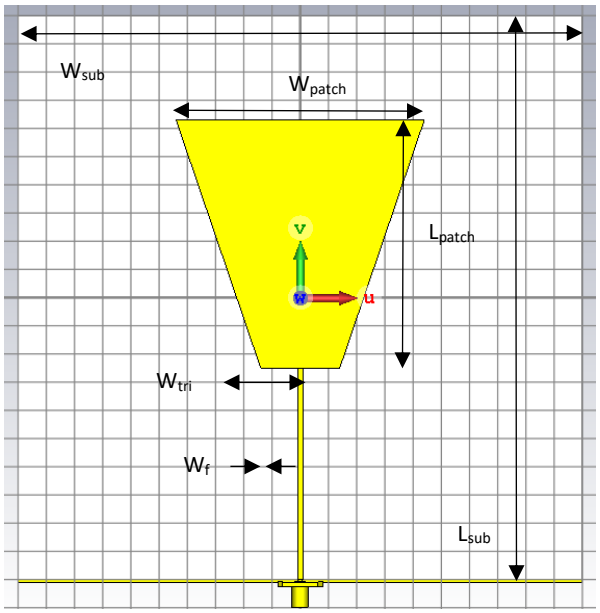

Figure 3.15 – Inverted trapezoidal patch monopole configuration

As in the simulations of the previous patch, W_{tri} ranges from 88 mm to 4 mm with 4 mm intervals and the results shown in figure 3.16 are obtained. The dimensions of the designed monopole are summarized in table 3.4.

Table 3.4 – Dimensions of the inverted trapezoidal patch monopole

Substrate width (W_{sub})	200 mm
Substrate length (L_{sub})	200 mm
Substrate thickness (h)	1.6 mm
Ground plane width (W_{gnd})	200 mm
Ground plane length (L_{gnd})	70 mm
Microstrip width (W_f)	2 mm
Patch width (W_{patch})	88 mm
Patch length (L_{pacth})	20 mm
Gap (g)	5 mm
Trapezoidal patch width (W_{tri})	4 – 88 mm

Figure 3.16 contains the reflection coefficient results corresponding to only a few values of W_{tri} to make the analysis easier. It is noticeable that with W_{tri} = 28 mm the reflection coefficient S_{11} is under -10 dB at the lower frequency limit of the working band (f = 700 MHz), which has been one of the main requirements in the antenna design. It also covers almost all required bandwidth except between 750 MHz and 1350 MHz. Compared with the previous model, the square patch with W_{patch} = L_{patch} = 88 mm, which also satisfied the lower frequency limit, the inverted trapezoidal patch presents a larger bandwidth.

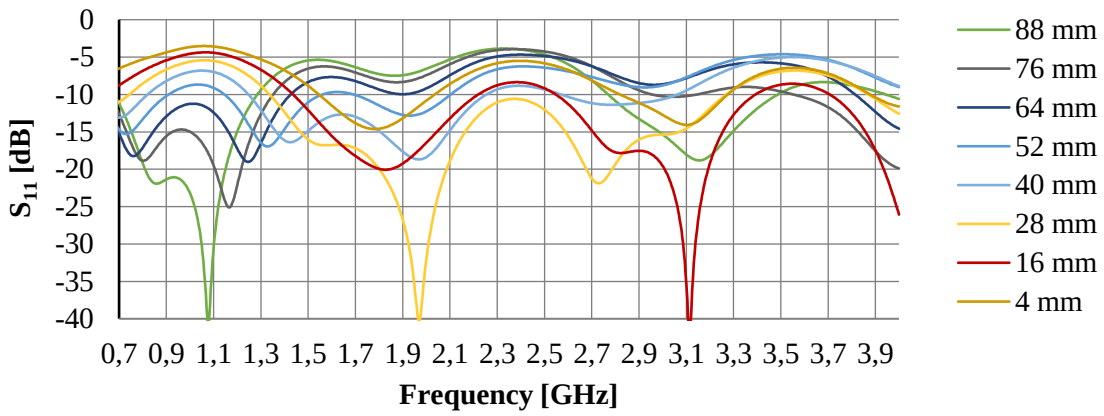

Figure 3.16 – Input reflection coefficient for inverted trapezoidal patch monopole

Keeping the parameters of the previous simulations W_f = 2 mm, W_{tri} = 28 mm, L_{sub} = W_{sub} = 200 mm, L_{gnd} = 70 mm, W_{patch} = L_{patch} = 88 mm, the parameter g is also studied for this model due to its promising S_{11} behaviour. The parameter is varied between 2 mm and 6 mm in intervals of 0.5 mm. The corresponding S_{11} results are shown in figure 3.17. For the sake of clarity only results of a few g values are included.

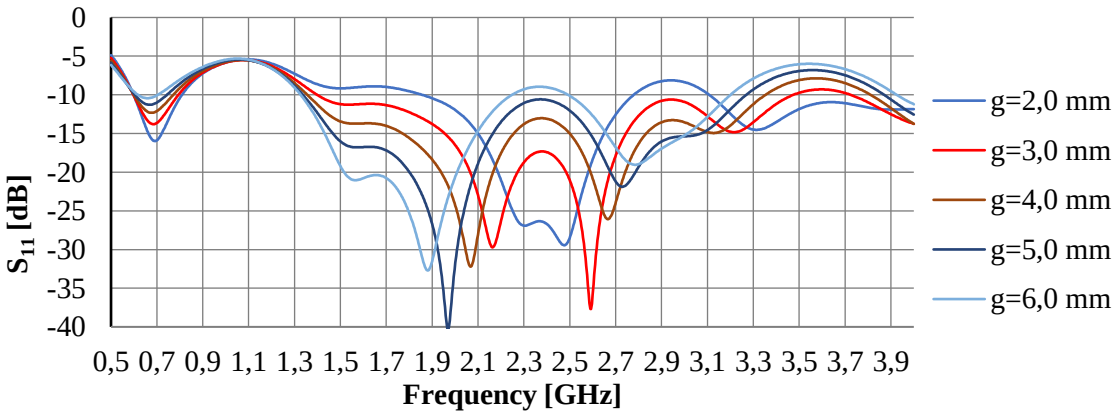

Figure 3.17 – Input reflection coefficient for inverted trapezoidal patch monopole gap g variation

From figure 3.17, it can be concluded that for this inverted trapezoidal patch the parameter g that optimizes the S_{11} is 3 mm. With this configuration, almost the entire frequency band presents an acceptable S_{11} except between the frequency 800 and 1400 MHz.

3.3.5 Octagonal Patch Monopole

A new octagonal patch monopole configuration, shown in figure 3.18 with the following parameters, W = 36 mm, L = 36.8 mm, W_{patch} = L_{patch} = 75 mm, W_f = 2 mm, g = 2 mm, L_{sub} = W_{sub} = 200 mm, L_{gnd} = 73 mm and g = 2 mm is tested. This initial design started with a square patch from which triangles were removed from the four corners. The dimensions of the designed monopole are summarized in table 3.5.

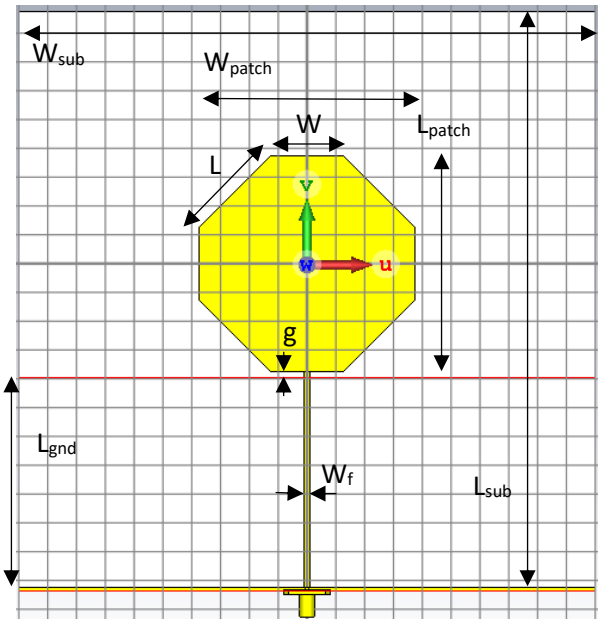

Figure 3.18 – Octagonal patch monopole configuration

Table 3.5 – Dimensions of the octagonal patch monopole

Substrate width (W_{sub})	200 mm
Substrate length (L_{sub})	200 mm
Substrate thickness (h)	1.6 mm
Ground plane width (W_{gnd})	200 mm
Ground plane length (L_{gnd})	73 mm
Microstrip width (W_f)	2 mm
Patch width (W_{patch})	75 mm
Patch length (L_{pacth})	75 mm
Gap (g)	2 mm
Octagonal side (W)	36 mm
Octagonal side (L)	36.8 mm

The corresponding S_{11} simulation results are shown in figure 3.19.

This octagonal patch monopole configuration has a better performance than all the others simulated, since S_{11} is below -10 dB for almost all the required working bandwidth between 700 MHz and 3.5 GHz. However S_{11} > -10 dB around the frequency 1.1 GHz. The results of the previous simulations were taken into account so that the following simulations in this configuration were performed in order to decrease the minimum frequency for which S_{11} < -10 dB and the maximum at f = 1.1 GHz.

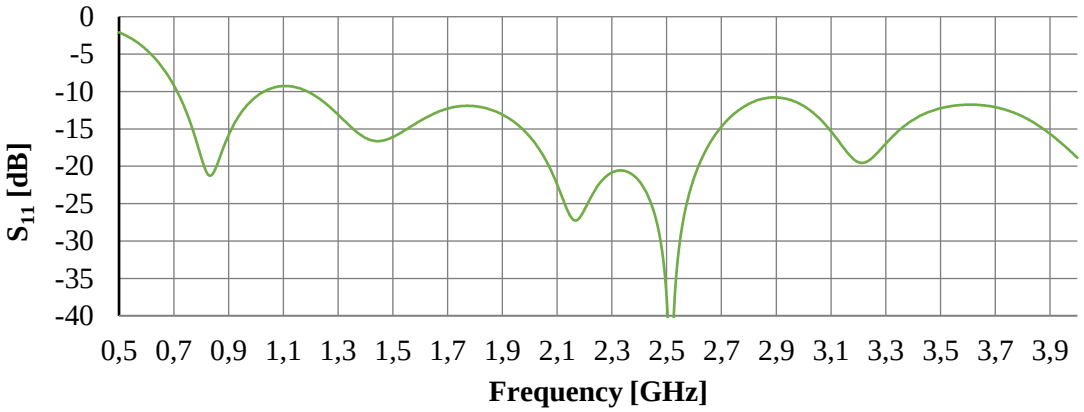

Figure 3.19 – Input reflection coefficient of the octagonal patch monopole

- Octagonal Patch Monopole – Cooplanar Feed

Using the new dimensions of the octagonal patch, a new cooplanar configuration is tested in which the ground is no longer in the lower plane of the substrate. The octagonal patch and the ground plane are printed on the same side of the dielectric substrate shown in figure 3.20. The antenna is fed by the central strip of the coplanar waveguide (CPW) by a SMA connector. The ground plane in the upper plane creates a new variable k that represents the distance between the ground planes and the strip (figure 3.21).

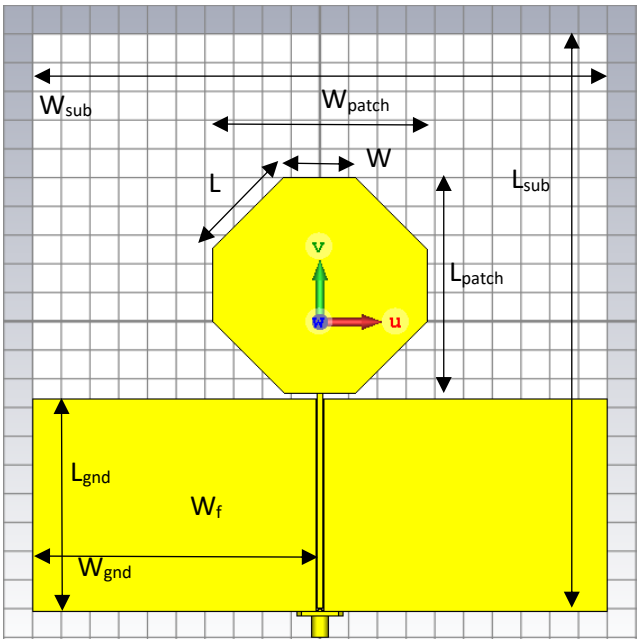

Figure 3.20 – Octagonal patch monopole configuration with CPW feed

Table 3.6 - Dimensions of the CPW

Ground plane length (L_{gnd})	73 mm
g	1 - 4 mm
k	0.36 – 0.6 mm

Keeping the parameters of the previous simulations, W = 25 mm, L = 35.35 mm, W_{patch} = L_{patch} = 75 mm, W_f = 2 mm, L_{sub} = W_{sub} = 200 mm, L_{gnd} = 73 mm a scan of values is simulated for parameters g and k. For parameter g, a variation from 1 mm to 4 mm is made with 0.5 mm intervals. For parameter k a variation is made from 0.35 mm to 0.6 mm with intervals of 0.05 mm.

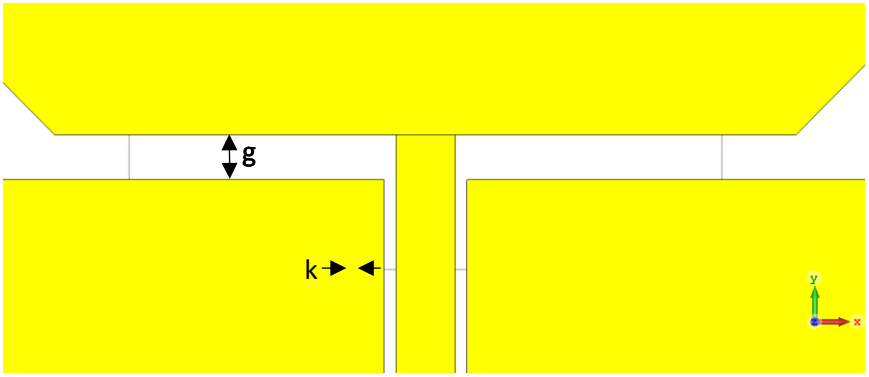

Figure 3.21 – Zoom of the octagonal patch monopole CPW feeding

The S_{11} results obtained by simulation are shown in figures 3.22 and 3.23.

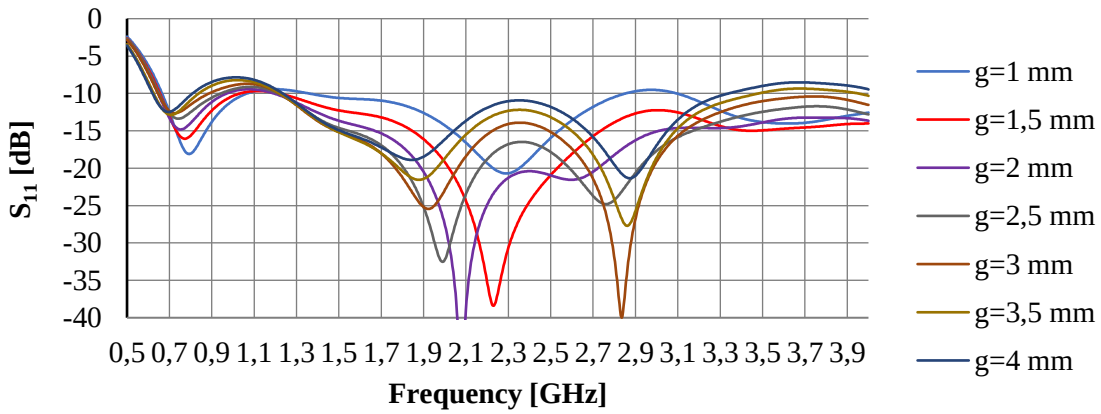

Figure 3.22 – Input reflection coefficient of the CPW feed octagonal monopole for parameter g variation

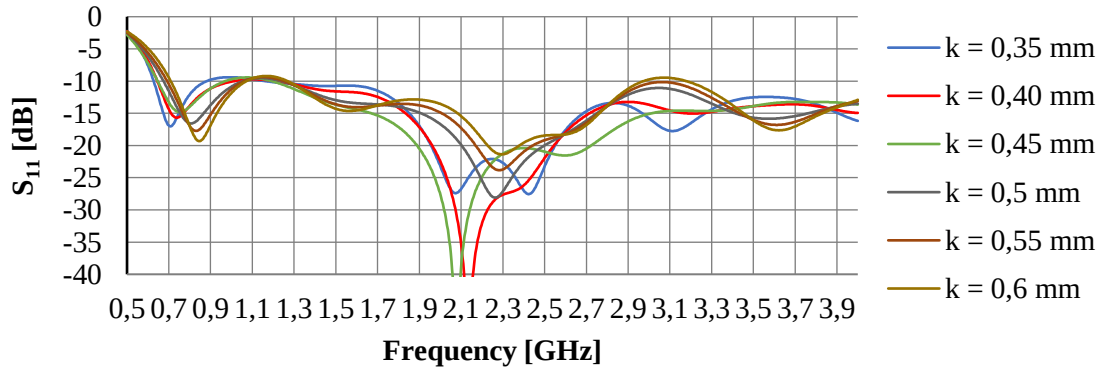

Figure 3.23 - Input reflection coefficient of the CPW feed octagonal monopole for parameter k variation

By analysing the obtained results, with the parameter g = 1.5 mm, it is possible to obtain the best reflection coefficient curve for this configuration since the maximum between 1000 MHz and 1200 MHz is smaller, approaching the -10 dB limit. Regarding parameter k, k = 0.4 mm was considered the best option for which the reflection coefficient at 1100 MHz is lower.

- Modified Octagonal Patch Monopole – Cooplanar Feed

To obtain the desired bandwidth, small isosceles triangles were added to the previous configuration (figure 3.24). These triangles vary in dimensions from 5 mm to 17.5 mm in relation to the sides and from 7.07 mm to 24.75 mm in relation to the hypotenuse. Keeping all previous parameters constant, W = 25 mm, L = 35.35 mm, W_{patch} = L_{patch} = 75 mm, W_f = 2 mm, L_{sub} = W_{sub} = 200 mm, L_{gnd} = 73 mm, g = 1.5 mm and k = 0.4 mm, simulations were carried out for a changing a parameter. The results obtained are shown in figure 3.25.

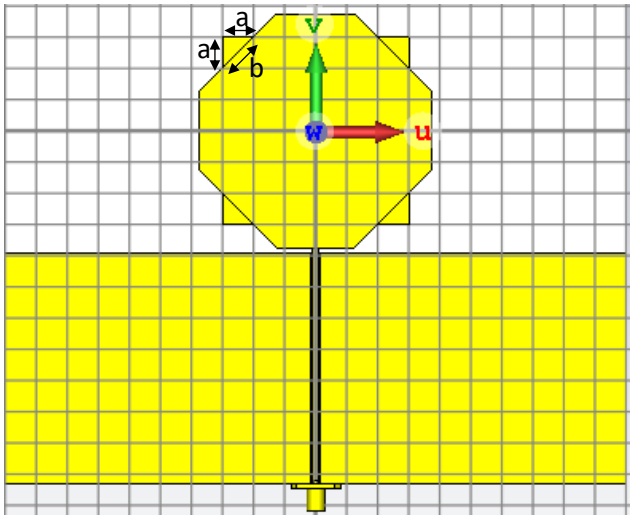

Figure 3.24 – Modified octagonal patch monopole configuration with CPW feeding

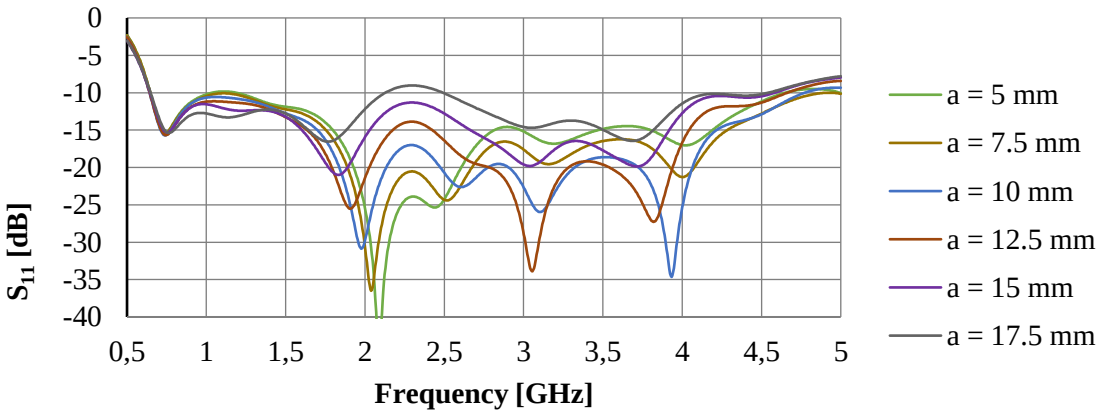

Figure 3.25 – Input reflection coefficient of the modified octagonal patch monopole for triangle dimensions variation

It is clear that with the addition of the small triangles the reflection coefficient takes acceptable values for the entire required band with S_{11} < -35 dB for a = 10 mm. These triangles behave as an additional inductive element that generates additional resonant modes, which is used for either dual or multiband operations, or it

is combined with the fundamental mode to improve the overall bandwidth [22]. Changing the sleeves shape has a strong effect on the second resonance frequency and the impedance matching over the frequency band of interest, such that the best result is obtained when using the triangular shape [22].

- Modified Octagonal Patch Monopole with CPW - Miniaturization

Since the overall size of the antenna is a critical requirement for the project, the objective of this study is to understand the impact that the size of the dielectric substrate and the ground plane have in the antenna´s reflection coefficient. Maintaining the height of the ground plane as 73 mm and the patch dimensions, four different designs were simulated, first reducing the dielectric substrate height above the octagonal patch and then reducing the ground plane width. The first design is 20 x 20 cm, the second is 20 x 15 cm, the third is 15 x 15 cm and the last one is 10 x 15 cm (figure 3.26).

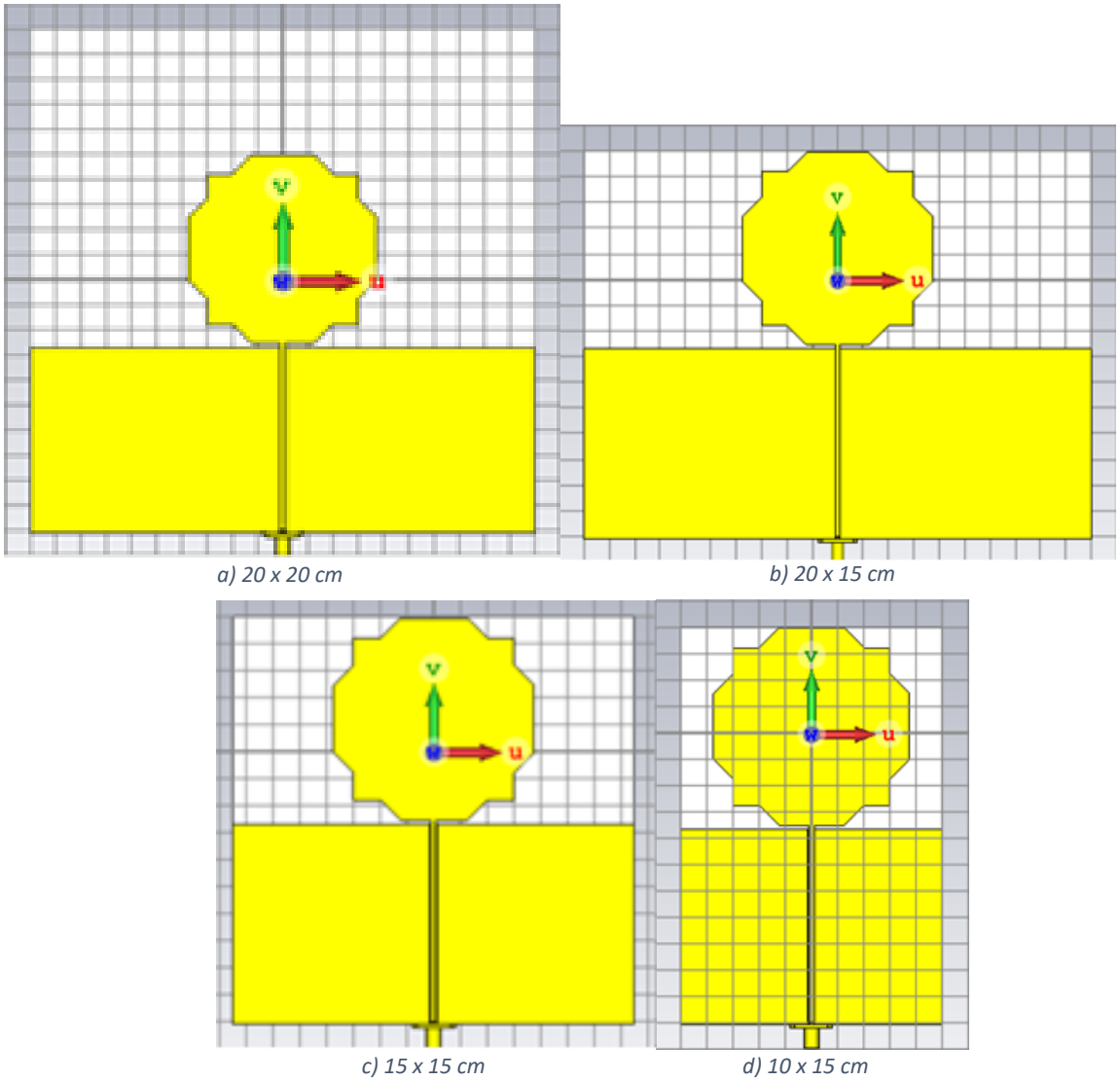

a) 20 x 20 cm *b) 20 x 15 cm*

c) 15 x 15 cm *d) 10 x 15 cm*

Figure 3.26 – Modified octagonal patch configuration with CPW

The S_{11} result presented in figure 3.27 show a comparison of the four simulated configurations.

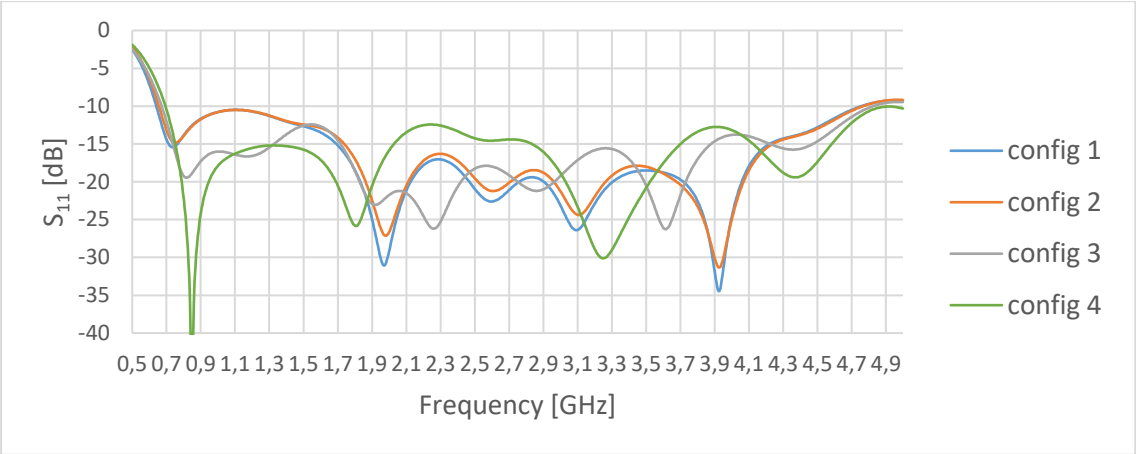

Figure 3.27 - Reflection coefficient comparison - Printed Monopole Octagonal Patch CPW

The input reflection coefficient of the four configurations is under -10 dB for all the required frequency range. By reducing the size of the dielectric substrate and the ground plane, it is noticeable that the lowest frequency where the antenna reflection coefficient its bellow -10 dB increases. Despite this increase when the width of the ground plane decreases, it is possible to observe a better behaviour of the S_{11}. This indicates one important step for size reduction and optimization before manufacturing the prototype that will be to determine how much one can reduce W_{gnd} before compromising the antenna´s bandwidth performance.

The second configuration was chosen even though the third and fourth had lower reflection coefficients since the author had in mind a cooplanar configuration with 2 monopoles. In configurations 3 and 4, the ground plane is too small to accommodate another patch monopole.

The radiation patterns for configuration 2 are presented in figure 3.28 for different frequencies. As expected, the radiation pattern of this configuration is similar to the radiation pattern of the simple straight monopole (section 3.3.1). However, in this case, higher values of E field are obtained.

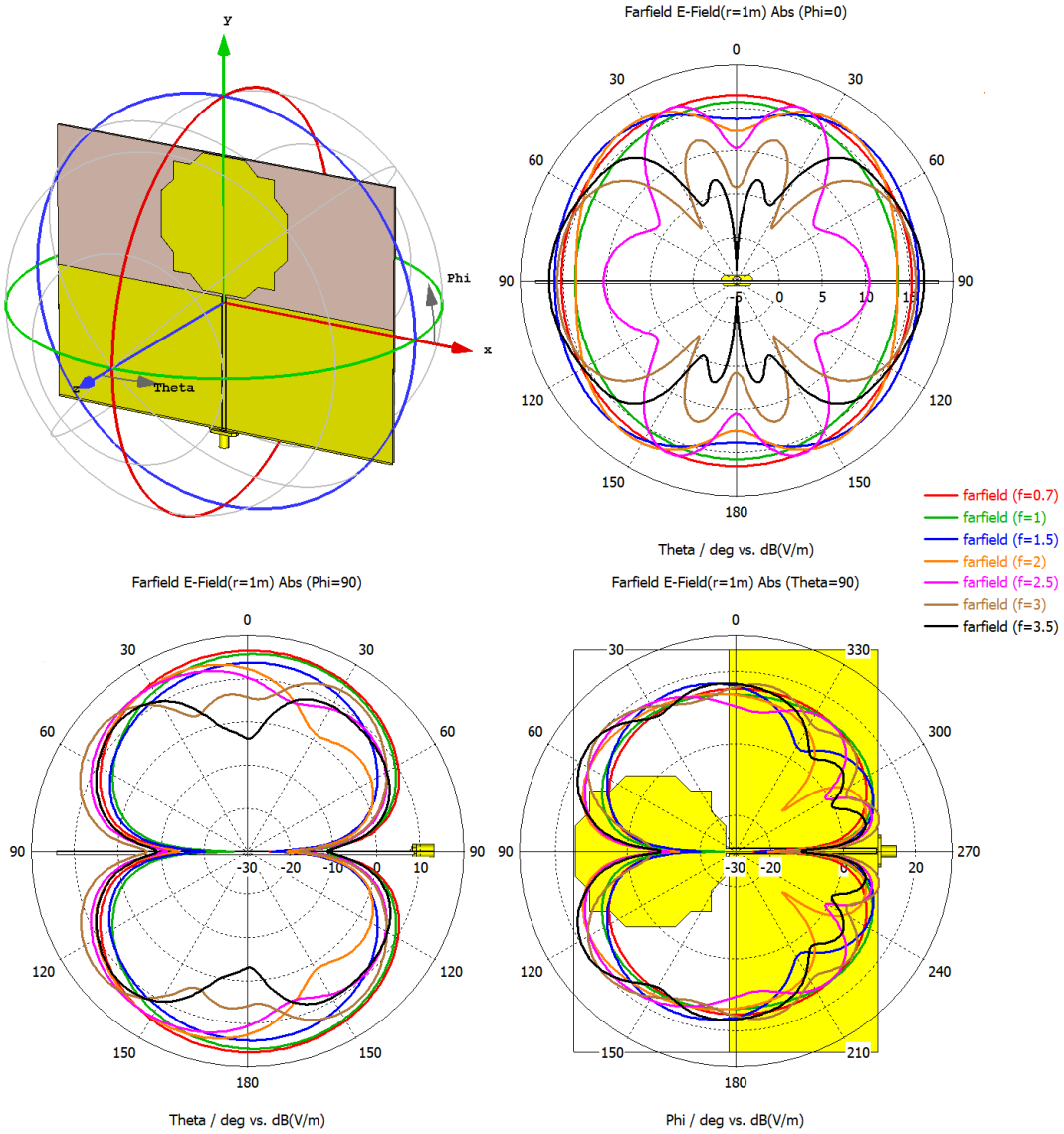

Figure 3.28 - Radiation patterns of the modified octagonal patch monopole with CPW feed

- Dual Linear Polarization Modified Octagonal Patch Monopole with CPW Feed

It is important to match the polarization of the antenna to the receiving signal, so that the maximum signal is obtained. If the antenna does not match of the signal, there is a corresponding decrease in the level of the signal. In the specific case, the polarization of the incident wave is unknown therefore it makes sense to implement a dual linear polarization configuration.

This configuration is designed based on the monopole with a octagonal patch with slight modifications. The antenna displayed in figure 3.29 is fed by two symmetrical CPW lines connected to two SMA connectors. The ground plane is 10 x 10 cm to accommodate the two CPW lines with a reasonable separation to avoid strong coupling. The patch design it is the same from the previous section with the four triangles with W_{patch} = L_{patch} = 75 mm, W_f = 2 mm, L_{sub} = W_{sub} = 190 mm, g = 1.5 mm, k = 0.4 mm and a = 10 mm.

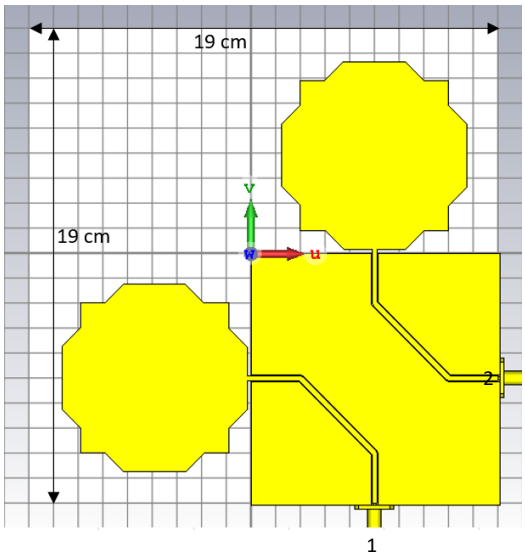

Figure 3.29 – CPW fed dual linear polarization octagonal patch monopole configuration

Figure 3.30 shows the S-parameters for the dual linear polarization configuration. S_{11} represents the reflection coefficient in the horizontal monopole of port 1 and S_{22} represents the reflection coefficient in the vertical monopole of port 2. Due to the physical symmetry of the antenna, $S_{11} = S_{22}$ and due to reciprocity $S_{12} = S_{21}$.

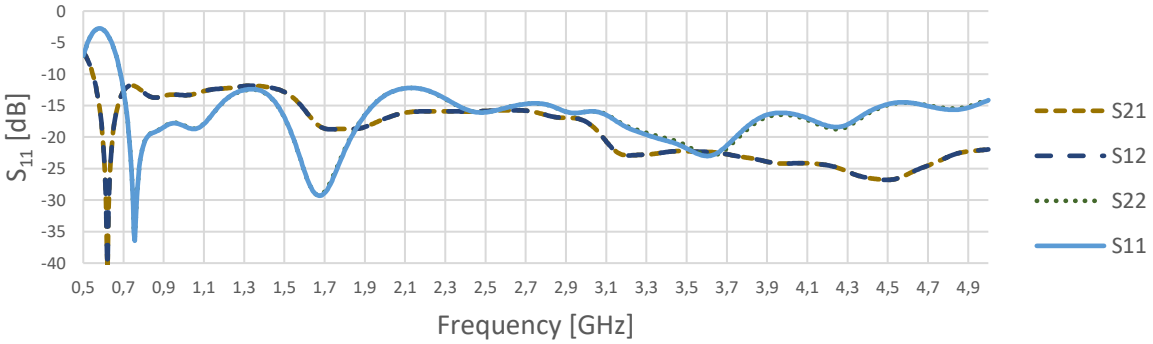

Figure 3.30 – S-parameters of the CPW fed dual linear polarization octagonal patch monopole configuration

It is noticeable that all the required bandwidth is satisfied with this configuration, in which the minimum frequency for S_{11} < - 10 dB is 680 MHz. Since the simulations were made from 500 MHz to 5 GHz, it is not possible to know the upper limit of the bandwidth obtained. Moreover, S_{21} is below -13 dB in the whole frequency range of interest.

3.4 Monopole with Foam Absorber

The printed monopole with CPW-feeding and dual linear polarization configuration developed up to this point achieves the required bandwidth between 700 MHz and 3.5 GHz, but since it is a monopole, it has almost omnidirectional radiation pattern and radiates to both the front and back planes.

The monopole is meant to be used integrated in a professional safety vest that is coated with a metallic shielding film. One solution to overcome the negative effects of this shield on the monopole performance is to insert a thick layer of lossy material between the monopole and the shield. Naturally, the monopole's efficiency decreases but, that is not critical for the envisaged application. In fact, if the efficiency is know it can be taken into account in the estimation of the incident electromagnetic field.

3.4.1 Absorber Foam Characterisation

For the lossy material, two absorber foams have been considered, one of them was not known but was available in the laboratory of IT/IST (CF) and the other one was fabricated by Laird. The absorber foam from Laird available in the laboratory, is the Eccosorb AN-75. It is made from polyurethane foam that is treated with special filler and assembled in a laminate construction to generate a controlled conductivity gradient.

Figure 3.31 – Multi-layer gradient Eccosorb AN-75

In order to assess what is the best option to take, a characterization is made for each foam and in the case of the Eccosorb for each layer.

$$\varepsilon_r' - j\varepsilon_r'' = \varepsilon_r - j\frac{\sigma}{\omega\varepsilon_0} = \varepsilon_r(1 - j\ \tan\delta) \quad (3.1)$$

Where $\varepsilon_r$is the relative electric permittivity, σ is the conductivity, $\varepsilon_0$is the electric permittivity of vacuum, ω is the angular frequency and $\tan\delta$ is the loss tangent.

In figure 3.32 is represented the theoretical electric dispersion (ε_r',ε_r'') between 500 MHz and 4 GHz for all the different layers of the Eccosorb AN-75, front, middle and back [45]. It is also represented the average (in black) so this values can be compared with the ones obtained in laboratory. It is noticeable that for the front side of the foam, the relative dielectric constant real and imaginary part are the lowest. On the other hand, in the backside, the relative dielectric constant is higher.

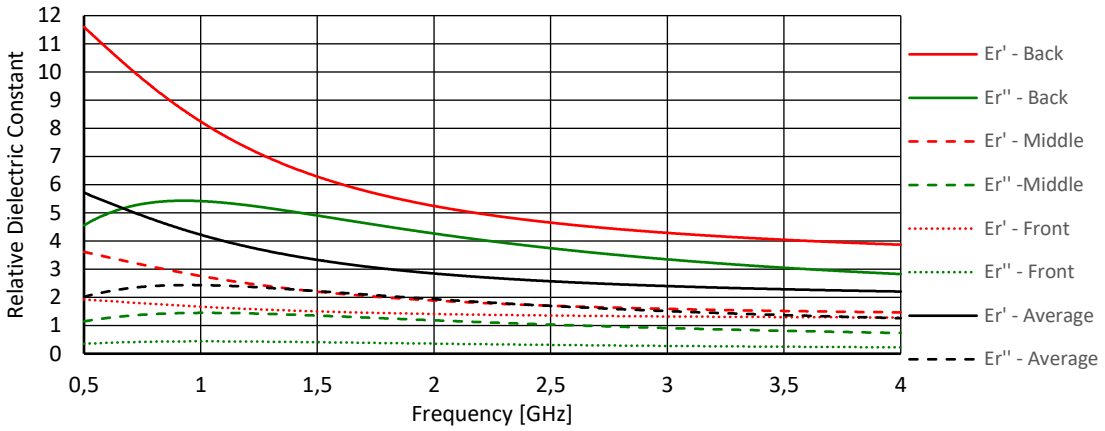

Figure 3.32 - Electric dispersion for Eccosorb AN-75 layers

The absorber foam Eccosorb AN-75 plate present in the IT/IST laboratory has approximately 29 mm of thickness and has been tested in order to characterize its dielectric constant as shown in figure 3.33.

Figure 3.33 – Setup for the experimental macroscopic characterization of Eccosorb AN-75

This measurement was made in the operating band from 1.5 GHz to 2.75 using two rectangular horn antennas. According to the dispersion equation,

$$\gamma^2 - j\omega\mu(\sigma + j\omega\varepsilon) = 0 \tag{3.1}$$

In the general case with losses, $\gamma = \alpha + j\beta$, therefore,

$$\gamma = \sqrt{j\omega\mu_0(\sigma + j\omega\varepsilon)} \tag{3.2}$$

$$(\alpha + j\beta)^2 = \alpha^2 + j2\alpha\beta - \beta^2 = \omega\mu_0(\sigma + j\omega\varepsilon) = j\omega\mu_0\sigma - \omega^2\varepsilon\mu_0) \tag{3.3}$$

$$\begin{cases} 2\alpha\beta = \omega\mu_0\sigma \\ -\beta^2 + \alpha^2 = -\omega^2\varepsilon\mu_0 \end{cases} \Rightarrow \begin{cases} \sigma = \frac{2\alpha\beta}{\omega\mu_0} \\ \varepsilon_r = \frac{\beta^2-\alpha^2}{\omega^2\varepsilon_0\mu_0} = \frac{\beta^2-\alpha^2}{\beta_0^2} \end{cases} \qquad \beta_0 = \frac{\omega}{c_0} \tag{3.4}$$

$$\alpha = \frac{A_{[dB]}}{d_{[m]}} \times \frac{\ln(10)}{20} \tag{3.5}$$

$$A_{[dB]} = \frac{E_{FS\,[dB]}}{E_{sample\,[dB]}} \quad (3.6)$$

$$\beta = \beta_0 + \frac{Fase_{FS} - Fase_{sample}}{d_{[m]}}\ [rad.m^{-1}] \quad (3.7)$$

Being E_{FS} the received electric field and respective phase $Fase_{FS}$ in free space (without sample) and E_{sample} being the received electric signal and respective phase $Fase_{sample}$ with absorber sample.

The following results were obtained:

Freq. [GHz]		1.75	2	2.5	2.75
CF	ε_r	1.368	2.003	2.789	2.203
	σ [S/m]	0.160	0.157	0.357	0.454
	tan δ	1.202	0.708	0.922	1.348
Eccosorb AN-75	ε_r	1.370	1.653	1.818	1.656
	σ [S/m]	0.037	0.036	0.106	0.116
	tan δ	0.277	0.196	0.422	0.458

Table 3.7 - Experimental macroscopic characterization of absorbers

Comparison between the values provided by the software library of CST for ε_r of Eccosorb AN-75 and the experimental values obtained is presented in figure 3.34.

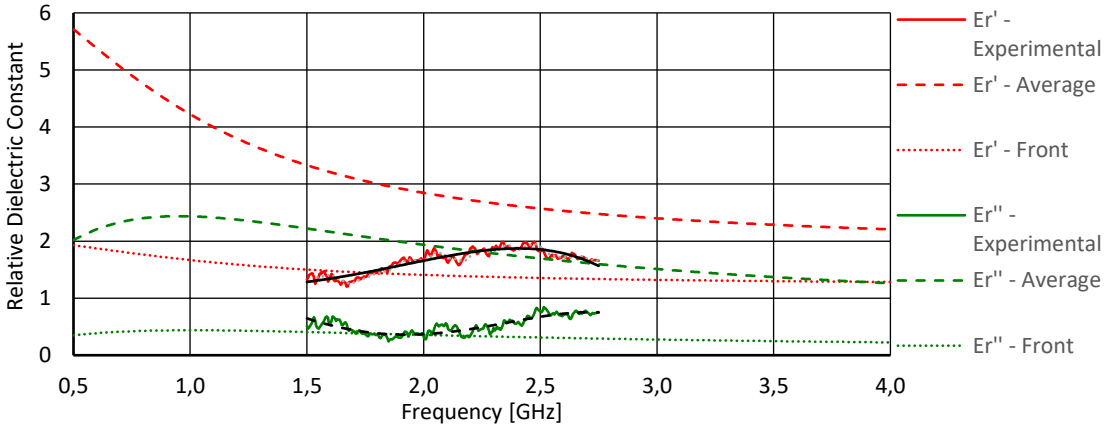

Figure 3.34 – Comparison of theoretical and experimental Eccosorb AN-75 characteristics

From figure 3.34, it is possible to identify clear differences between the experimental values of ε_r and the average of the theoretical values. It is noticeable that the experimental ε_r' and ε_r'', are relatively similar in terms of values to the lines that corresponds to the front layer of the Eccosorb AN-75, ε_r'- Front and ε_r''- Front. The measured data have a reasonable similarity but not in terms of behaviour because a different type of absorber variation is observed.

The CF foam has 30 mm of thickness, and has been tested in the same way of Eccosorb AN-75, in order to characterize its dielectric constant as shown in figure 3.35.

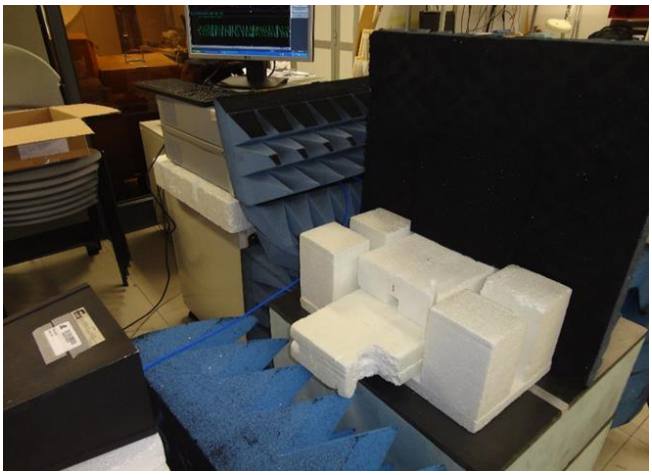

Figure 3.35 – Setup for the experimental macroscopic characterization of CF absorber

In figure 3.36 is presented a comparison between the experimental values of ε_r measured for Eccosorb AN-75 and the experimental values of ε_r measured for CF foam. It turns out that the CF foam introduces more losses due to a higher value of ε_r''.

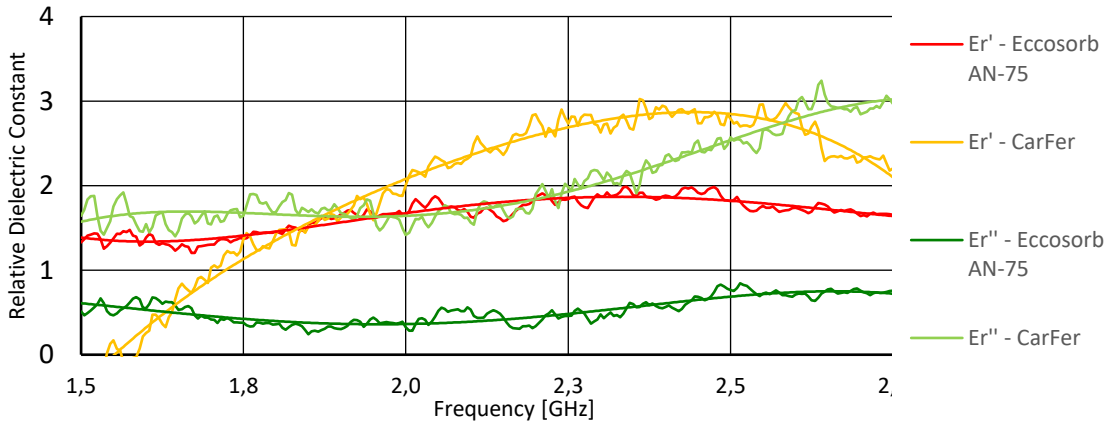

Figure 3.36 – Comparison between experimental characteristics of Eccosorb AN-75 and CF absorbers

Since the CF foam is not in the CST material library, in order to continue simulations to optimize the antenna with the foam thickness, it was necessary to choose witch layer of the Eccosorb AN-75 would be used for the simulations in CST. The next three figures show a comparison of the experimental values of ε_r measured for this foam and the values from CST material library for Eccosorb AN-75 layers.

Analysing figures 3.37, 3.38 and 3.39, in the front layer the measured values of ε_r are much higher, in the middle layer the values are relatively similar and in the back layer they are very low. Therefore, in terms of the CST models for the Eccosorb AN-75, the layer that is more similar to the CF absorber is the middle layer.

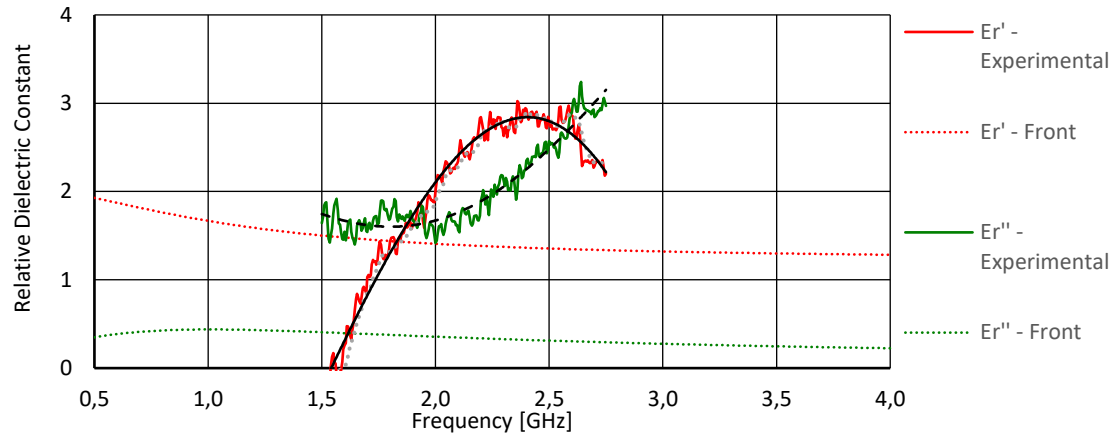

Figure 3.37 – Comparison between experimental CF absorber characteristics and CST library values of absorber Eccosorb AN-75 front layer

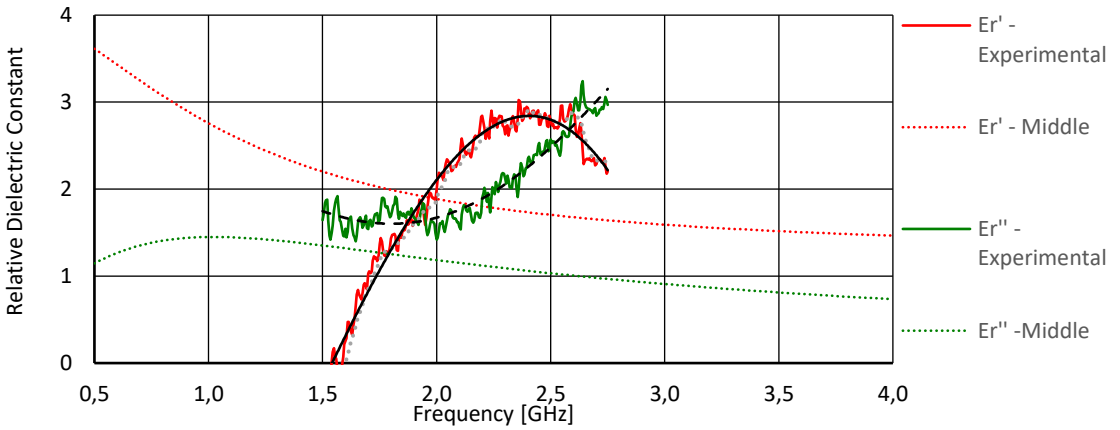

Figure 3.38 - Comparison between experimental CF absorber characteristics and CST library values of absorber Eccosorb AN-75 middle layer

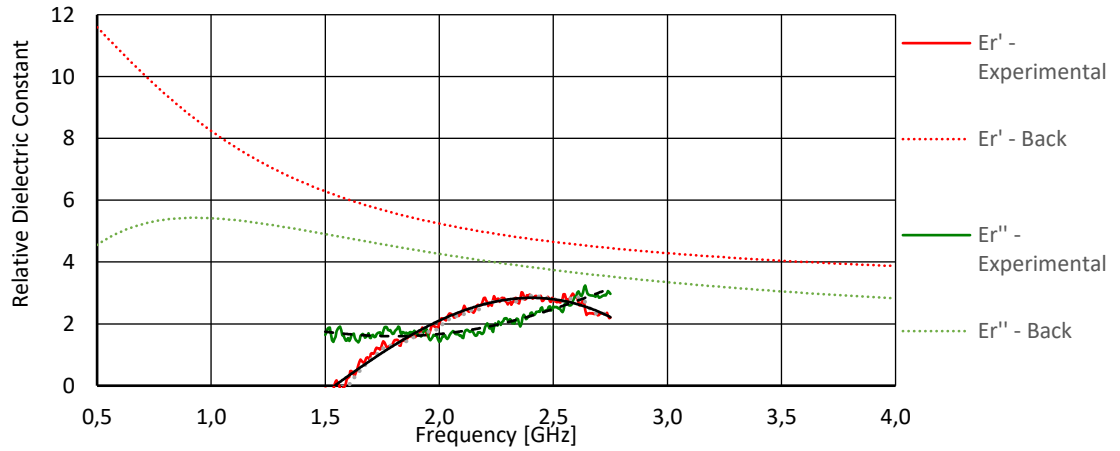

Figure 3.39 - Comparison between experimental CF absorber characteristics and CST library values of absorber Eccosorb AN-75 back layer

3.4.2 Absorber Effects

Using the dispersive model from middle layer of Eccosorb AN-75, some simulations were made with the last optimized monopole varying the foam thickness. The printed monopole with CPW feed and dual linear polarization is now backed with absorber foam and a shield cooper plate with 1 mm thickness behind as shown in figure 3.40. Maintaining all the parameters of the antenna, the foam thickness is simulated between 5 mm and 30 mm in 5 mm intervals.

Since the middle layer of Eccosorb is the one that resembles the CF foam in terms of values, the results obtained using the Eccosorb foam in CST are expected to be slightly worse than the experimental measurements using the CF foam since experimental ε_r is higher.

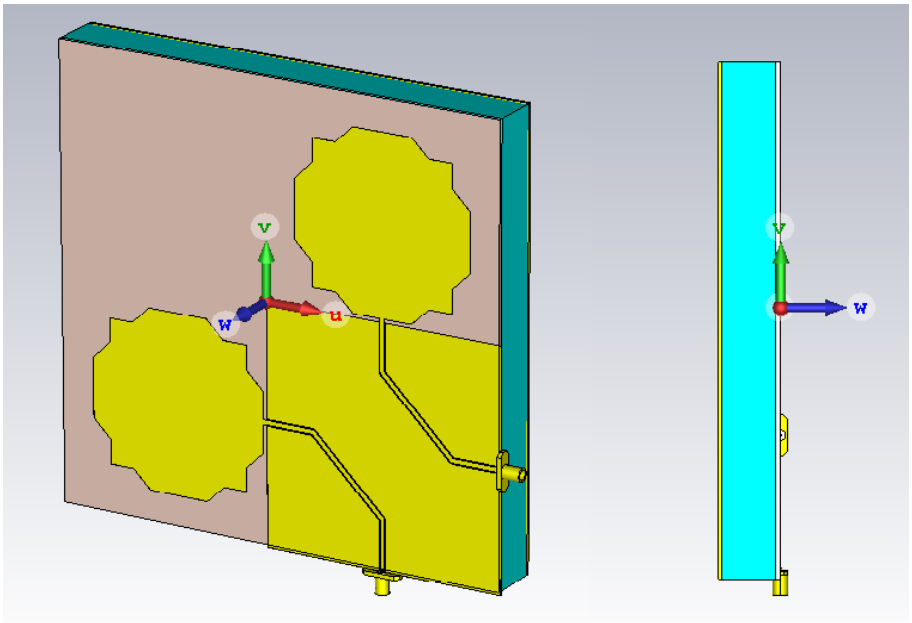

Figure 3.40 – Octagonal monopole with CPW feed dual linear polarization backed by absorber foam and shield

As expected, with the introduction of the cooper shield and the absorber foam on the back of the antenna, a new behaviour of the input reflection coefficient is observed specially for low frequencies. Figure 3.41 shows a comparison between the results for different values of the foam thickness from 5 mm to 30 mm. It is shown that by simulating the antenna using absorber foam with a thickness of 30 mm, represented in red, it is possible to obtain a reflection coefficient bellow -10 dB for almost all the working bandwidth except for a peak of -8.7 dB between 630 MHz and 750 MHz.

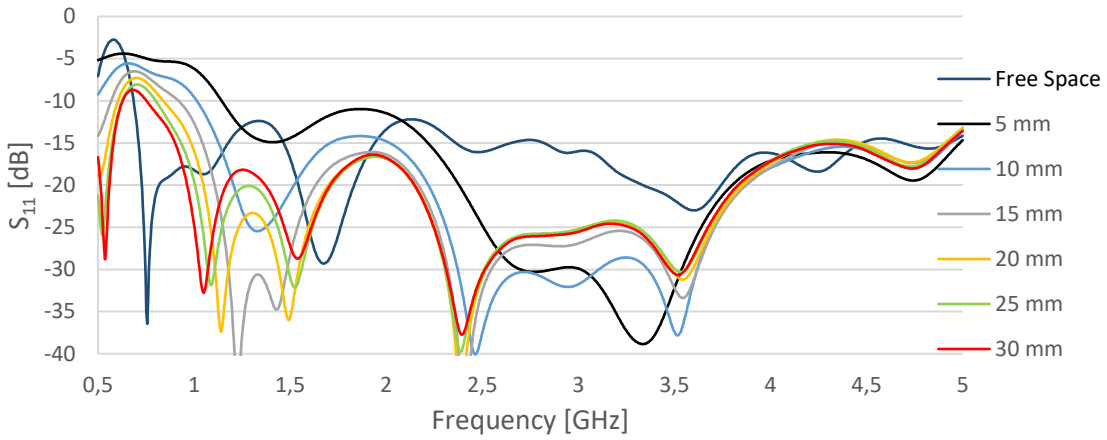

Figure 3.41 – Input reflection coefficient for different foam thickness

Compared with the foam-free model, represented in dark blue, for the case with a thickness of 5 mm, the minimum frequency for which S_{11} <-10 dB increases due to proximity coupling between the antenna and the 1 mm thick copper shield behind. Increasing the thickness of the foam, increases the distance between the shield and the antenna, therefore this minimum frequency decreases, creating a peak around 700 MHz. Since the foam used on the simulations, Eccosorb AN-75 middle layer, introduces fewer losses than the CF foam, better results are expected for the prototype tests.

3.5 Optimized Antenna

This section describes the outcome of the design procedure, resulting in the optimized configuration that fulfils the specifications. It presents the configuration to be used in the prototype antennas.

3.5.1 Antenna Configuration

From figure 3.42, it is noticeable that the designed antenna has a square shape with two octagonal patch monopoles. The overall size of the antenna is 190 x 190 mm. The dielectric substrate used is FR-4, a material with a relative permittivity of 4.3, loss tangent of 0.025 @ 10 GHz and a thickness of 1.6 mm. Regarding the feeding technique, the antenna is fed through CPW lines by SMA connectors.

The optimized antenna has the following characteristics: The dielectric substrate dimensions are L_{sub} = W_{sub} = 190 mm, the octagonal patch dimensions are W_{patch} = L_{patch} = 75 mm and for the octagonal sides W = 25 mm, L = 35.35 mm and a = 10 mm. The symmetric microstrip lines dimensions are L_{f1} = L_{f3} = 20 mm, L_{f2} = 42.5 mm and W_f = 2 mm, the ground plane dimensions are W_{gnd} = 100 mm, L_{gnd} = 100 mm, the gap between the patch and the ground plane is g = 1.5 mm, and k = 0.4 mm is the gap between the ground plane and the microstrip. Figure 3.43 shows that for a thickness of the absorber foam of 25 mm, the reflection factor is below -10 dB for all the bandwidth except between 625 MHz and 800 MHz. Therefore, the chosen thickness for the absorber foam was 25 mm, simulating with Eccosorb AN-75 middle layer, since better results are expected with the CF foam.

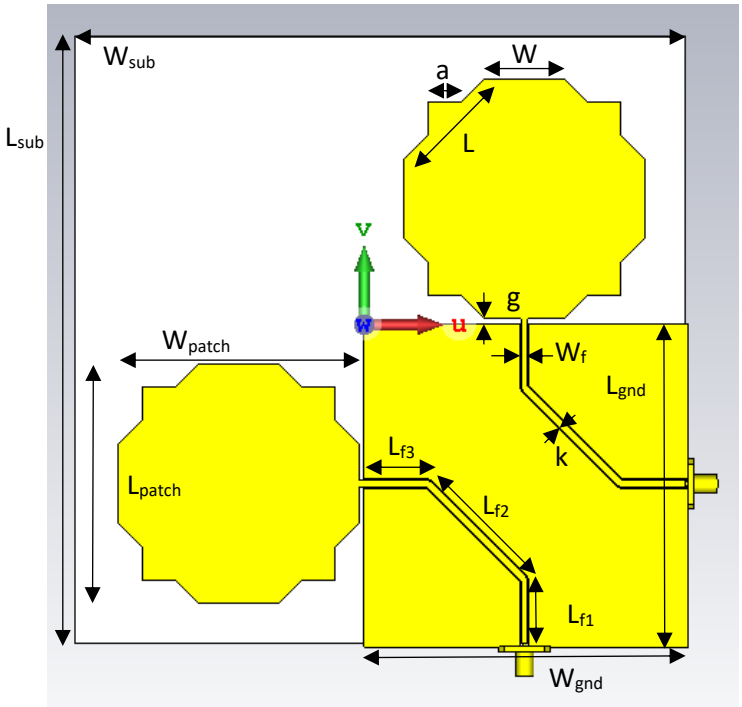

Figure 3.42 - Optimized printed monopole antenna

All the metal layers were designed and simulated using annealed cooper, a lossy material, of thickness 0.04375 mm. The feeding microstrip lines width, size and position are a very important part of the printed monopole antenna since they have a strong influence on the antenna impedance. All the materials used in the simulations will match the ones used in the prototypes.

3.5.2 Input Reflection Coefficient

Since this result will be compared with the experimental result of the fabricated prototype, the antenna was simulated with the best and most accurate solver accuracy and settings, in the same frequency range as the experimental S_{11} results, from 500 MHz to 5000 MHz.

Figure 3.43 shows the simulated magnitude of S parameters in dB. According to the presented results, the antenna verifies the criteria of S_{11}<-10 dB from 800 MHz to the upper limit of the simulated frequency band, having one peak of -8 dB within the band of interest around 750 MHz. In addition, the average S_{11} of the desired bandwidth of operation is -20 dB, which gives enough margin to guaranty any discrepancies between the simulated and experimental results.

This margin is important to guaranty an experimental S_{11} result below the reference point (of -10 dB), since despite CST being a great tool for simulation, the results do not model exactly the reality since the simulation is performed in a controlled environment using a specific solver and certain characteristics. Moreover, any deviation in the fabrication process (e.g. fabrication tolerances) from the designed antenna can cause differences in these results

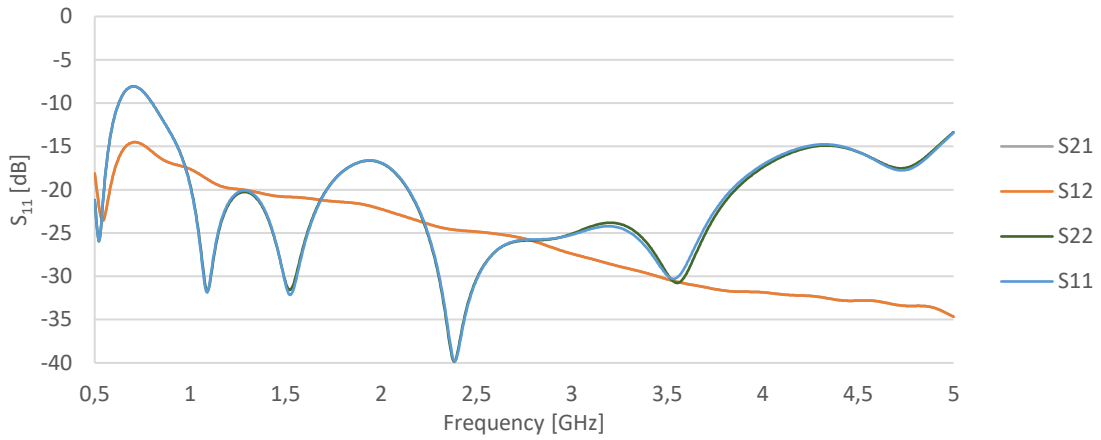

Figure 3.43 - S parameters of the optimized dual linear polarization monopole configuration

3.5.3 Realized Gain and Efficiency

The simulated antenna realized gain and radiation efficiency results are presented in figures 3.44 and 3.45 respectively. For this simulation, a sweep frequency from 500 MHz to 5 GHz with a step size of 5 MHz was used.

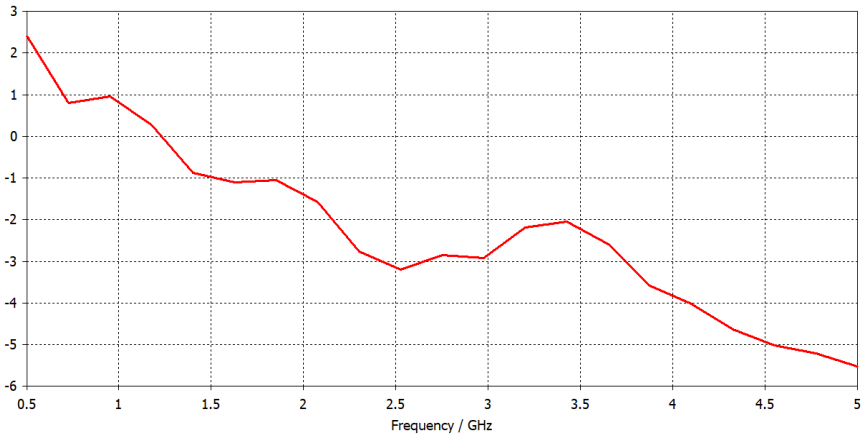

Figure 3.44 - Simulated realized gain of the optimized antenna

Figure 3.44 shows an average gain of -2.2 dB from 500 MHz to 5 GHz. The negative average gain is expected since the presence of the absorber foam introduces losses. As expected the gain decreases as the frequency increases.

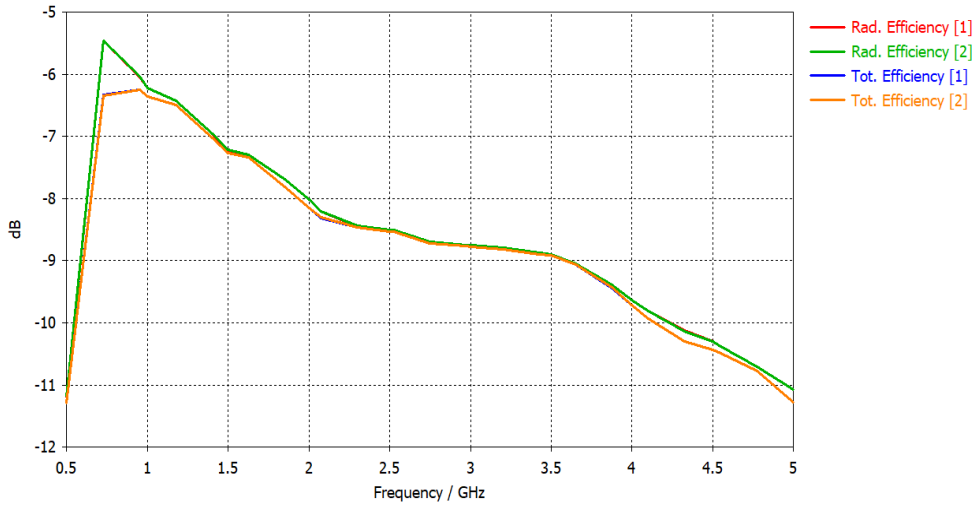

Figure 3.45 – Simulated efficiency of the optimized antenna

3.5.4 Radiation Patterns

This section presents the simulated results related to the antenna`s overall performance. First, a representation of the antenna, with its system of coordinates is presented. It shows how Phi and Theta angles are defined for the antenna which is very important since every radiation pattern in this section will use these coordinates.

3.5.4.1 System of coordinates

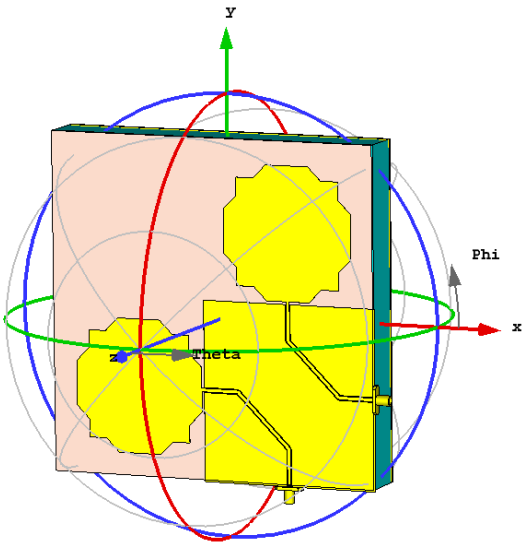

Figure 3.46 - Printed monopoles antenna in the system of coordinates

3.5.4.2 Polar Plots

Below are presented the radiations pattern cuts for the main planes for specific frequencies of f = (700, 1000, 1500, 2000, 2500, 3000, 3500) MHz, which were carefully chosen to show how the radiated fields change with frequency.

As expected, the presence of the absorber foam attenuates the back radiation. This can be verified by analysing the cuts were phi is 0° and 90° for theta variation of [0°, 180°]. In this specific cases, the back radiation takes values around -10 dB while the front radiation takes values around 5 dB.

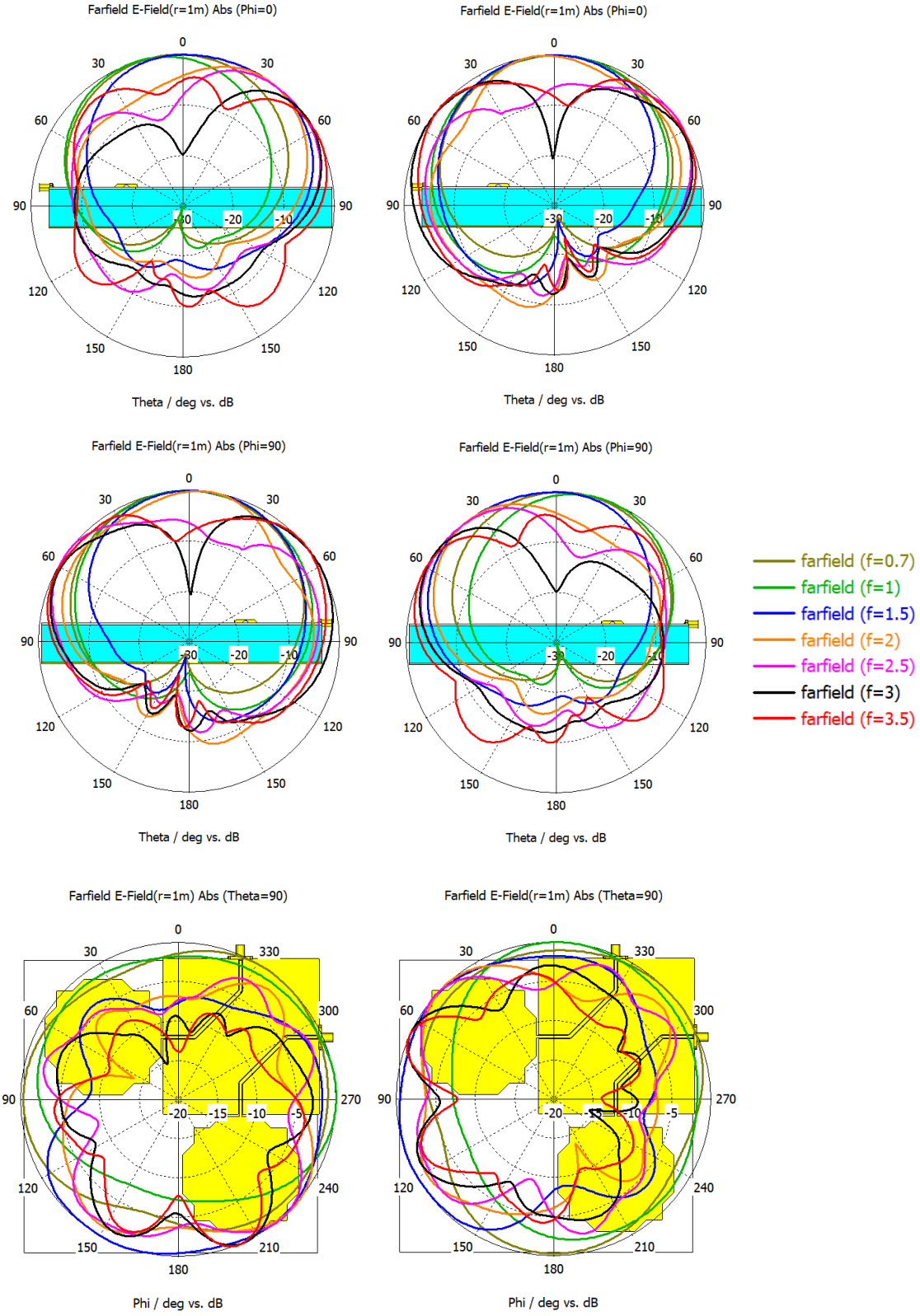

Figure 3.47 - Radiation patterns for different frequencies

Figure 3.47 represents the radiation patterns for different frequencies between 700 MHz and 3500 MHz. The left column refers to the power supply through port 1 and the right column refers to the power supply through port 2. It is possible to observe in the phi=0° and phi=90° cuts for the two ports, a strong attenuation in the radiation pattern caused by the absorber foam.

3.5.4.3 Current Density

Below (figure 3.48) is a representation of how the current travels along the structure for different frequencies for port 1 (port 2 is loaded with 50 Ω). The results are presented for port 1 only since they are symmetrical to port 2.

When the frequency is minimum the current is concentrated mostly around both microstrips, while as the frequency increases the current is much more intense in the active port and is distributed along the CPW feed and octagonal patch.

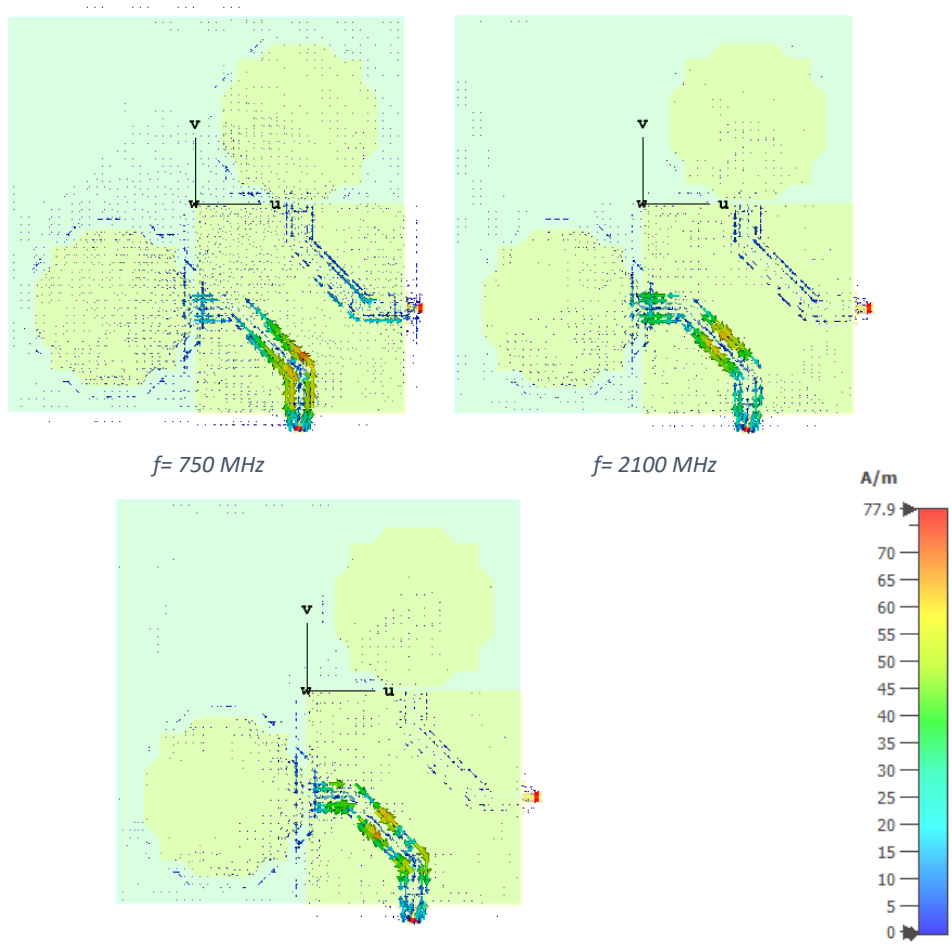

f= 750 MHz

f= 2100 MHz

f= 3500 MHz

Figure 3.48 - Current density

3.5.4.4 3D realized Gain

Below (figure 3.49) is a 3D far field representation of the antenna realized gain at some frequency points of the frequency range of interest. The left column refers to the power supply through port 1 and the right column refers to the power supply through port 2. It is possible to observe a strong attenuation in the radiation pattern caused by the absorber foam.

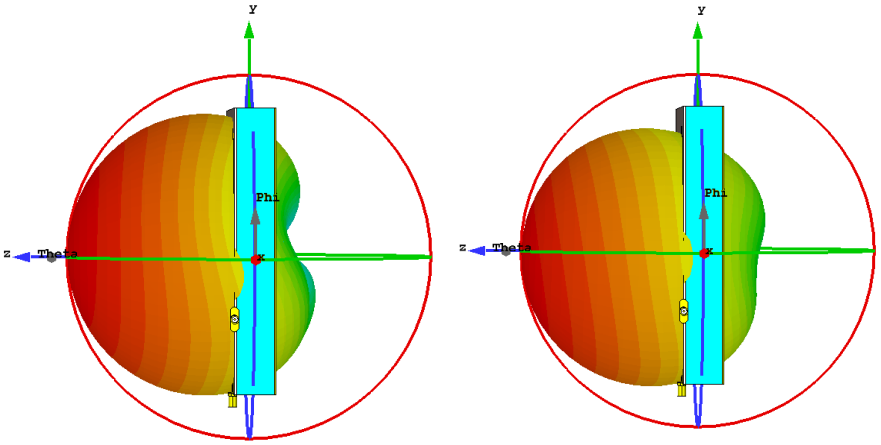

f= 750 MHz

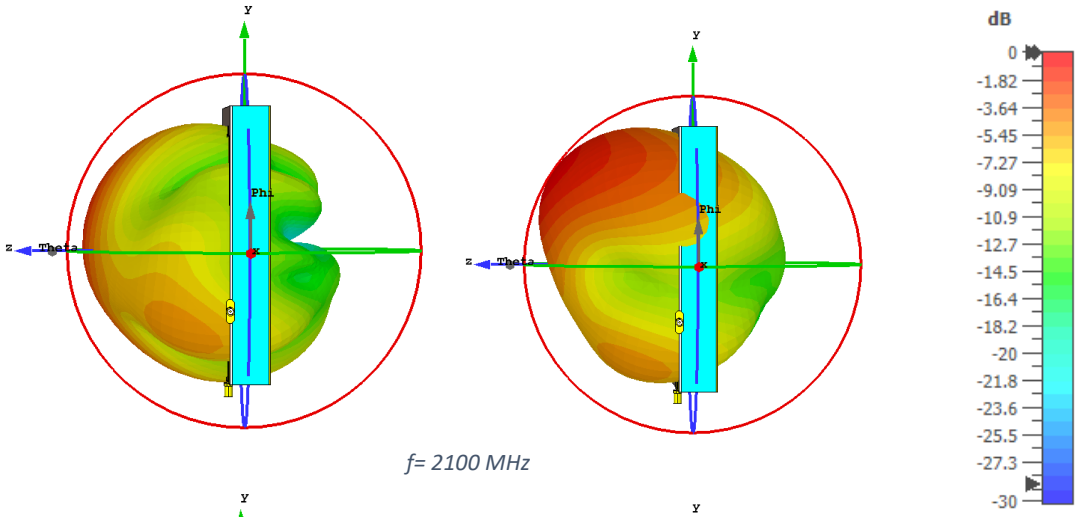

f= 2100 MHz

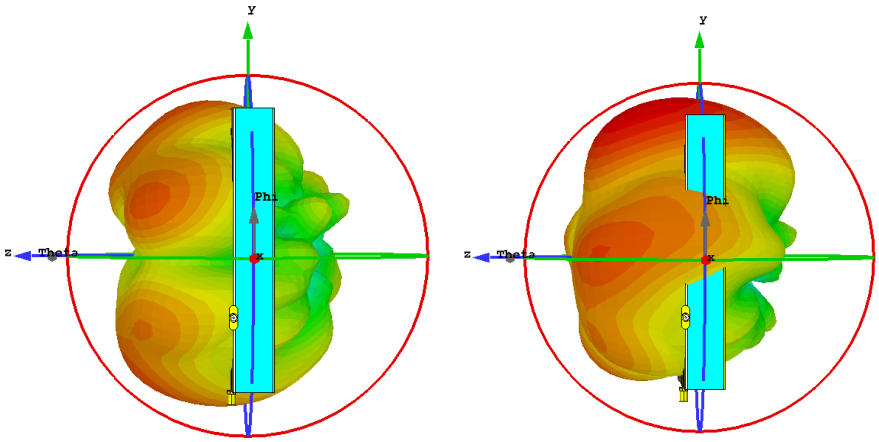

f= 3500 MHz

Figure 3.49 - Realized gain

4. Antenna Fabrication and Test

This chapter explains how the antenna prototypes were manufactured in the IT/IST laboratory of printed circuits and how they were measured.

4.1 Photolithography Fabrication Process

The fabrication process used to manufacture the printed monopole in FR4 was the photolithography technique. It started by producing the masks of the circuit, represented in figure 4.1, which is a 2D section of the circuit where the copper (metal part) is represented in black. The masks are then used to print a transparent film of the simulated circuit at a chosen scale. To produce the masks, the author used a script to import a DXF file from CST to further mark the metal parts and then export to PDF, with the defined scale size, for them to be copied into the transparent film.

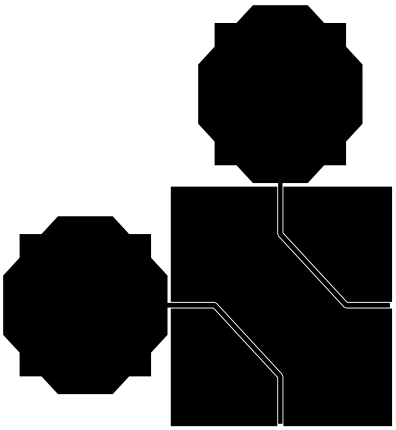

Figure 4.1 - Printed monopole mask

After the mask is printed and properly aligned, the manufacturing process starts by cutting the dielectric substrate into a square shape and cleaning its surface of any grease or impurities. To apply the pre-treatment, the PCB board is scrubbed with a brush, detergent and water in order to be completely clean.

Once the PCB board is completely clean and dry, the second step was to cover its entire surface with a photoresist solution. This must be done in a room with special light and in a clean, dust-free atmosphere. After applying the photoresist spray, the PCB board was left to dry in the dark for 24 hours. To speed up the process, the author used a thermostatically controlled oven.

Figure 4.2 - Applying the photoresist solution Positiv 20

The step 3 is very important, as this is where all preparations are made before the unwanted copper areas are exposed to the UV-light. To do that, a positive original transparent film material opaque to light, representing the circuit drawing, was prepared and inserted on top of the PCB board.

Further, in step 4, the circuit is exposed to the UV-light. The time of exposure depends on both the thickness of the coating and on the intensity of the light source.

Figure 4.3 - UV machine

After that, the next steps 5 and 6, were to remove the film mask and to submit the circuit board to caustic soda and water in dark conditions for the detailed pattern of copper start to appear.

Finally, in the last steps, 7 and 8, is the cleaning process, were the board was immersed in the etchant composed by a mixture of hydrochloric, hydrogenperoxide and water to etch the copper plates and then the softened resist was washed away using an alkaline solution (acetone or another solvent available). At the end, a Soldering Varnish SK 10 was applied to protect the circuit form oxidation and to help the soldering process. The steps of the process are described in figure 4.4.

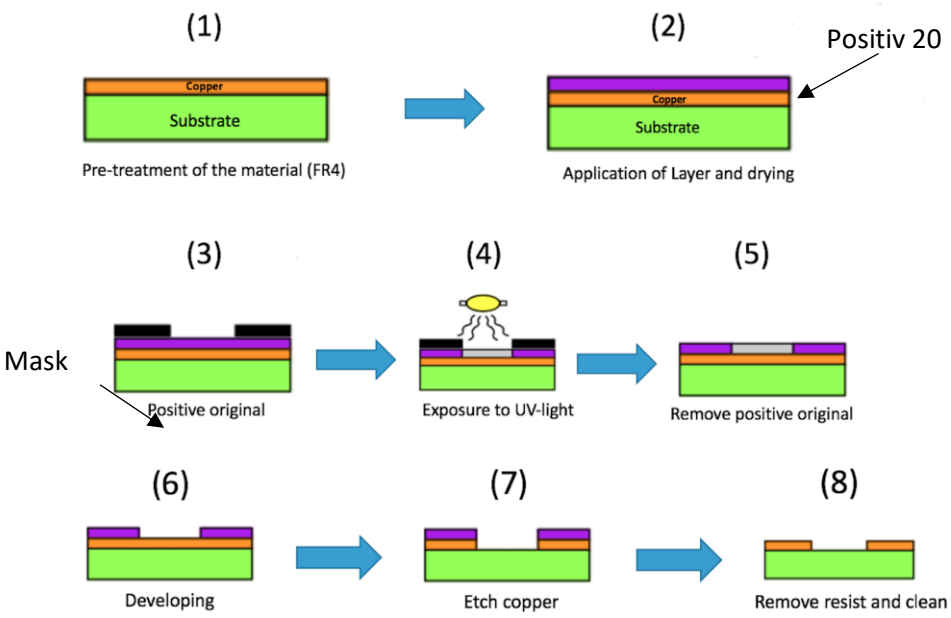

Figure 4.4 - Photolithography process [44]

The first prototype produced was the single octagonal patch monopole with cooplanar ground plane configuration. Followed by the second prototype, the dual linear polarization configuration of the previous one shown in figure 4.5.

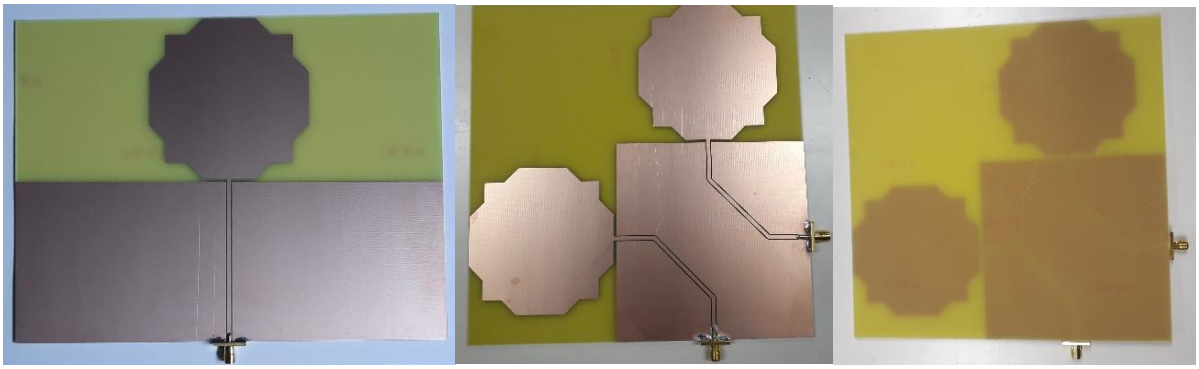

Figure 4.5 - First and second prototypes

4.2 Antenna Test Procedure

4.2.1 S - Parameters Measurement

In order to measure the S-parameters of the prototypes, an Agilent Technologies E5071C vector network analyser (VNA) from IT/IST was used. The antenna was connected through the SMA connectors and to compensate internal and external errors an electronic calibration procedure was made at the ports. The stimulus signal is injected into the DUT and the VNA measures both the signal that's reflected from the input side, as well as the signal that passes through to the output side of the DUT. The VNA receivers measure the resulting signals and compare them to the known stimulus signal (figure 4.6). The measured results are then processed by either an internal or external PC and sent to a display. Additional information of how a VNA works can be found in [43].

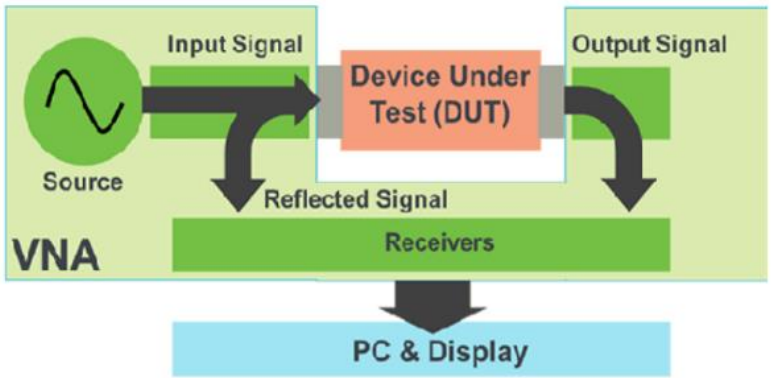

Figure 4.6 - VNA measurements scheme

The experimental reflection coefficient was measured from 200 MHz to 5000 MHz using an interval of 1 MHz for both prototype antennas.

During the experimental measurement of the dual linear polarization antenna, three configurations were tested, the antenna without absorber foam and cooper shield, the antenna with cooper shield without the absorber foam and finally the antenna with both absorber foam and copper shield. For all experiments, a piece of white foam material was placed under the antenna to minimize the electromagnetic radiation reflected from the ground (figure 4.7).

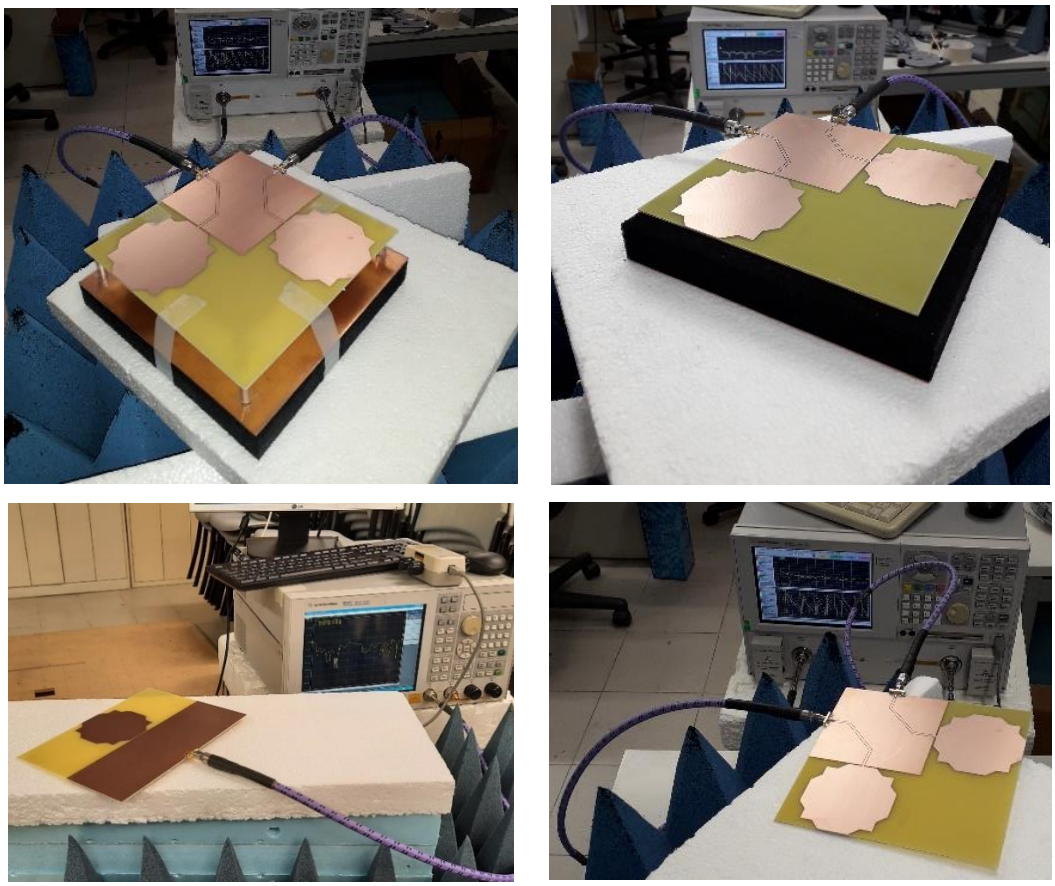

Figure 4.7 – S-parameters measurement setup for the two prototypes

4.2.2 Radiation Pattern Measurement

Measuring the radiation pattern of an antenna is very important, since it shows its far-field radiation properties. In this specific case due to the dual linear polarization configuration of the antenna, the radiation pattern is determined in the far region for constant frequency and distance, with the antenna performance described in terms of vertical and horizontal plane cuts.

Inside the IT/IST far-field anechoic chamber, the walls are covered with pyramidal shape foam that absorbs the electromagnetic radiation, it has length of 8.5 m, width of 4.6 m and height of 3.6 m. There are two mounting places, one for the receive antenna and the other for the transmit antenna, both with polarization positioners allowing measurements in the horizontal and vertical plane. A scheme of the IT/IST anechoic chamber system and equipment associated is presented in figure 4.8.

N5183A: Agilent MXG Microwave Analog Signal Generator, 100 kHz to 20 GHz; **N5264A**: Agilent PNA-X Measurement Receiver for Antenna Test; **N5280A**: Agilent Frequency Down Converter; **AL-4906**: Orbit/FR Positioner Control; **AL-4146-2**: Orbit/FR Local Control Unit; **AL760**: Orbit/FR Azimuth Positioner; **AL560**: Orbit/FR DUT Polarization Positioner; **AL360**: Orbit/FR Probe Positioner.

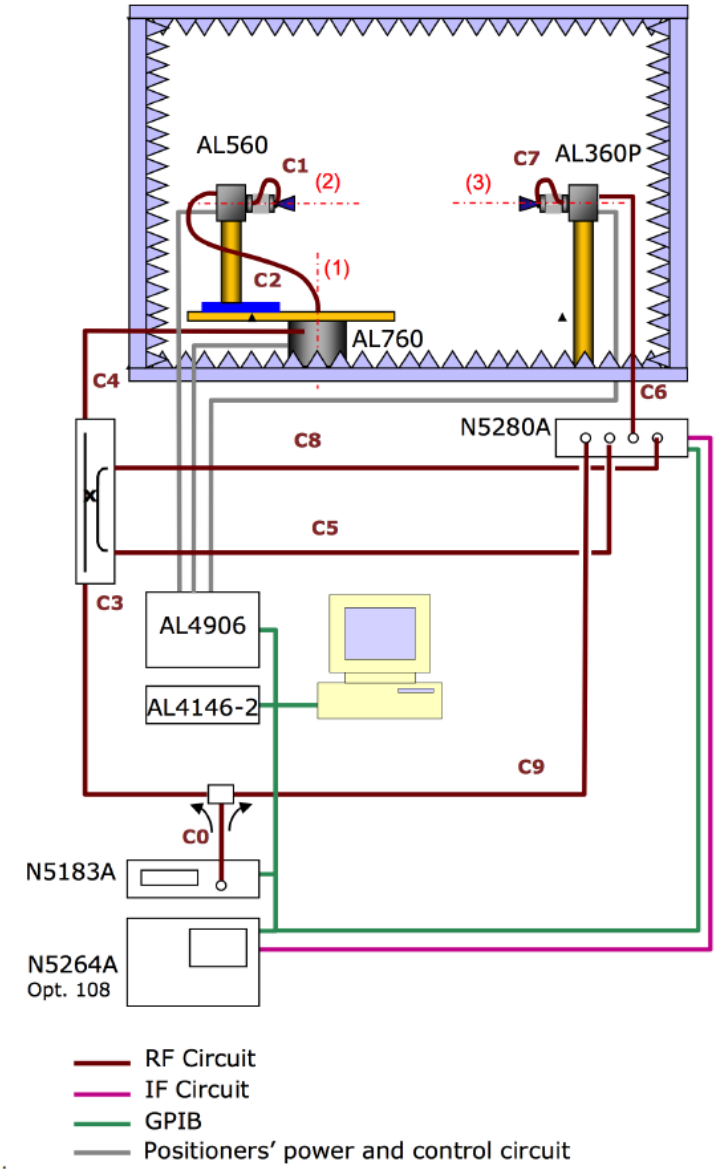

Figure 4.8 - IT/IST anechoic chamber measurements scheme [44]

4.2.2 Gain Measurement

In order to measure the gain of an antenna, there are two main methods, absolute gain and gain transfer techniques. The absolute gain method does not require previous information of the transmitting or receiving antenna gain. If the transmitting antenna is identical to the receiving antenna, one measurement and use of the Friis transmission formula is sufficient to determine the gain [11].

Suppose the transmitting antenna is separated from the receiving antenna at a distance r. Here, P_t and P_r represent the transmitted and received power respectively while A_{et} and A_{er} are the effective apertures of transmitting and receiving antennas.

As the two antennas are identical, therefore,

$$A_{et} = A_{er} = \frac{G_0\lambda^2}{4\pi} \tag{4.1}$$

By Friis's transmission equation,

$$\frac{P_r}{P_t} = \left(\frac{A_{et}A_{er}}{\lambda^2 r^2}\right) = \left(\frac{G_0\lambda^2}{4\pi}\right)\left(\frac{G_0\lambda^2}{4\pi}\right)\frac{1}{\lambda^2 r^2} \tag{4.2}$$

Thus,

$$\frac{P_r}{P_t} = \left(\frac{G_0\lambda}{4\pi r}\right)^2 \Leftrightarrow \sqrt{\frac{P_r}{P_t}} = \frac{G_0\lambda}{4\pi r} \Leftrightarrow G_0 = \frac{4\pi r}{\lambda}\sqrt{\frac{P_r}{P_t}} \tag{4.3}$$

From the above equation, it is clear that the power transmitted by the transmitter and received by the receiver is measured, then for the known value of separation distance and wavelength, the gain of each antenna can be determined.

The other method is the gain-transfer method and must be used in parallel with standard gain antennas to determine the absolute gain of the antenna under test (AUT). Each technique has its own unique advantages and disadvantages in terms of accuracy, cost and measurement time.

The gain-transfer method provides an accurate and simple solution for measuring the antenna gain. This method consists in performing two measurements of received power. It uses a standard antenna with its known characteristics, such as the reflection coefficient and gain to determine the gain of an AUT with the equation bellow.

$$G_{AUT} = \frac{P_r^{AUT} G_{SGH}}{P_r^{SGH}(1-|\tau_t|^2_{AUT})}\left(\frac{d_{AUT}}{d_{SGH}}\right)^2 \tag{4.4}$$

The parameters P_r^{AUT}, G_{AUT} and $|\tau_t|^2_{AUT}$ represent the received power, unknown gain, the reflection coefficient regarding the AUT while d_{AUT} represents the distance between the AUT and the transmitting antenna. Further, d_{SGH}, P_r^{SGH} and G_{SGH} are the distance between the standard gain antenna and the transmitting antenna, the received power associated with the standard gain antenna and standard antenna gain respectively.

4.3 Experimental Results

4.3.1 S - Parameters

Figure 4.9 contains the measured and the simulated reflection coefficient results of the first prototype, the printed octagonal patch monopole with cooplanar ground plane.

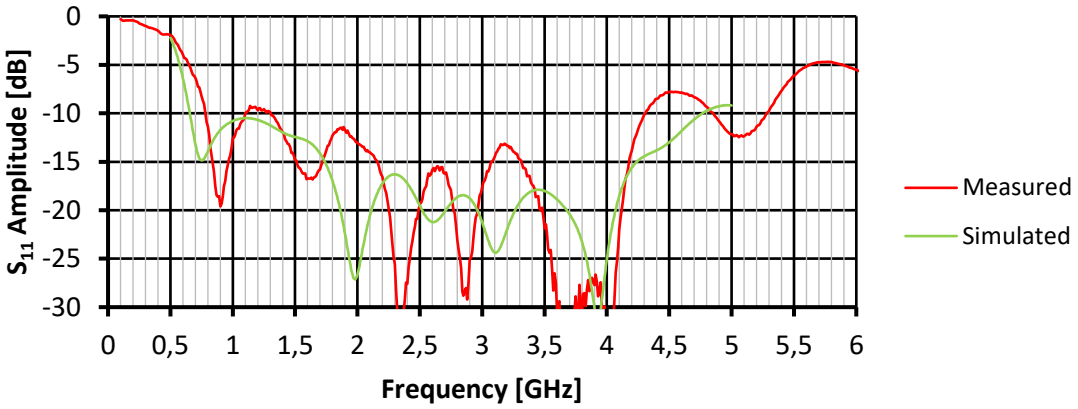

Figure 4.9 - Simulated vs measured S_{11} results of the single octagonal patch monopole

The simulated and measured results have good agreement and fulfill the requirement of S_{11} < -10 dB for almost the entire working bandwidth. It is observed in the measured results that the minimum frequency for the condition S_{11} < -10 dB is higher and there is also a peak slightly above -10 dB around 1.2 MHz.

Regarding the second prototype, three different configurations were tested. The first configuration is the simplest, the antenna is tested without the reflector and the absorber foam in order to validate the simulated results. In the second configuration, the antenna is tested at a distance of 2.5 cm from a reflecting plane without absorber in order to verify its interference. Finally, in the third configuration, the antenna is measured with the selected absorber foam and the reflecting plane.

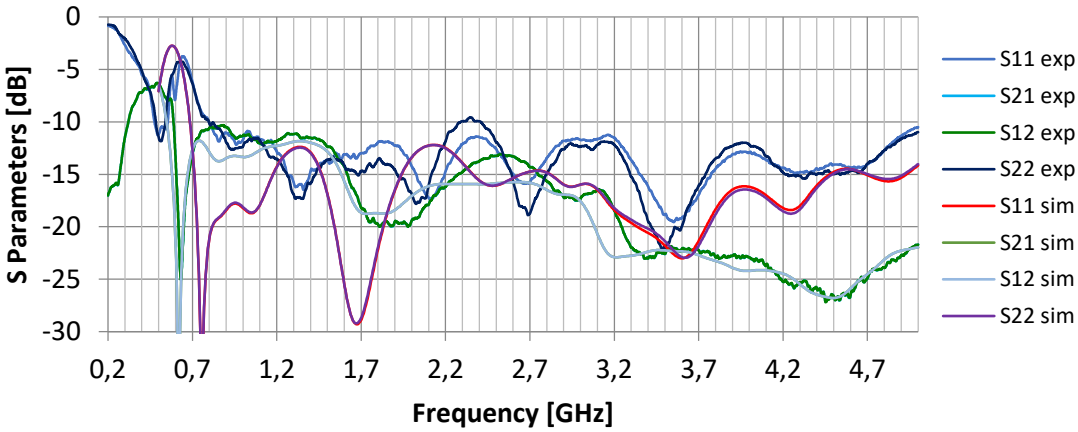

Figure 4.10 - Simulated vs measured S-parameters results of configuration 1

Comparison of simulation and experimental S-parameters results for configuration 1 are shown in figure 4.10. The measured reflection coefficient S_{11} is below -10 dB from 800 MHz to the end of the working bandwidth while the simulated reflection coefficient in the CST presents lower values in the whole band, as expected.

The difference between the simulated and the experimental results can be caused by the simulator itself (accuracy and mesh used), and by the test environment. In addition, there are always factors that happen during the manufacturing process that can cause these little discrepancies such as the way the antenna was cut, the

soldering and connection of the cable that introduce losses and even the materials used, specially FR4 which is not a high quality substrate.

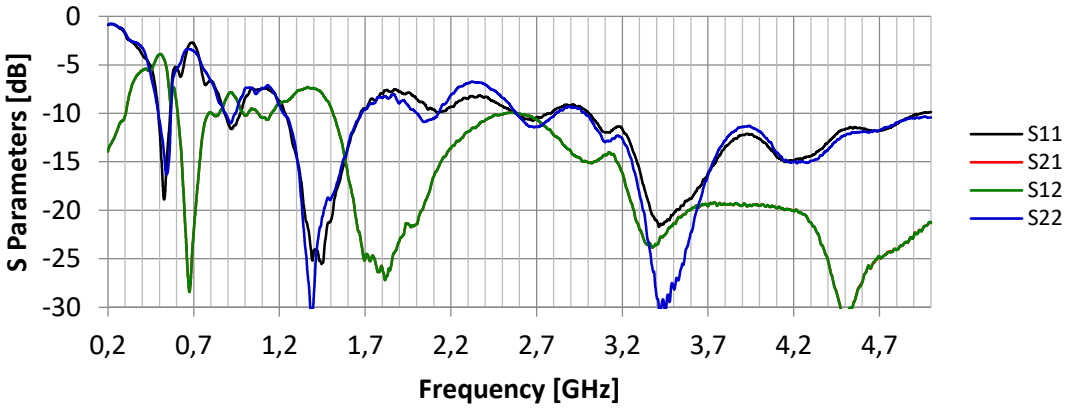

Figure 4.11 - Measured S-parameters results of configuration 2

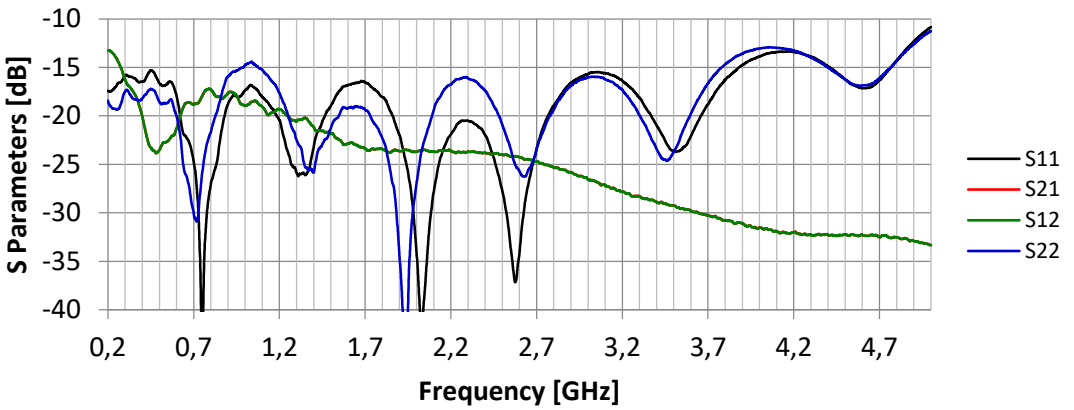

Figure 4.12 - Measured S-parameters results of configuration 3

Figure 4.11 shows the very negative impact of the reflecting (and shielding) plane in the antenna performance. This negative interference justifies the use of the absorber foam to mitigate it. The absorber foam causes the reflection coefficient to drop below -15 dB across the entire measured bandwidth improving the antenna performance (figure 4.12). It is therefore confirmed experimentally the expected effect of the absorber foam.

4.3.2 Radiation Pattern and Gain Measurement

Due to the restrictions imposed by the coronavirus disease (COVID-19) pandemic, it was not possible to measure radiation pattern and gain.

5. System of Antennas

5.1 Introduction

After the design, optimization and measurement of the printed monopole antenna with absorber foam developed in the previous 3 chapters, a new configuration with spatial diversity is considered. The main objective of this system of antennas is to measure the incident radiation on its user and at the same time protect him from that same radiation. To measure the incident radiation, five antennas identical to the one developed before are used, placed in strategic positions in order to obtain spatial diversity.

5.2 System Characteristics

The antenna system, shown in figure 5.1, is composed of five identical printed monopole antennas developed in the previous chapters. To simulate the user's body, the author used a hollow copper block covered with Eccosorb AN-75 (middle layer) of varying thickness between 1 mm and 0,5 mm shown in figure 5.2.

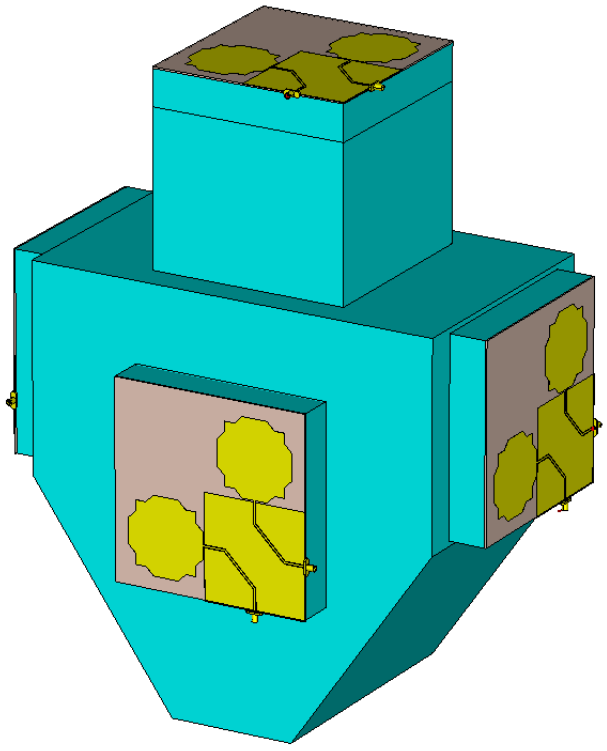

Figure 5.1 - System of antennas - perspective

The antenna designed in chapter 3 consists of two octagonal monopoles, one for horizontal polarization and the other for vertical polarization. In order to obtain the results of incident radiation around the user, the antennas were placed on the chest, back, shoulders and head, achieving spatial diversity. All the dimensions of

the antenna system are shown in figure 5.2, where different views of the antennas integrated in the user model are also presented.

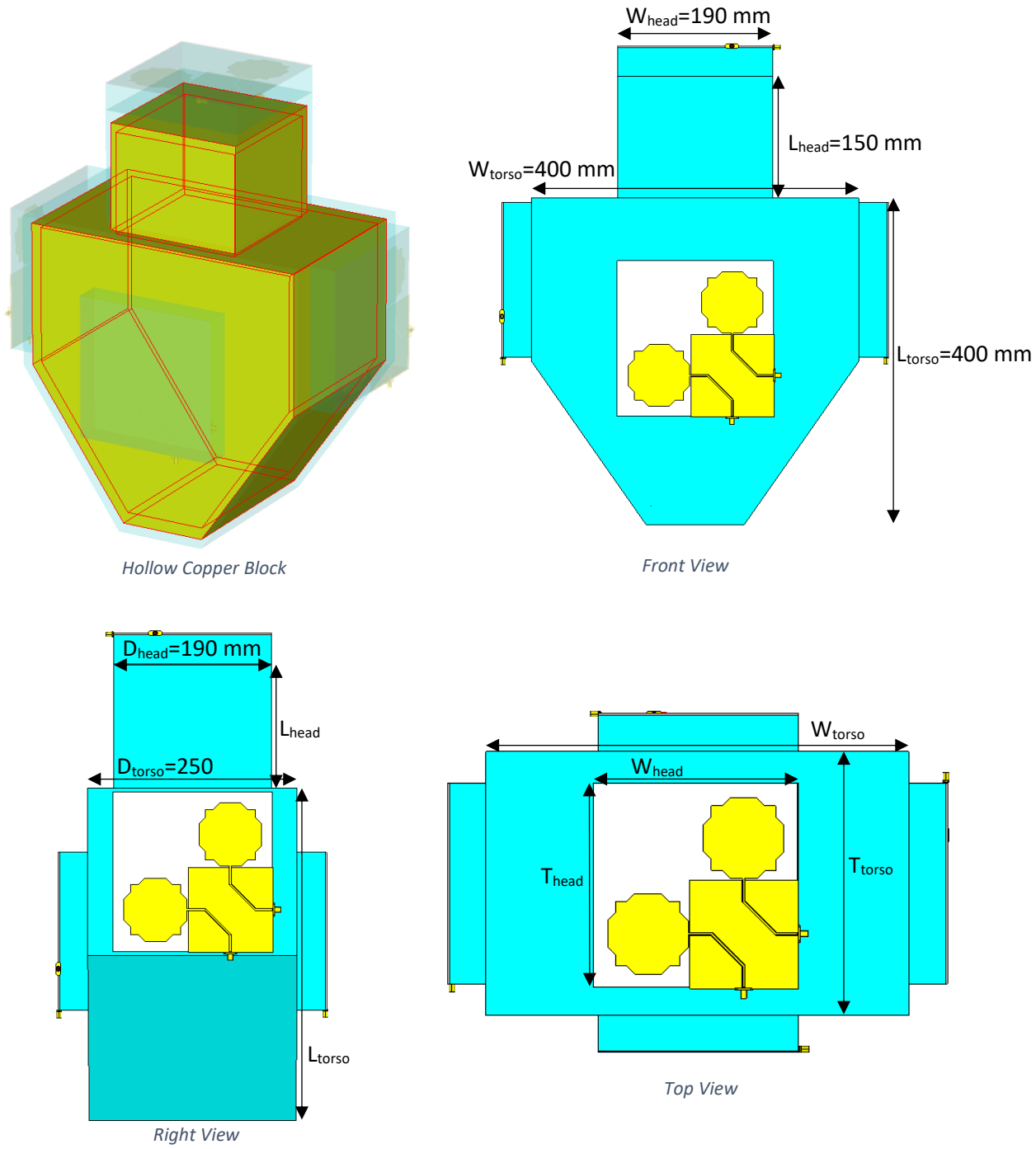

Hollow Copper Block

Front View

Right View

Top View

Figure 5.2 - System of antennas

A simple model of the upper part of the user body has been chosen. The head is represented by a parallelepiped with a width and depth of 190 mm but with a height of 150 mm and the chest is represented by a cutted parallelepiped with 400 mm in height and width and 250 mm of depth.

The reflection coefficients for each port were simulated from 700 MHz to 3,5 GHz to verify the impedance matching. Once well matched, the system is no longer fed by the ports but rather excited by a plane

wave of 1 V/m from various directions and polarizations. The system was simulated for a phi and theta variation with a range of [0°, 360°[with 45° intervals.

Using voltage monitors at the SMA conector of each monopole it is expected to observe a higher voltage at the monopoles that are printed on a plane perpendicular to the direction of the incident wave and aligned with the polarization of the incident wave.

A 50 Ω load has been inserted between the inner and outer conductors of the SMA connectors. Therefore, the voltage monitors provide the voltage created on these matched 50 Ω resistance loads (figure 5.3).

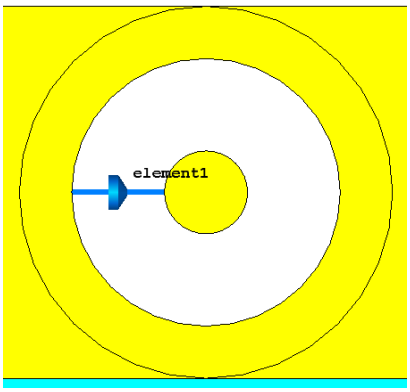

Figure 5.3 - 50 Ω load inserted between the inner and outer conductor of the SMA connector

5.3 Simulated Results

The port numbers were chosen as follows: ports with an odd number correspond to the horizontally polarized monopoles. Even-numbered ports correspond to vertically polarized monopoles, as shown in figure 5.4. The monopole on the chest are numbered 1 and 2, on the back 3 and 4, on the right shoulder by 5 and 6, on the left shoulder by 7 and 8, and finally on the head by 9 and 10.

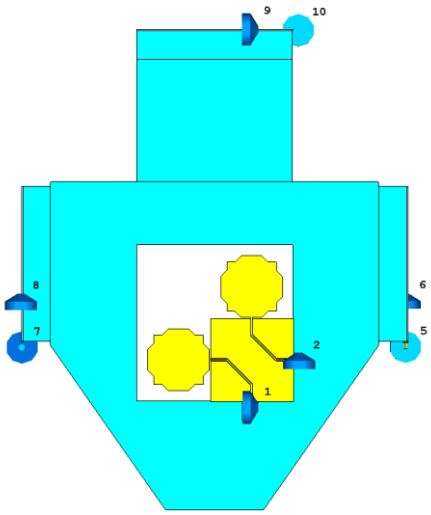

Figure 5.4 - System of antennas - ports numbers

As explained before, the antennas were simulated using waveguide ports exciting each monopole with the best and most accurate solver accuracy and settings. Figure 5.5 shows the simulated magnitude of the S parameters in dB. According to the presented results, the system verifies the criteria of S < -10 dB from 700 to 3500 MHz for all monopoles except for monopoles 4, 6 and 7. In relation to monopole fed by port 4 there is a maximum of –9,2 dB in the reflection coefficient between 2,51 GHz and 2,87 GHz. In relation to monopoles fed by the ports 6 and 7, the reflection coefficient is slightly above -10 dB from 2,98 GHz and 3,164 GHz, respectively.

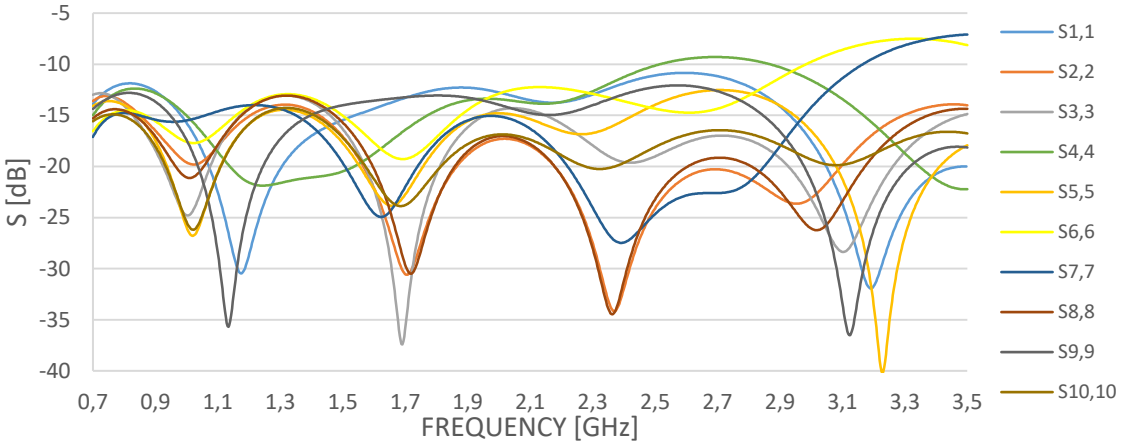

Figure 5.5 - System of antennas – S-parameters

Having the monopoles adequately matched, the system is powered by a plane wave with 1 V/m. Three different polarizations of the incident wave were simulated, horizontal, vertical and linear polarization at 45 degrees for a scan from 0 to 315 degrees of the angles Theta and Phi. They are represented in figure 5.7. A representation of the system, with its coordinates is presented in figure 5.6. It shows how Phi and Theta angles are defined.

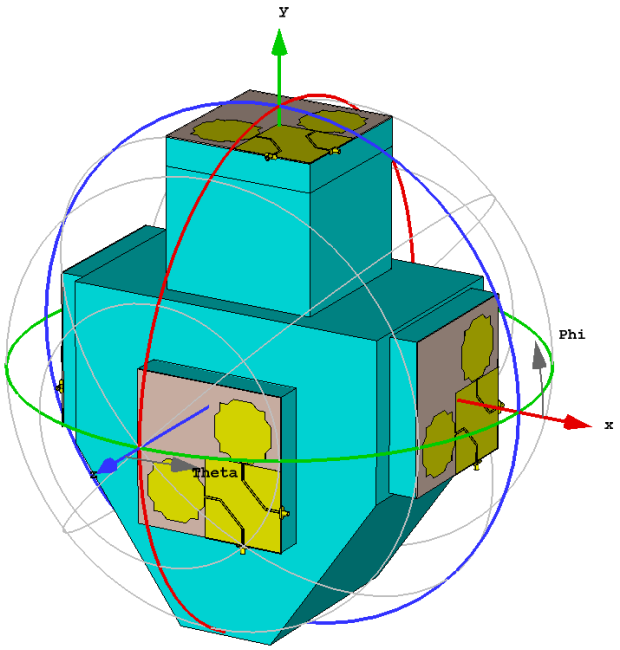

Figure 5.6 - System of coordinates - perspective view

5.3.1 Theta Scan (Phi = 0°)

Figure 5.7 contains the antenna system powered by a plane wave with vertical polarization. For the case of the theta sweep from 0 to 315 degrees, only the first three results theta = 0, 45 and 90 are represented for the three types of polarizations since due to (almost) symmetry they provide enough information regarding the voltage at the monopole terminals with the polarization and incident wave direction. The results corresponding to the remaining angles of incidence (135°, 180°, 225°, 270° and 315°) are presented in appendix B.

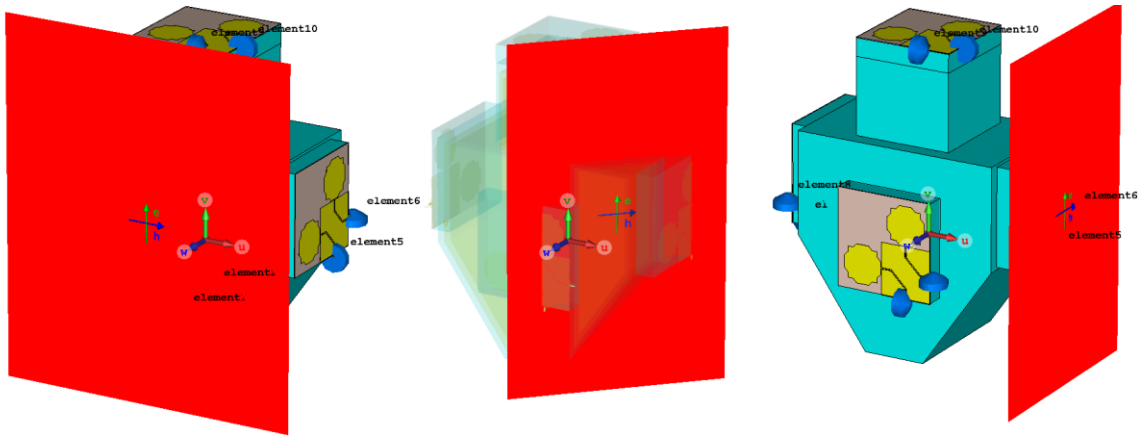

Figure 5.7 - System of antennas for theta scan (0°, 45°, 90°) and phi = 0°

In the case of the incident wave with vertical polarization, the voltage induced at each port, as a function of frequency, is shown in figures 5.8, 5.9 and 5.10.

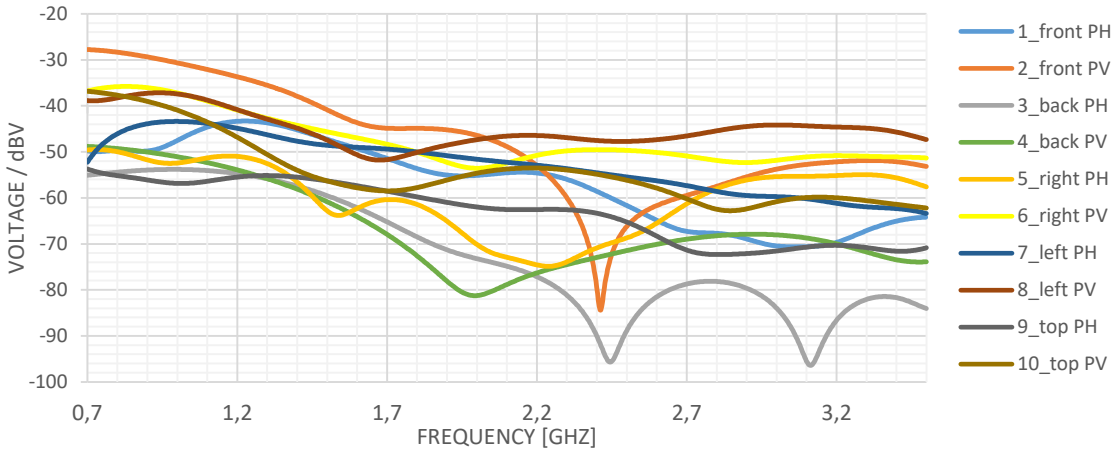

Figure 5.8 – Voltage induced at each port for Θ=0° and vertical polarization

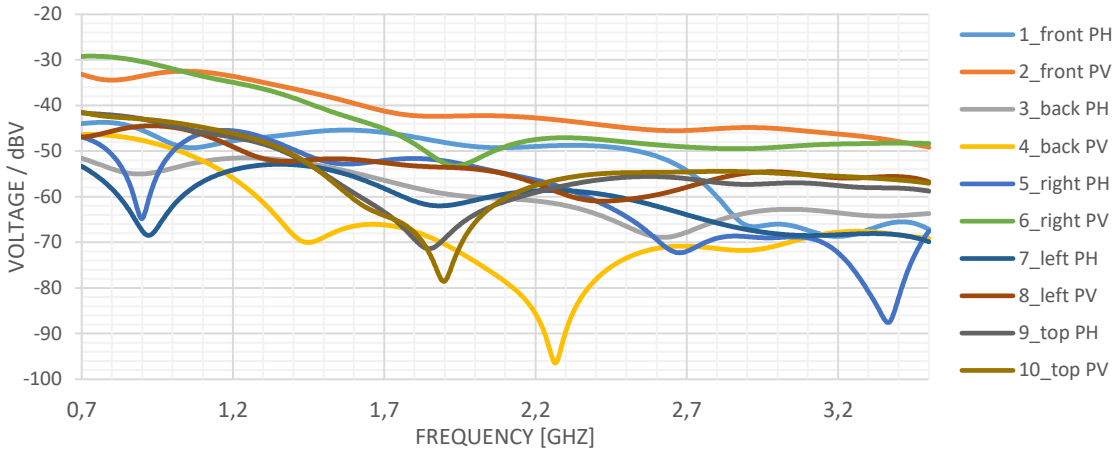

Figure 5.9 - Voltage induced at each port for Θ=45° and vertical polarization

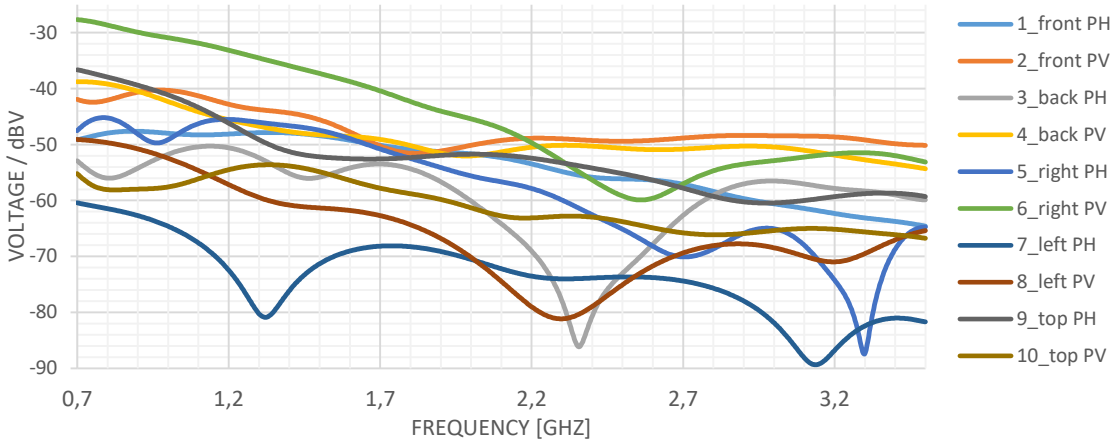

Figure 5.10 - Voltage induced at each port for Θ=90° and vertical polarization

In the case of the incident wave with horizontal polarization the results are shown in figures 5.11, 5.12 and 5.13.

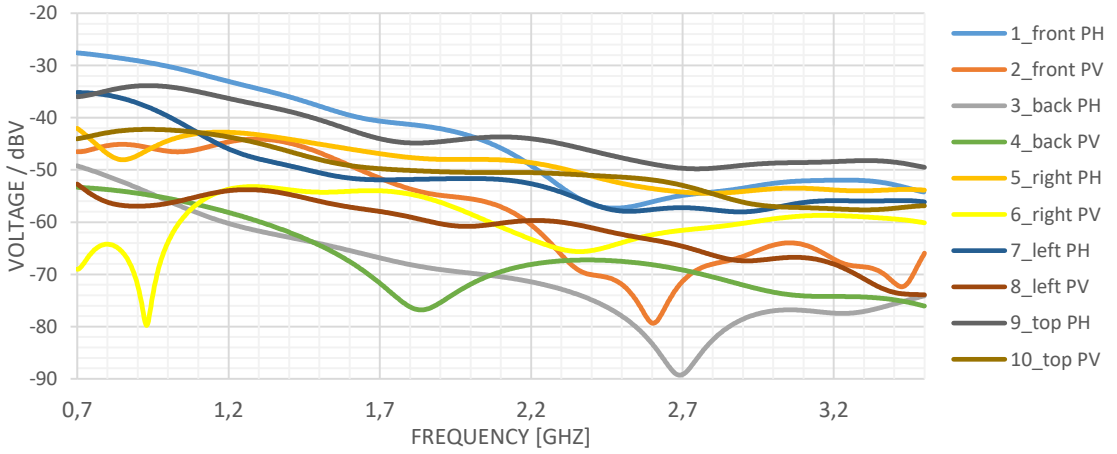

Figure 5.11 - Voltage induced at each port for Θ=0° and horizontal polarization

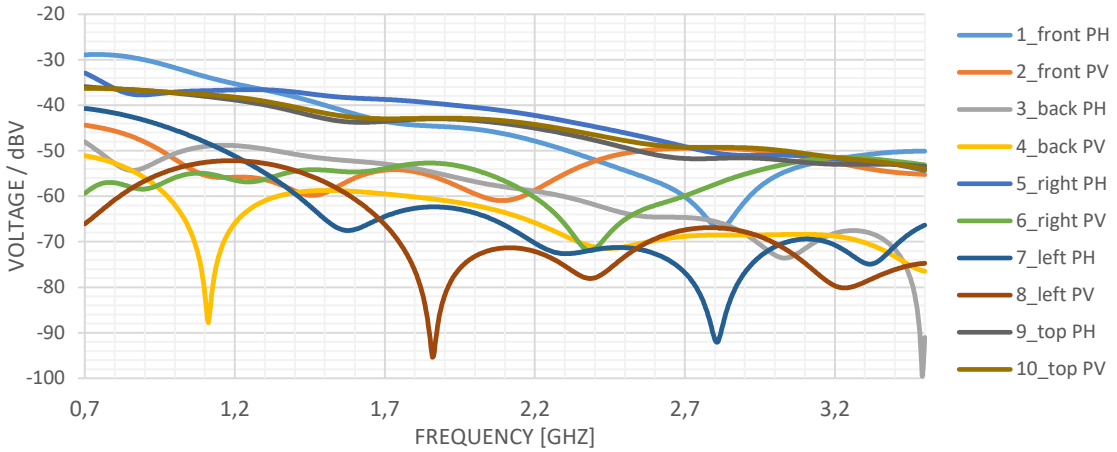

Figure 5.12 - Voltage induced at each port for Θ=45° and horizontal polarization

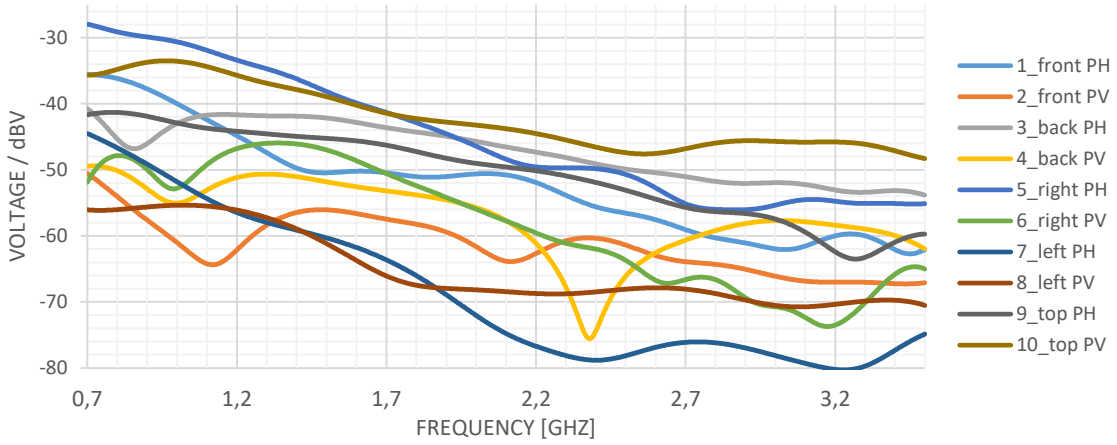

Figure 5.13 - Voltage induced at each port for Θ=90° and horizontal polarization

Finally, in the case of the incident wave with linear polarization at 45 degrees the results are shown in figures 5.14, 5.15 and 5.16.

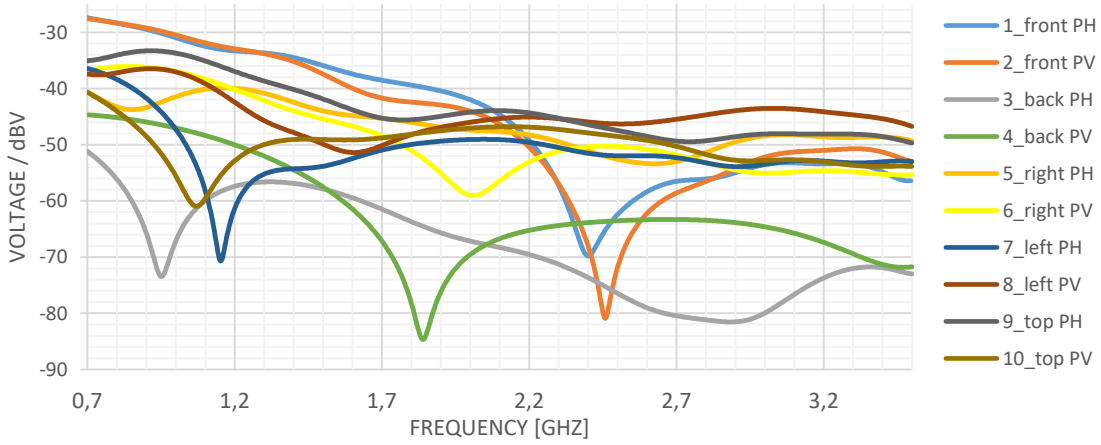

Figure 5.14 - Voltage induced at each port for Θ=0° and 45° linear polarization

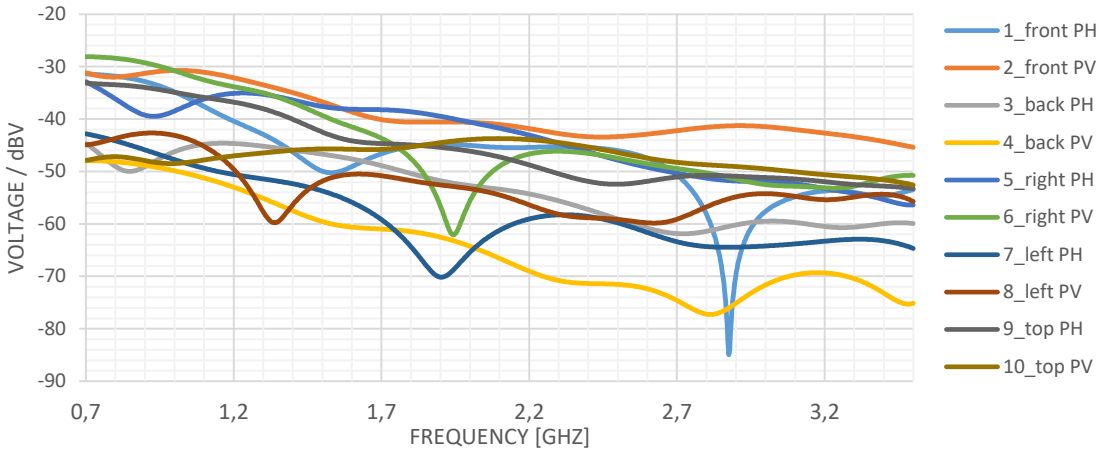

Figure 5.15 - Voltage induced at each port for Θ=45° and 45° linear polarization

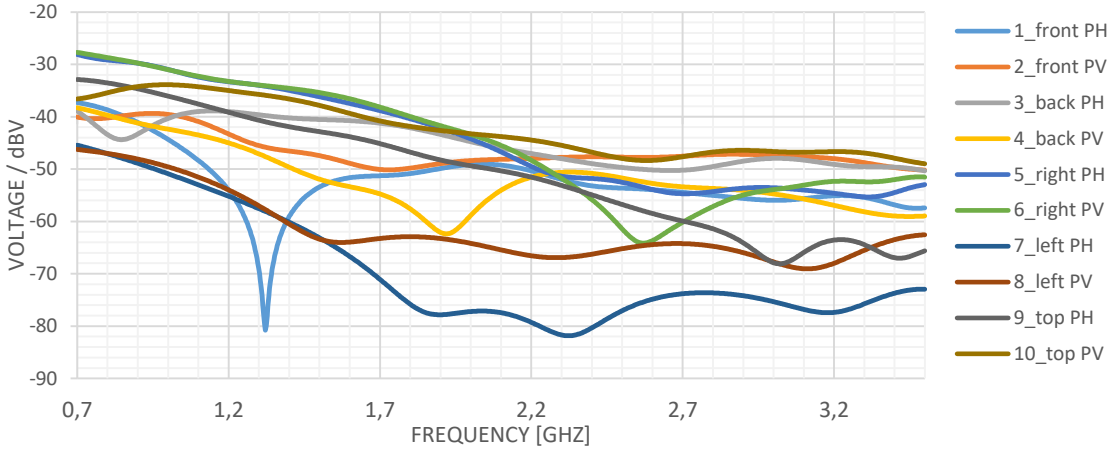

Figure 5.16 - Voltage induced at each port for Θ=90° and 45° linear polarization

From the results presented in the figures 5.8 to 5.16 it can be concluded that the monopoles that have higher voltages at their terminals are the ones that are directly in front of the incident wave and that have the configuration of polarization of the incident wave. For example, when the incident wave has a vertical polarization, and Theta=0, the monopoles that present a higher voltage are the front, left, right and top with the vertical polarization configuration. On the other hand, if Theta=45 the monopoles that present higher voltages at their terminals are the front, right and top with the vertical polarization configuration as well. The same behaviour of the system is observed for the other values of Theta and for the case of the incident wave having horizontal polarization.

For the case where the incident wave has linear polarization at 45 degrees, it is observed that the monopoles that present higher voltages at their terminals are the ones that are directly in front of the incident wave. For example, when the incident wave has linear polarization at 45 degrees, and Theta=90°, the monopoles that present higher voltages are the right, back, front and top, regardless of their polarization settings.

In all presented voltage results, there is a decrease as frequency increases caused by the increase of the absorber foam losses.

5.3.2 Phi Scan (Theta = 90°)

For the case of the phi sweep from 0 to 315 degrees, only the first three results phi = 0°, 45° and 90° are represented for the three types of polarizations since again due to symmetry, it provides enough information regarding the voltage at the monopoles terminals with the polarization and incident wave direction. The results corresponding to the remaining angles of incidence (135°, 180°, 225°, 270° and 315°) are presented in appendix C.

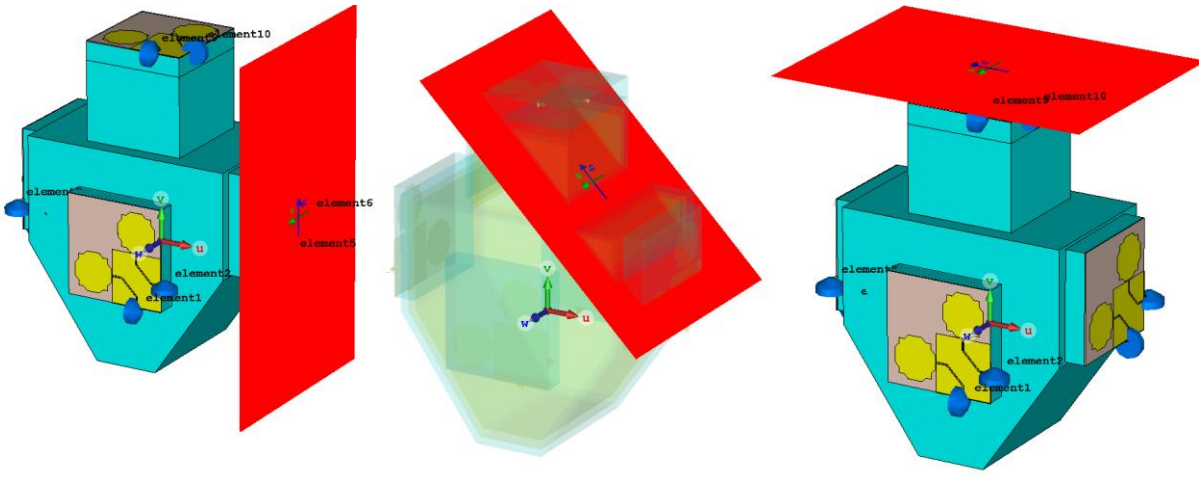

Figure 5.17 - System of antennas for a phi scan (0°, 45°, 90°) and theta = 90°

In the case of the incident wave with vertical polarization the voltage induced at each port, as a function of frequency, is shown in figures 5.18, 5.19 and 5.20.

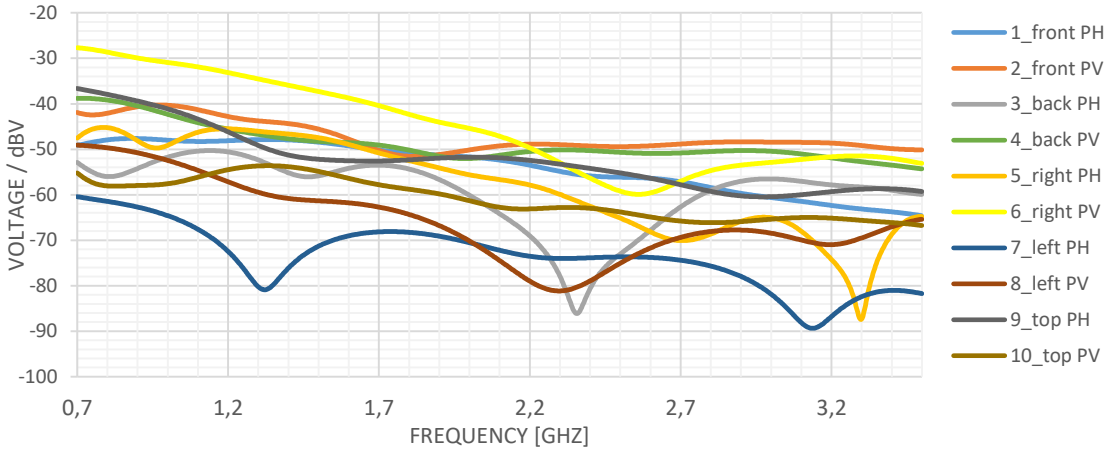

Figure 5.18 - Voltage induced at each port for φ=0° and vertical polarization

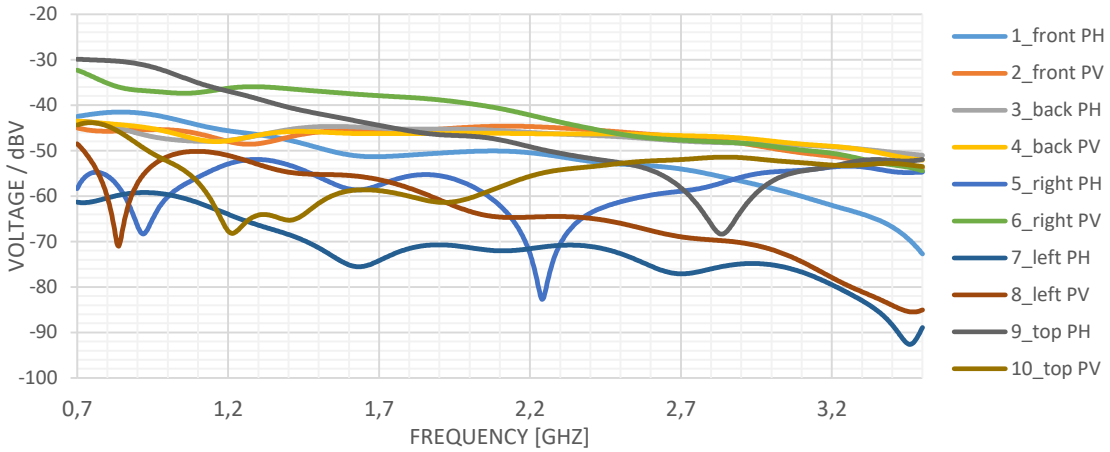

Figure 5.19 - Voltage induced at each port for φ=45° and vertical polarization

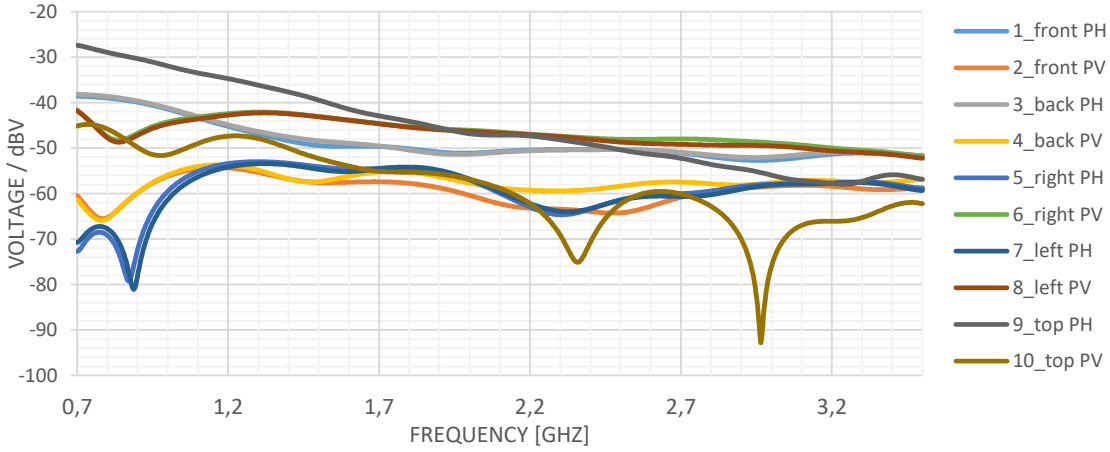

Figure 5.20 - Voltage induced at each port for φ=90° and vertical polarization

In the case the of incident wave with horizontal polarization, the results are shown in figures 5.21, 5.22 and 5.23.

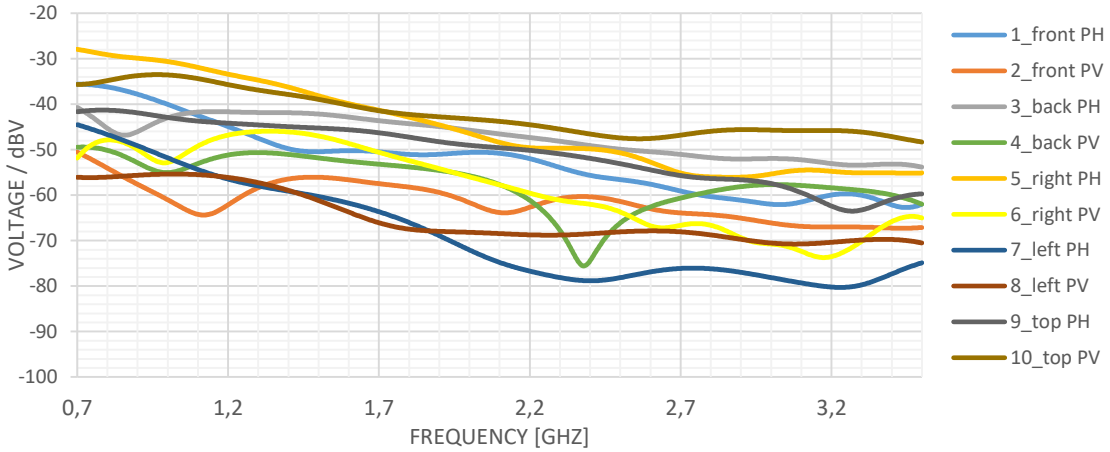

Figure 5.21 - Voltage induced at each port for φ=0° and horizontal polarization

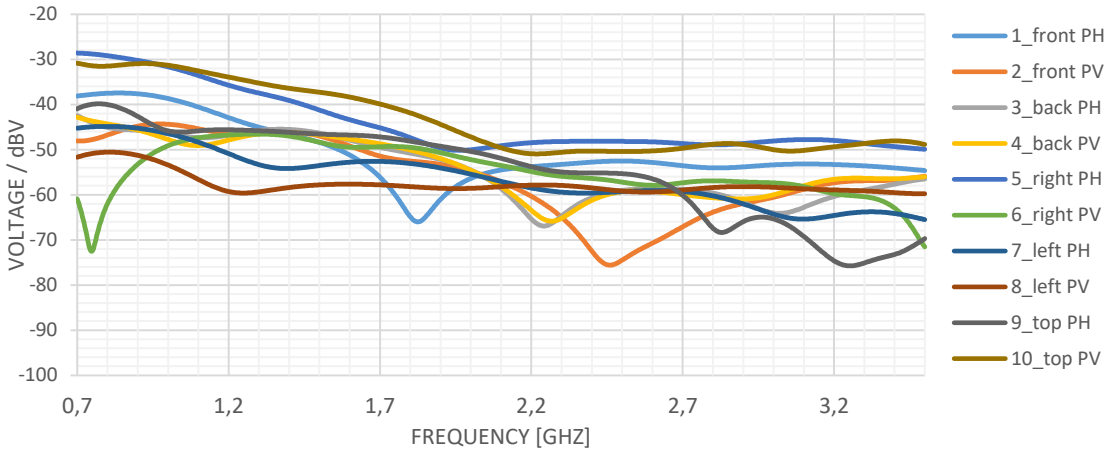

Figure 5.22 - Voltage induced at each port for φ=45° and horizontal polarization

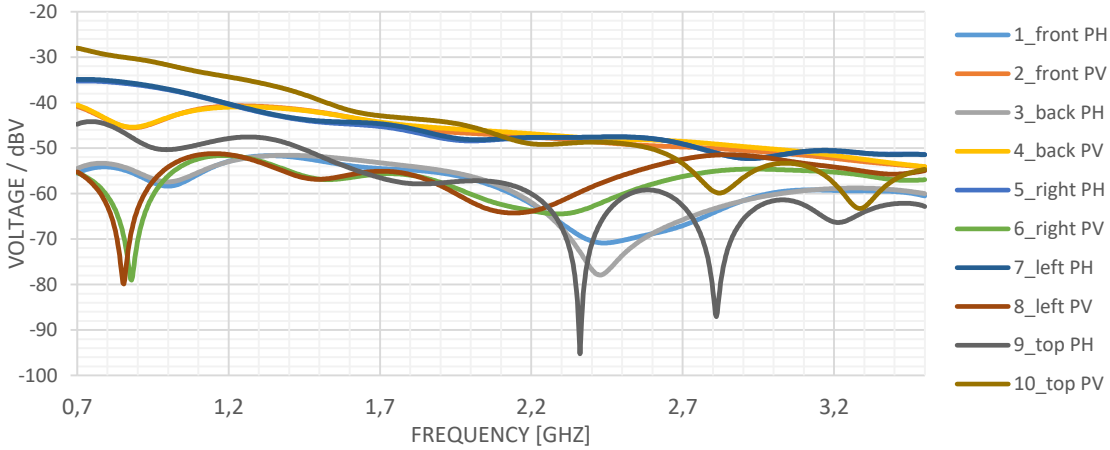

Figure 5.23 - Voltage induced at each port for φ=90° and horizontal polarization

Finally, in the case the incident wave with linear polarization at 45 degrees the results are shown in figures 5.24, 5.25 and 5.26.

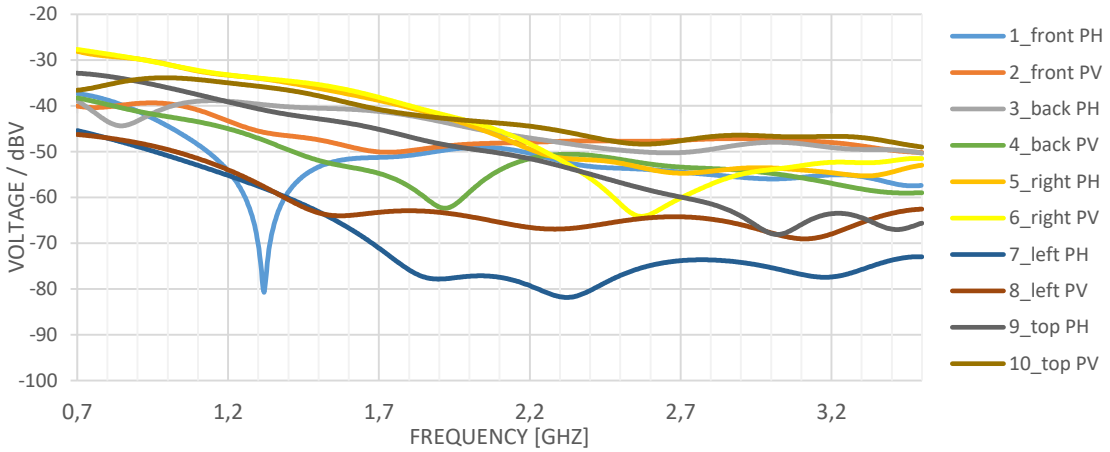

Figure 5.24 - Voltage induced at each port for φ=0° and 45° linear polarization

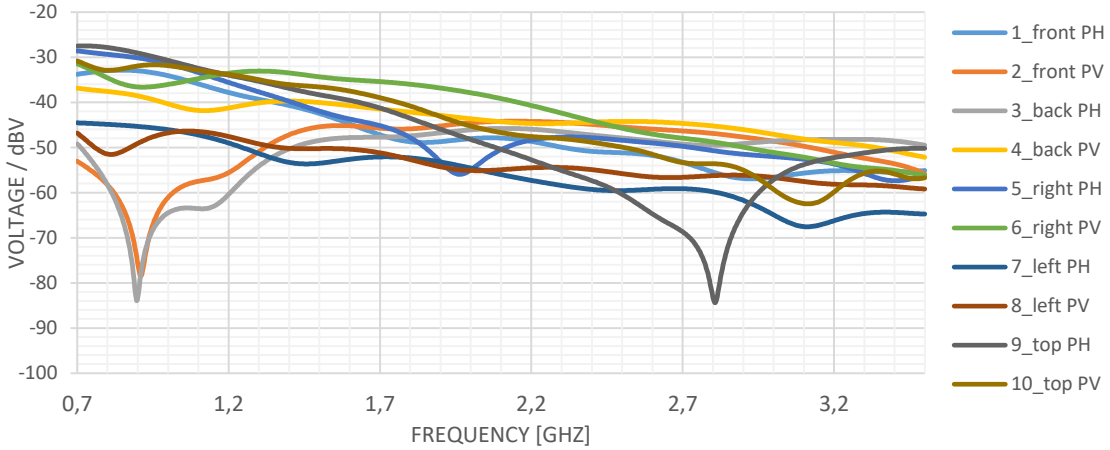

Figure 5.25 - Voltage induced at each port for φ=45° and 45° linear polarization

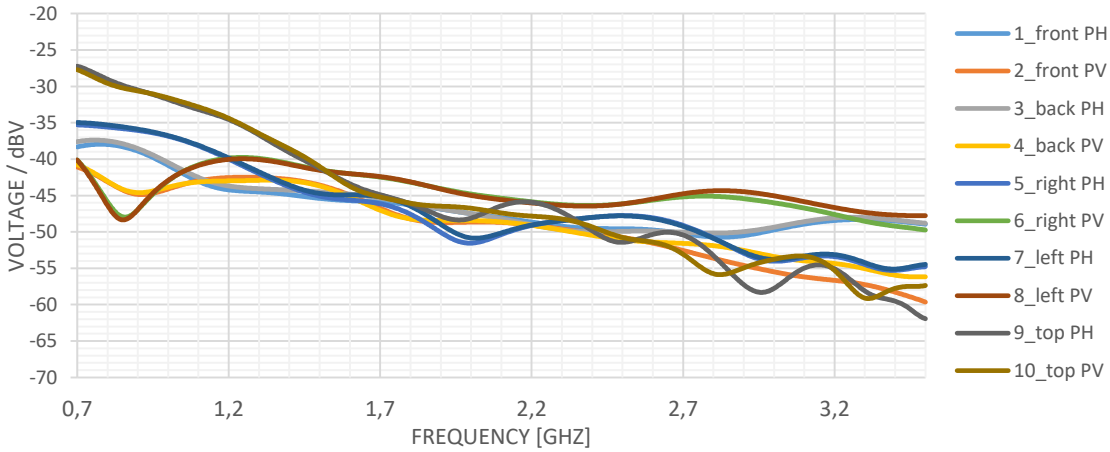

Figure 5.26 - Voltage induced at each port for φ=90° and 45° linear polarization

From the results presented in the figures 5.18 to 5.26 it can be concluded that the monopoles that present a higher voltage at their terminals are the ones who are directly in front of the incident wave and that have the configuration of polarization of the incident wave. For example, when the incident wave has a horizontal polarization, and Phi=90, the monopoles that present a higher voltage are the top, left and right with the

horizontal polarization configuration. On the other hand, if Phi=45 the monopoles that present a higher voltage to their terminals are the top, right, front and back with the horizontal polarization configuration as well. The same behaviour of the system is observed for the other values of Phi and for the case of the incident wave having vertical polarization.

For the case where the incident wave has linear polarization at 45 degrees, it is observed that the monopoles that present higher voltages at their terminals are the ones that are directly in front of the incident wave. For example, when the incident wave has linear polarization at 45 degrees, and Phi=0, the monopoles that present higher voltages are the right, front, back and top regardless of their polarization setting.

Again, in all presented voltage results, there is a decrease as frequency increases caused by the increase of the absorber foam losses.

5.4 Incident Electric Field Amplitude Estimation

The final purpose of the antenna system is to allow the estimation of the amplitude of the incident electric field. The equivalent Thevenin unloaded antenna voltage (V_0) can be obtained from [11].

$$V_0 = E\, h_e \sqrt{C_p} \tag{5.1}$$

E – incident electric field amplitude [$V.m^{-1}$]

h_e – antenna effective length [m]

C_p – antenna polarization mismatch coefficient

Moreover, the antenna effective length can be obtained from [11].

$$h_e = \lambda \sqrt{\frac{D}{\pi}\frac{R_r}{Z_0}} = \lambda \sqrt{\frac{G}{\pi}\frac{R_a}{Z_0}} \tag{5.2}$$

λ – free-space wavelength [m]

D – directivity

R_r – antenna radiation resistance [Ω]

Z_0 – free-space characteristic impedance [Ω]

G – antenna gain

R_a – antenna input resistance [Ω]

As $Z_0=120\pi$ [Ω] and Ra≈50 [Ω] then

$$h_e = \frac{\lambda}{\pi}\sqrt{\frac{5}{12}G} = \frac{6.164x10^7}{f}\sqrt{G} \tag{5.3}$$

and

$$E = \frac{V_0}{\sqrt{G\,C_p}}\frac{f}{6.164x10^7} \tag{5.4}$$

where f is the frequency [Hz].

Therefore an estimation of the amplitude of the incident electric field can be obtained from equation (5.4) as

$$E_{est}(f) = \frac{V_0(f)}{\sqrt{G(f)}}\frac{f}{6.164x10^7} \tag{5.5}$$

where $C_p=1$ was assumed.

In conclusion, the amplitude of the electric field of an electromagnetic wave incident on the antenna system can be estimated using the following procedure:

1. Read the unloaded voltage of all the monopoles and choose the highest value.
2. If the frequency of the incident electromagnetic wave is known then the amplitude of its electric field can be estimated from equation (5.5) using the corresponding gain value obtained in chapter 4.
3. If the frequency of the incident electromagnetic wave is not known a table of values of the amplitude of its electric field can be estimated, as a function of the frequency (in the range 0.7-3.5 GHz), from equation (5.5) using the gain values obtained in chapter 4.

It has been assumed that there is a filtering mechanism that allows selection of the received signals in a chosen narrow frequency band. One of the tasks that needs to be carried out to make this procedure more effective is the estimation of its accuracy.

6. Conclusions and Future Work

This chapter presents the main conclusions of this thesis, describing the most relevant results of the work done. In addition, some perspectives of future work are outlined.

6.1 Conclusions

The idea for the theme of this masters thesis was initially suggested by CeNTI, in the framework the project iP Vest. The iP Vest project aims to investigate and develop innovative solutions for technical and functional clothing with smart multi-risk protection, using new textile materials with advanced performance and new directly integrated sensor systems.

This thesis describes the study, design, optimization and fabrication of two wideband printed monopole antennas to cover a frequency band starting from 700 MHz to 3,5 GHz, specially challenging due to size constraints. Several of these monopoles will be combined to form an antenna system capable of estimating the unkown amplitude of the electric field received by the user in a professional unknown work environment. The main challenges of the problem under analysis come from the wideband (5:1), the small size and the unvoidable proximit of the antennas from the conducting protective shield.

A historical and scientific review is made about printed antennas, more specifically microstrip patch antennas and printed monopoles. The advantages and disadvantages of their use are discussed, as well as a review of wearable antennas. A detailed parametric study was performed, with all relevant parameter studied such as: monopole width, ground plane dimensions and geometry, dielectric substrate dimensions and patch geometry. Both free space and foam loaded enviroments have been considered. Moreover, ortogonal dual-linear polarization configuration have been developed.

After the antennas were optimized, meeting the required working bandwidth, a system was developed consisting of five of these printed antennas with absorber foam. A basic model for the user's body was used, simulated with a hollow copper block. The system was powered by a plane wave with an incident angle sweep in theta and phi for vertical, horizontal and linear polarizations at 45 degrees

After being developed, this antenna system can be used to measure the amplitude of the incident electric field on the system user from the voltage obtained at the terminals of each monopole The voltages decreases with an increase in frequency due to losses and higher voltages are verified for the monopoles where the wave falls in the direction of maximum radiation.

Due to the terrible Covid-19 virus pandemic, there were severe limitations on the experimental work. However, it was possible to fabricate two antenna prototypes and measure their S-parameters. A general agreement between numerical simulation and experimental results was obtained. Such concordance has validated the design procedure and provided proof of the proposed antenna concepts.

6.2 Future Work

There are many aspects that could have been addresed in this work, and there are also many issues that could be investigated to render the work more complete. A non-exhaustive list of future work topics is suggested below.

- Measurement of the radiation pattern (and associated parameters) of the fabricated prototypes in a anechoic chamber.
- Analysis of the polarization properties of the monopoles developed.
- Estimate the accuracy of the proposed estimation procedure of the amplitude of the incident electric field provided by the developed antenna system.
- Investigate the effects of increasing the number of dual-linear polarization monopoles and the best location for them.
- Investigate the effects of the bending of the monopoles caused by the integration into the vestment.
- Investigate the effects of the textiles of the garment that cover the antennas.

References

[1] [online accessed] https://www.centi.pt/projetos/texteis-avancados/ipvest-centi-nanotecnologia

[2] [online accessed] https://www.compete2020.gov.pt/noticias/detalhe/Proj33994-iPVest-MafaldaMotaPinto-NL232-20122019

[3 [online accessed] https://www.portugal2020.pt/content/projeto-ip-vest-investe-em-solucoes-inovadoras-para-vestuario-tecnico-e-funcional

[4] [online accessed] https://www.engn.pt/wp-content/uploads/2021/06/Electromagnetic-Field-EMF-Triaxial-Isotropic-Antenna.pdf

[5] G. Deschamps and W. Sichak, “Microstrip Microwave Antennas,” Proc. of Third Symp. on USAF Antenna Research and Development Program, pp. 18–22, October 1953.

[6] E. V. Byron, "A new flush-mounted antenna element for phased array application," Proc. Phased-Array Antenna Symp, pp. 187-192, 1970.

[7] R. E. Munson, "Microstrip Phased Array Antennas," Proceedings of the TwentySecond Symposium on the USAF Antenna Research and Development Program, October 1972.

[8] R. E. Munson, "Conformal Microstrip Antennas and Microstrip Phased Arrays," IEEE Transactions on Antennas and Propagation, Vol. 22, pp. 74-78, 1974.

[9] J. Q. Howell, "Microstrip Antennas," in IEEE AP-S Int. Symp. Digest, pp. 177-180, 1972.

[10] J. Q. Howell, "Microstrip Antennas," IEEE Transactions on Antennas and Propagation, Vol. 23, pp. 90-93, 1974.

[11] C. A. Balanis, “Antenna Theory Analysis and Design.”, 3rd Ed., John Wiley Sons, Inc., Hoboken, New Jersey, 2005.

[12] K. F. Fong Lee and K. M. Luk; “Microstrip Patch Antennas”, Imperial College Press, 2011.

[13] R. Bancroft, “Microstrip and Patch Antennas Design”, 2nd Ed., Scitech Publishing, 2009.

[14] D. M. Pozar, “Microstrip Antennas, “IEEE Antennas and Propagation Magazine, Vol. 80, No. 1, pp. 79-81, January 1992.

[15] I. J. Bahl and P. Bhartia, “Microstrip Antenna”, Artech House, Deaham, MA, 1980.

[16] K. R. Carver and J. W. Mink, “Microstrip Antenna Technology”, IEEE Transactions on Antennas and Propagation, Vol. AP-29, No. 1, January 1981.

[17] D. M. Pozar, “Microstrip Antennas”, Prococedings of IEEE, Vol. 80, No. 1, January 1992.

[18] D. M. Pozar, “A Microstrip Antenna Aperture Coupled to a Microstrip Line”, Eletronic Letters, Vol. 21, January 1985.

[19] Y. T. Lo, D. Solomon and W. F. Richards, “Theory and Experiment on Microstrip Antennas”, IEEE Transactions on Antennas and Propagation, Vol. AP-27, No. 2, March 1979.

[20] J. R. James and P. S. Hall, “Handbook of Microstrip Antennas”, Vol. 1 and 2, Peter Peregrinus, London, 1988.

[21] I. E. Rana and N. G. Alexopoulos, “Current Distribution and Input Impedance of Printed Dipoles”, IEEE Transactions on Antennas and Propagation, Vol. AP-29, No. 1, January 1981.

[22] H. Lebbar, M. Himdi, and J. P. Daniel, “Analysis and size reduction of various printed monopoles with different shapes”, Electronics Letters, Vol. 30, No. 21, 1994.

[23] H. Lebbar, M. Hinmdi and J. P. Daniel, “Transmission line analysis of printed monopole” ,Electronic Letters, Vol. 28, No. 14, 1992.

[24] Y. L. Kuo and K. L. Wong, “Printed double T monopole antenna for 2.4/5.2 GHz dual-band WLAN operations”, IEEE Transactions on Antennas and Propagation, Vol. 51, No. 9, 2003.

[25] W. C. Liu, C. M. Wu, and N. C. Chu, “A compact CPW fed slotted patch antenna for dual-band operation”, IEEE Antennas and Wireless Propagation Letters, Vol. 9, 2010.

[26] A. Z. Manouare, S. Ibnyaich, D. Seetharamdoo, A. E. Idrissi and A. Ghammaz, “Design, fabrication and measurement of a miniaturized CPW-Fed planar monoole antenna using a single vertical strip for multi-band wireless applications”, Jounal of Engineering Technology, Vol. 7, 2008.

[27] K. P. Ray, “Design Aspects of Printed Monopole Antennas for Ultra-Wide Band Applications”, International Jounal of Antennas and Propagation, 2008.

[28] K. P. Ray and Y. Ranga, “CPW-fed Modified Rectangular Printed Monopole Antenna with Slot”, International Microwave & Optoelectronics Conference, IMOC, 2007.

[29] K. P. Ray and Y. Ranga, “Printed Rectangular Monopole Antennas”, IEEE AP-URSI Int. Microwave Symp, US, June 2006.

[30] K. Mandal, “A Review on Printed Monopole Antenna for UWB Applications”, International Journal of Advanced Research in Computer and Communication Engineering, Vol. 4, December 2015.

[31] K. F. Jacob, “Printed Monopole Antenna for Ultra Wide Band Applications”, Master Thesis, Cochin University of Science and Technology, 2008.

[32] M. Wu, “Multibroadband Slotted Bow-tie Monopole Antenna”, IEEE Antennas and Wireless Propagation Letters, Vol. 14, 2015.

[33] X. J. Liang, C. C. Chiau, X. D. Chen, and C. G. Parini, “Study of a printed circular disc monopole antenna for UWB systems”, IEEE Transactions on Antennas and Propagation 2005, Vol. 53 No. 11, pp. 3500-3504.

[34] K. N. Paracha, S. K. A. Rahim, P. J. Soh and M. Khalily, “Wearable Antennas: A Review of Materials, Structures, and Innovative Features for Autonomous Communication and Sensing”, IEEE Access, Vol. 7, 2019.

[35] P. Friess, “Internet of Things: Converging Technologies for Smart Environments and Integrated Ecosystems.” Gistrup, Denmark: River Publishers, 2013.

[36] S. Bhattacharyya, N. Das, D. Bhattacharjee and A. Mukherjee, Handbook of Research on Recent Developments in Intelligent Communication Application. Philadelphia, PA, USA: IGI Global, 2016.

[37] M. Chan, D. Estève, J.-Y. Fourniols, C. Escriba and E. Campo, ‘‘Smart wearable systems: Current status and future challenges,’’ Artif. Intell. Med., Vol. 56, No. 3, November 2012.

[38] C. Oliveira, “Characterisation of on-body Communications”, PhD Degree Thesis, Instituto Superior Técnico 2013.

[39] R. Salvado, C. Loss, R. Gonçalves and P. Pinho, “Textile Materials for the Design of Wearable Antennas: A Survey”, Sensors ISSN 1424-8220, 2012.

[40] N. Rais, P. Soh, F. Malek, S. Ahmad, N. Hashim and P. Hall, “A Review of Wearable Antenna”, University Malaysia Perlis 2009.

[41] S. Zhang, A. Chauraya, W. Whittow, R. D. Seager, T. Acti, T. Dias and J. Y. C. Vardaxoglou, “Embroidered wearable antennas using conductive threads with different stitch spacings”, Antennas and Propagation Conference, Nov 2012.

[42] The International Commission on Non-Ionizing Radiation Protection, ‘‘Guidelines for limiting exposure to time-varying electric, magnetic, and electromagnetic fields (up to 300 GHz),’’ Health Phys., Vol. 74, No. 4, April, 1998.

[43] Anritsu, “Understanding vector network analysis,” 2013, [online accessed], http://www.anritsu.com.

[44] G. C. Vieira, “Log-Periodic Dipole Antennas in Printed Circuit Technology”, Master Thesis, Instituto Superior Técnico, 2018.

[45] [online accessed] https://www.laird.com/products/microwave-absorbers/microwave-absorbing-foams/eccosorb-an.

[46] C. Mendes, “A Wearable Dual-Mode Printed Antenna for Body-Centric Applications”, PhD Degree Thesis, Instituto Superior Técnico, 2017.

Appendices

A. CST Software Tool – Algorithms and Solvers Used

CST Microwave Studio (CST MWS) is a powerful tool, as it gives access to multiple electromagnetic (EM) simulation solvers which use methods such as the finite element method (FEM), the finite integration technique (FIT), and the transmission line matrix method (TLM). The seamless integration of the solvers into one user interface in CST Studio Suite enables the easy selection of the most appropriate simulation method for a given problem class, delivering improved simulation performance and reliability through cross-verification.

Off all the available solvers, the author chose the Frequency Domain Solver, based on the finite element method (FEM), offering excellent simulation performance for many types of components. Because the Frequency Domain Solver can calculate all ports at the same time, it is also a very efficient way to simulate multi-port systems such as the ones presented providing broadband frequency domain results such as S-parameters. The Frequency Domain Solver is the best for wideband or planar antennas and it can deliver farfield results for numerous frequencies in one simulation.

CST Studio Suite offers automatic optimization routines for electromagnetic systems. CST models can be parameterized with respect to their geometrical dimensions or material proprieties. Considering the optimization algorithms, CST contains several both local and global. Local optimizers provide fast convergence but risk converging to local minimum rather than the overall best solution. On the other hand, global optimizers search the entire problem space but typically require more calculations.

In relation to the optimization algorithms some were used whenever the user wanted to optimize some value, such as Classic Powell, Interpolated Quasi Newton, Covariance Matrix Adaptation Evolutionary, Trust Region Framework (TRF), Decap Optimization, Nelder Mead Simplex Algorithm, Particle Swarm Optimization and Genetic Algorithm.

All simulations were done using maximum accuracy settings according to the CST support recommendation whenever it was possible. There comes a point where increasing the precision of the simulations does not provide more accurate results while the simulation time continues to increase, so a compromise had to be reached throughout the simulation procedure.

B. System of Antennas – Theta Scan

In the case of the incident wave with vertical polarization, the voltage induced at each port, as a function of frequency, is shown in figures B.1 to B.5.

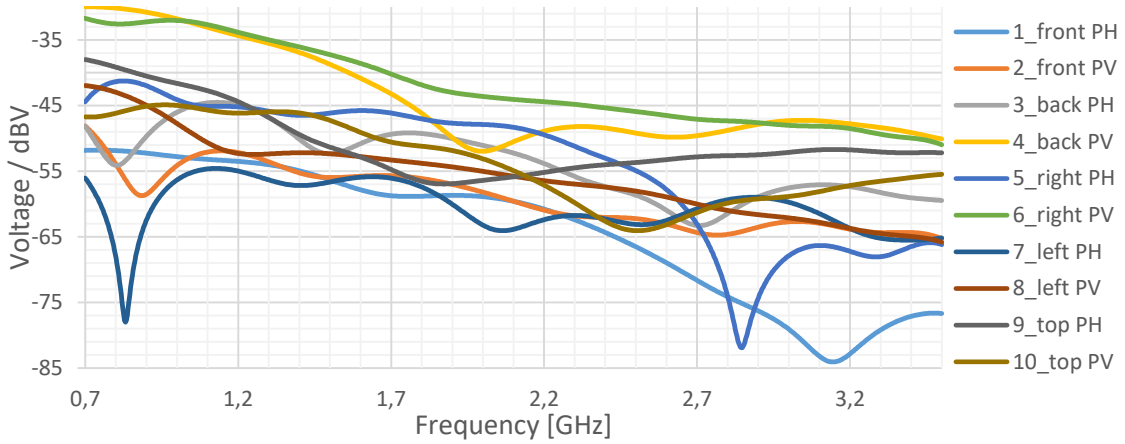

Figure B.B.1 - Voltage induced at each port for Θ=135° and vertical polarization

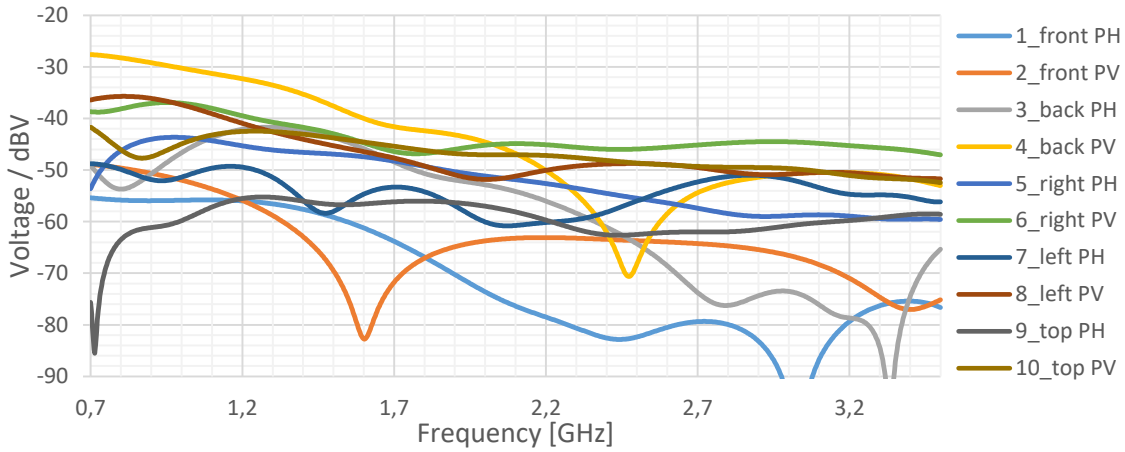

Figure B.B.2 - Voltage induced at each port for Θ=180° and vertical polarization

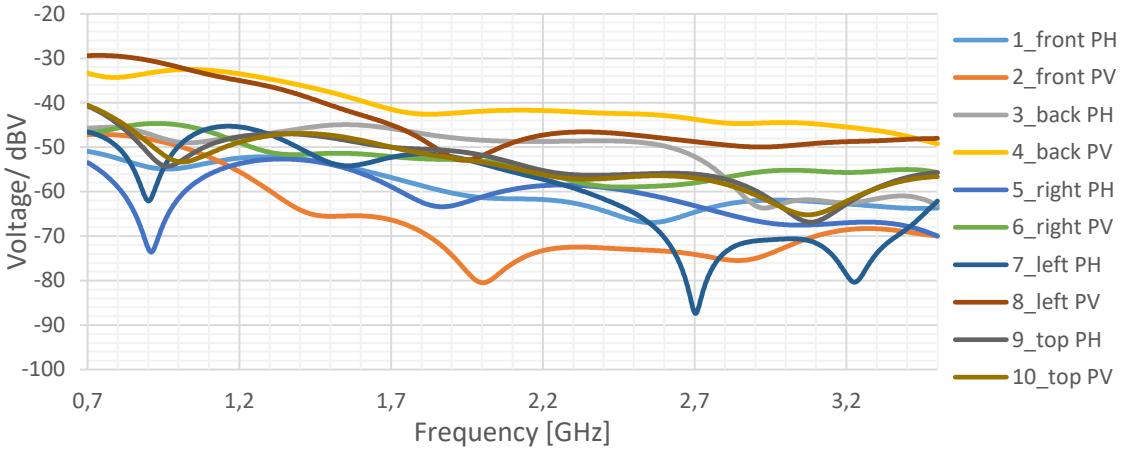

Figure B.B.3 - Voltage induced at each port for Θ=225° and vertical polarization

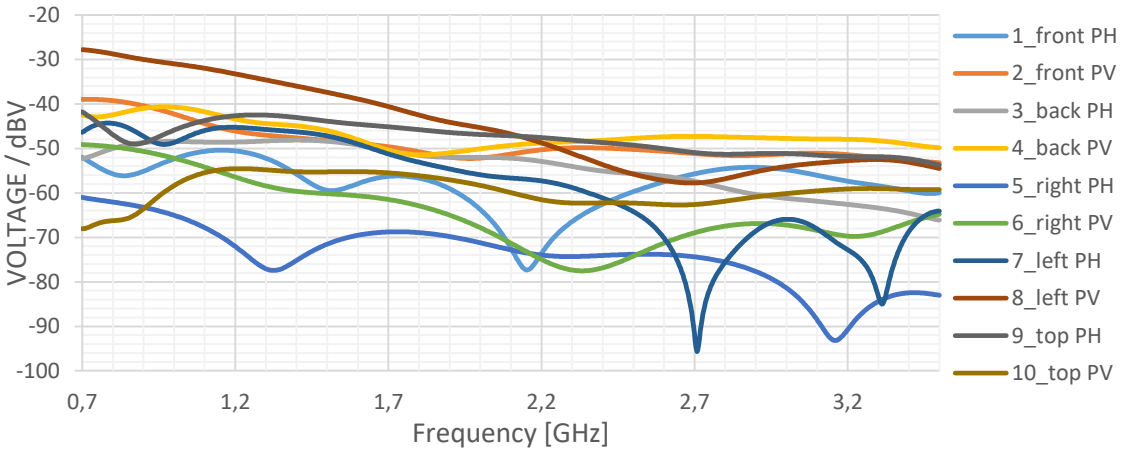

Figure B.B.4 - Voltage induced at each port for Θ=270° and vertical polarization

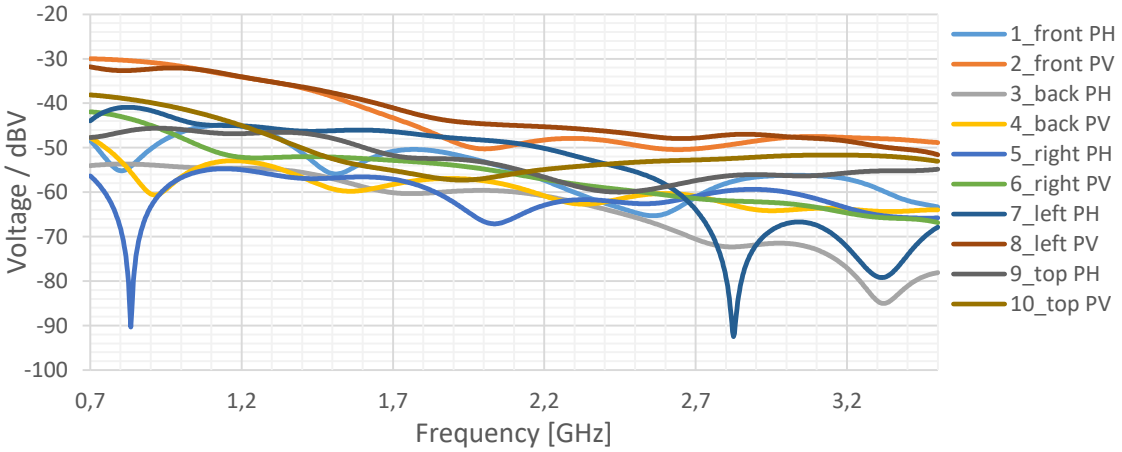

Figure B.5 - Voltage induced at each port for Θ=315° and vertical polarization

In the case of the incident wave with horizontal polarization, the voltage induced at each port, as a function of frequency, is shown in figures B.6 to B.10.

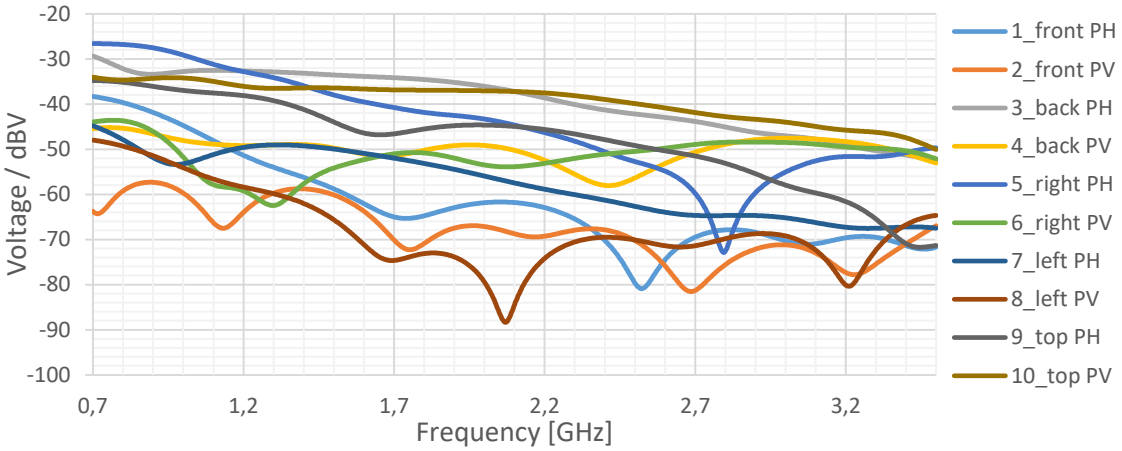

Figure B.6 - Voltage induced at each port for Θ=135° and horizontal polarization

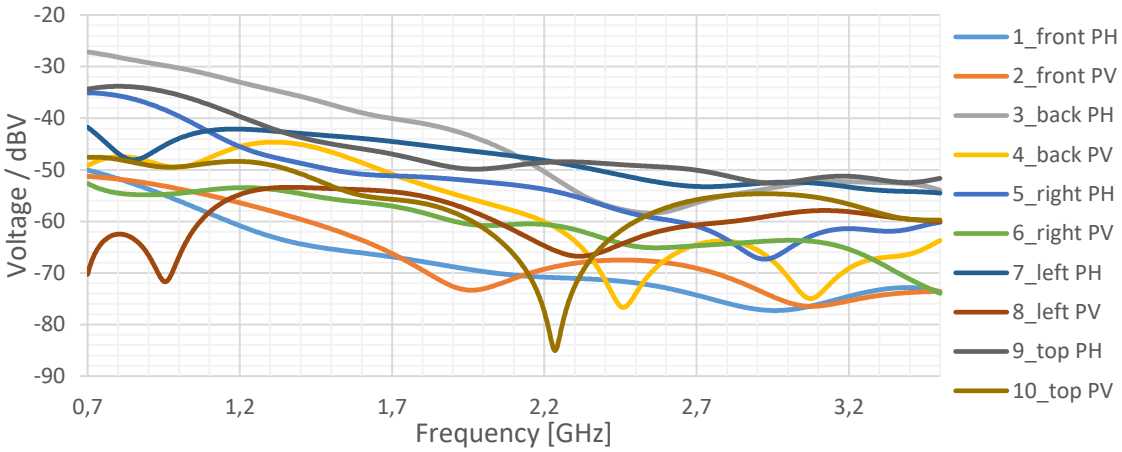

Figure B.7 - Voltage induced at each port for Θ=180° and horizontal polarization

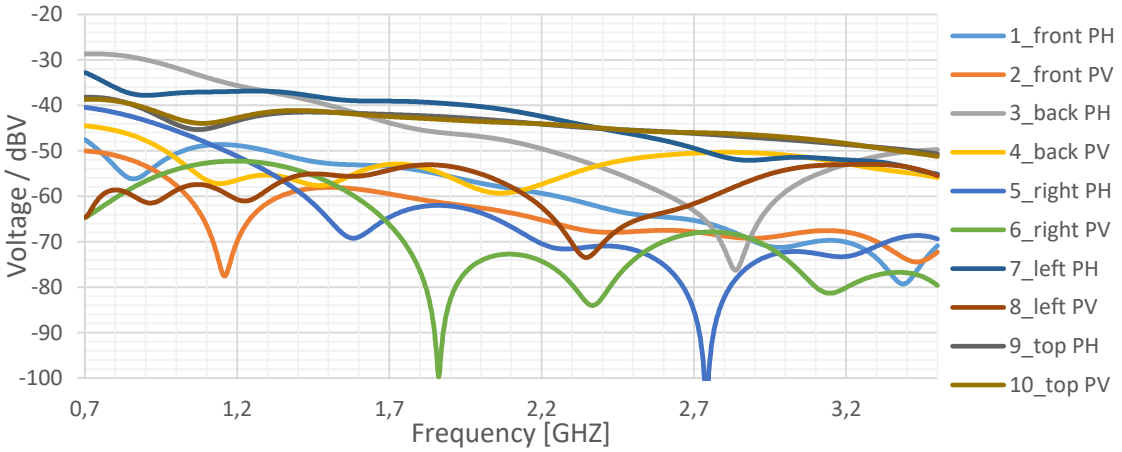

Figure B.8 - Voltage induced at each port for Θ=225° and horizontal polarization

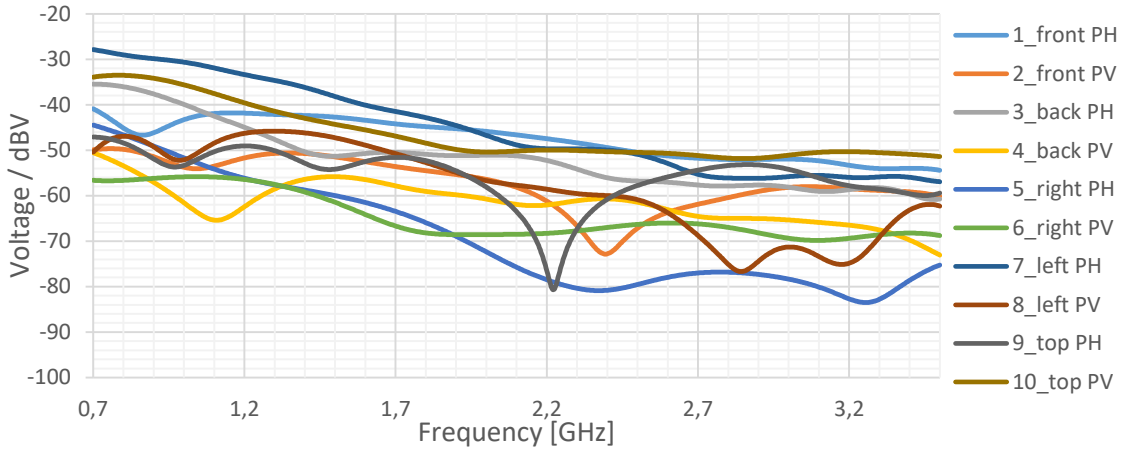

Figure B.9 - Voltage induced at each port for Θ=270° and horizontal polarization

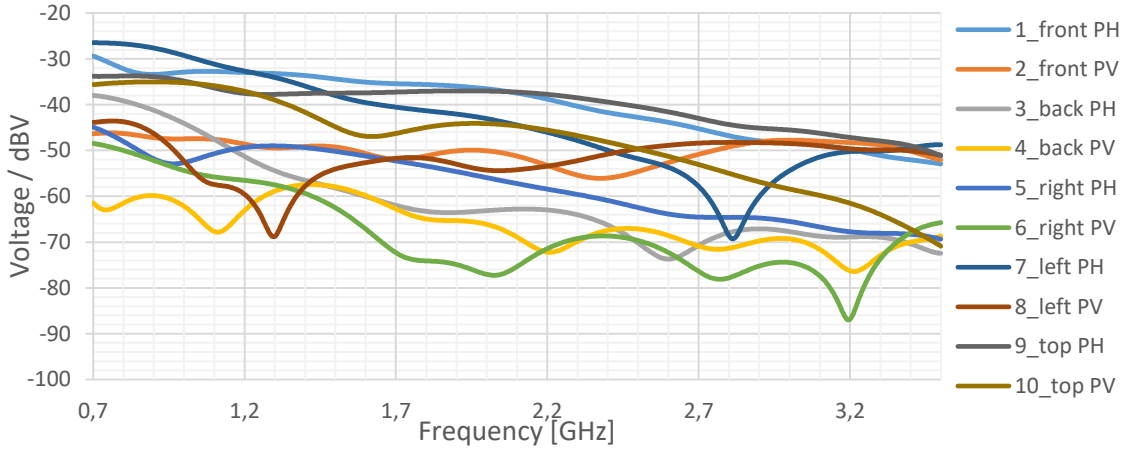

Figure B.10 - Voltage induced at each port for Θ=315° and horizontal polarization

Finally, in the case of the incident wave has linear polarization at 45 degrees the results are as shown in figures 5.11 to 5.15.

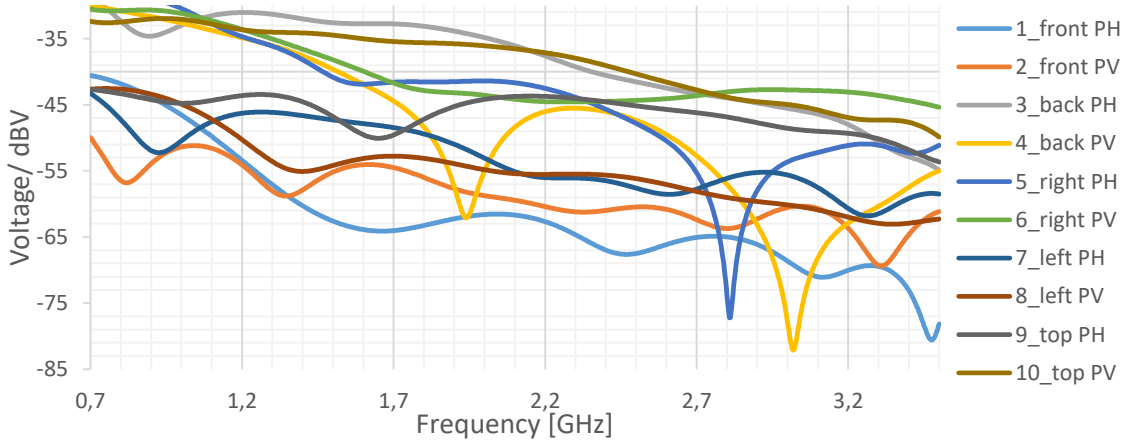

Figure B.11 - Voltage induced at each port for Θ=135° and 45° linear polarization

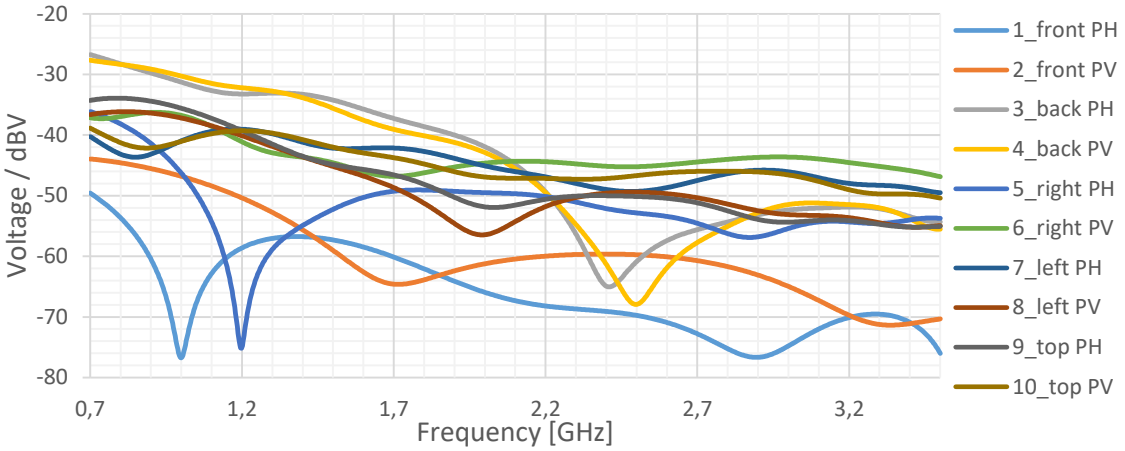

Figure B.12 - Voltage induced at each port for Θ=180° and 45° linear polarization

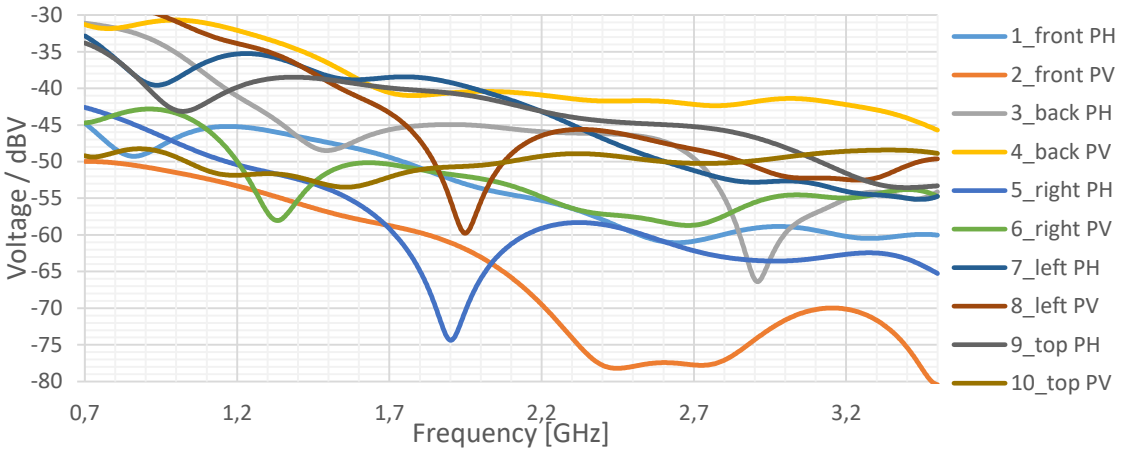

Figure B.13 - Voltage induced at each port for Θ=225° and 45° linear polarization

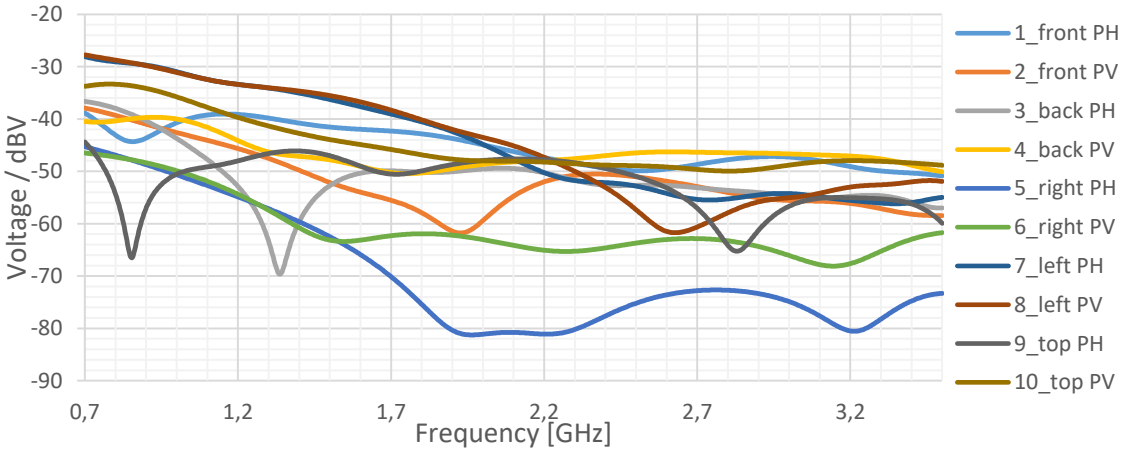

Figure B.14 - Voltage induced at each port for Θ=270° and 45° linear polarization

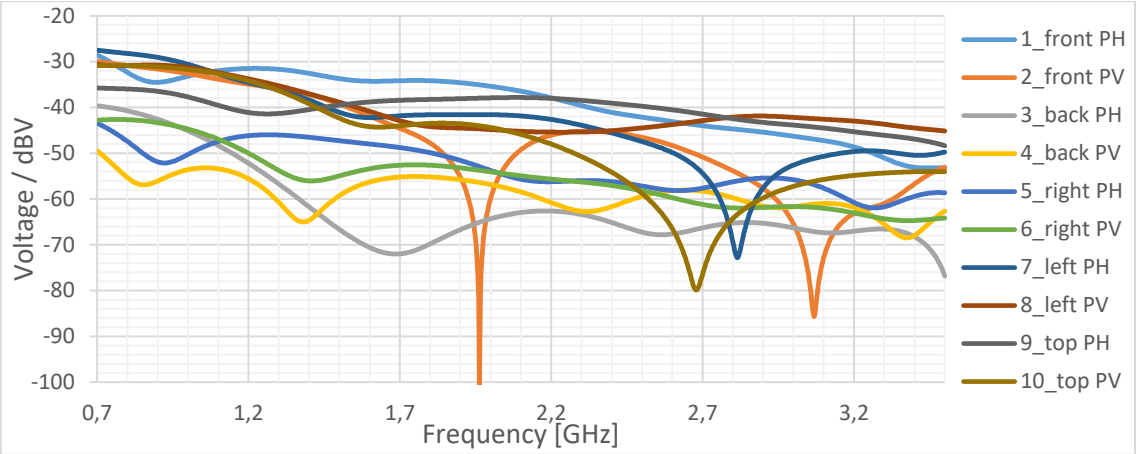

Figure B.15 - Voltage induced at each port for Θ=315° and 45° linear polarization

C. System of Antennas – Phi Scan

In the case of the incident wave with horizontal polarization, the voltage induced at each port, as a function of frequency, is shown in figures C.1 to C.5.

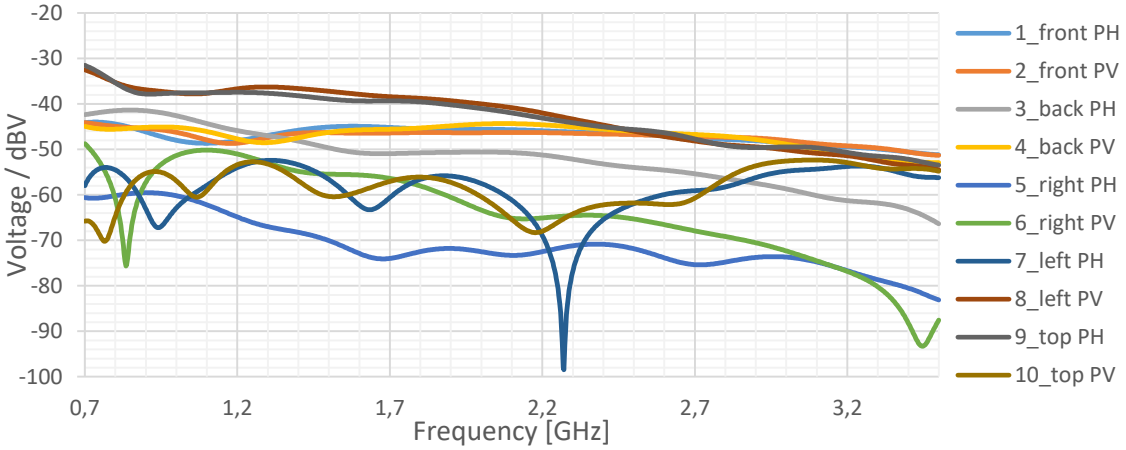

Figure C.1 - Voltage induced at each port for φ=135° and vertical polarization

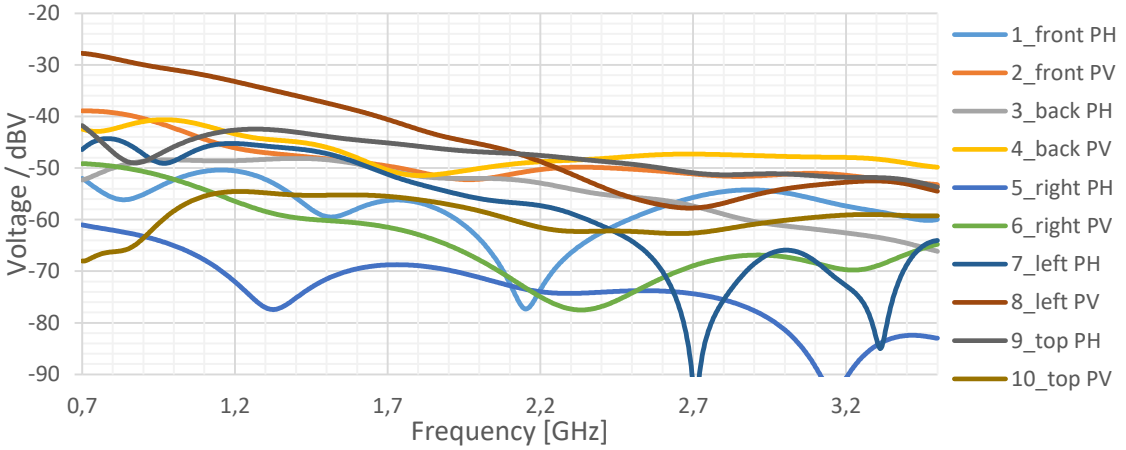

Figure C.2 - Voltage induced at each port for φ=180° and vertical polarization

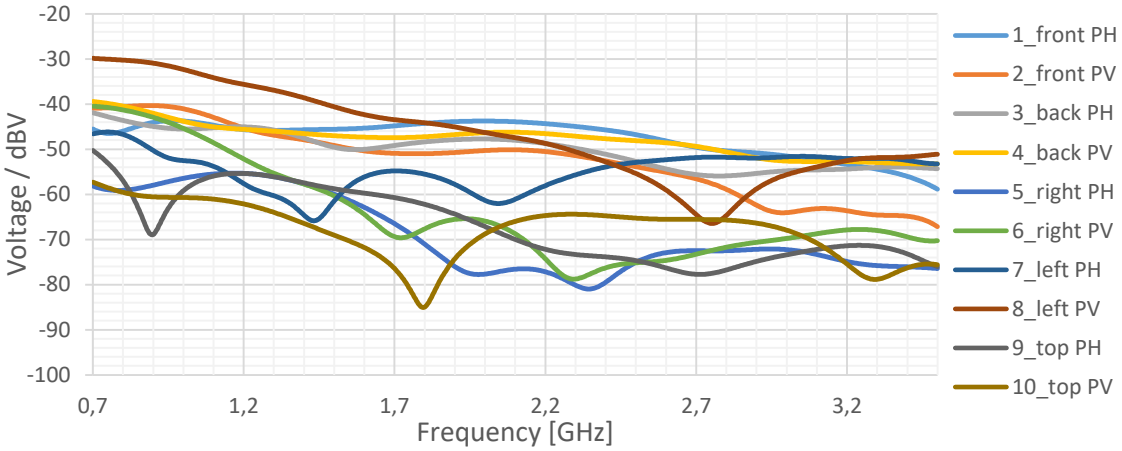

Figure C.3 - Voltage induced at each port for φ=225° and vertical polarization

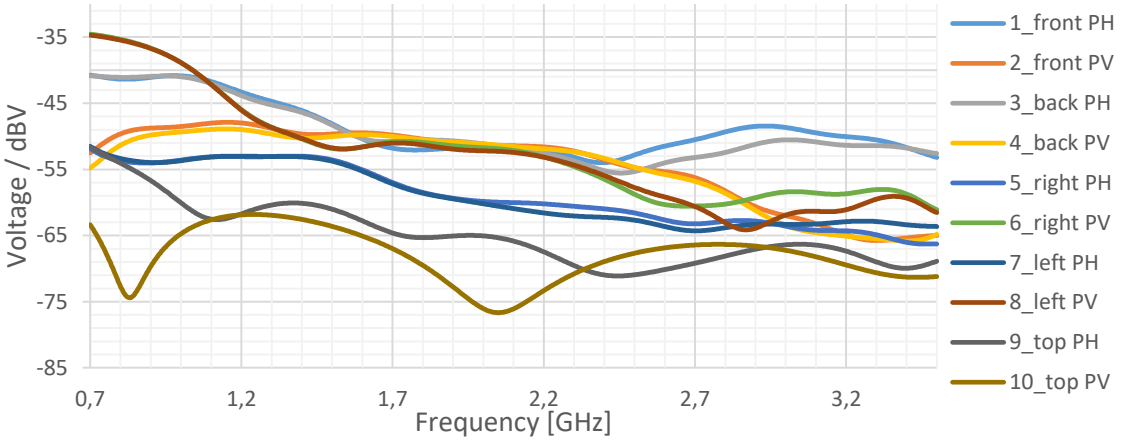

Figure C.4 - Voltage induced at each port for φ=270° and vertical polarization

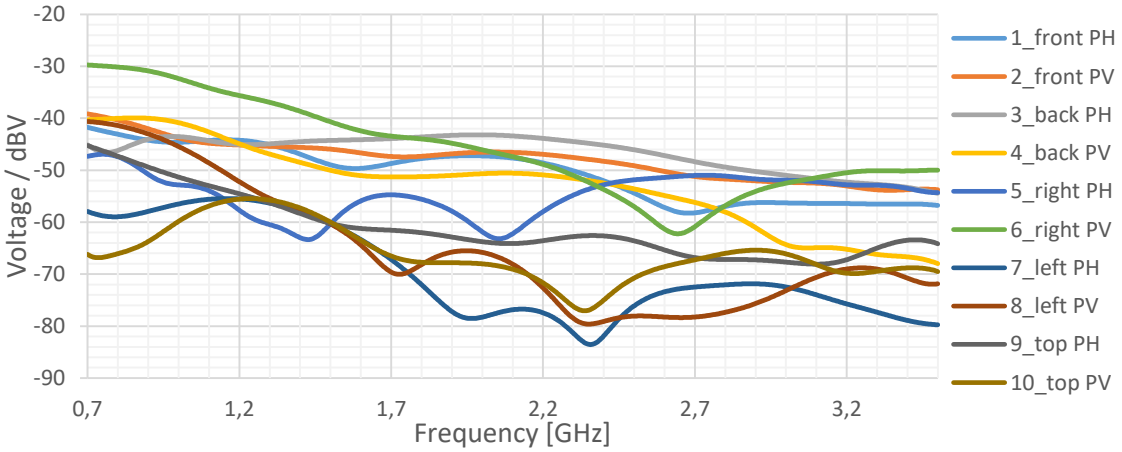

Figure C.5 - Voltage induced at each port for φ=315° and vertical polarization

In the case of the incident wave with horizontal polarization, the voltage induced at each port, as a function of frequency, is shown in figures C.6 to C.10.

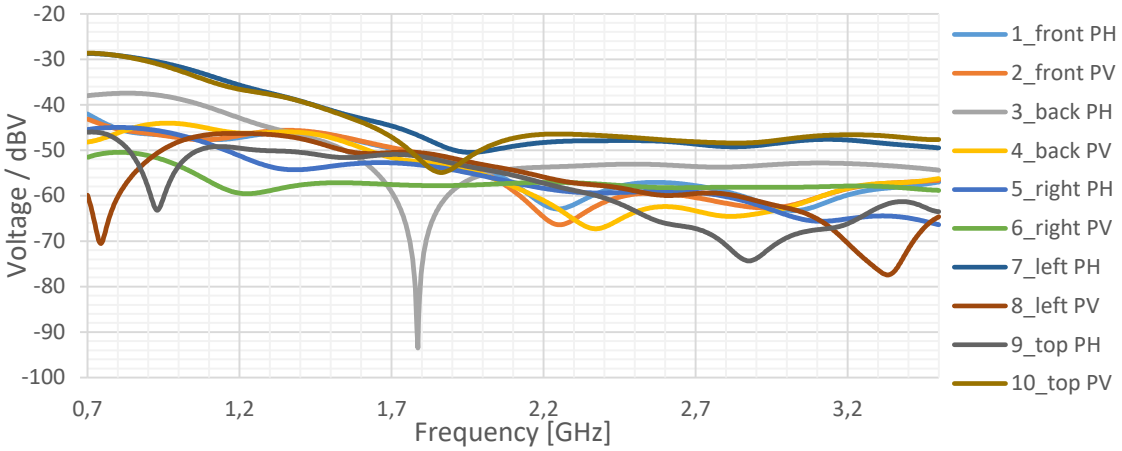

Figure C.6 - Voltage induced at each port for φ=135° and horizontal polarization

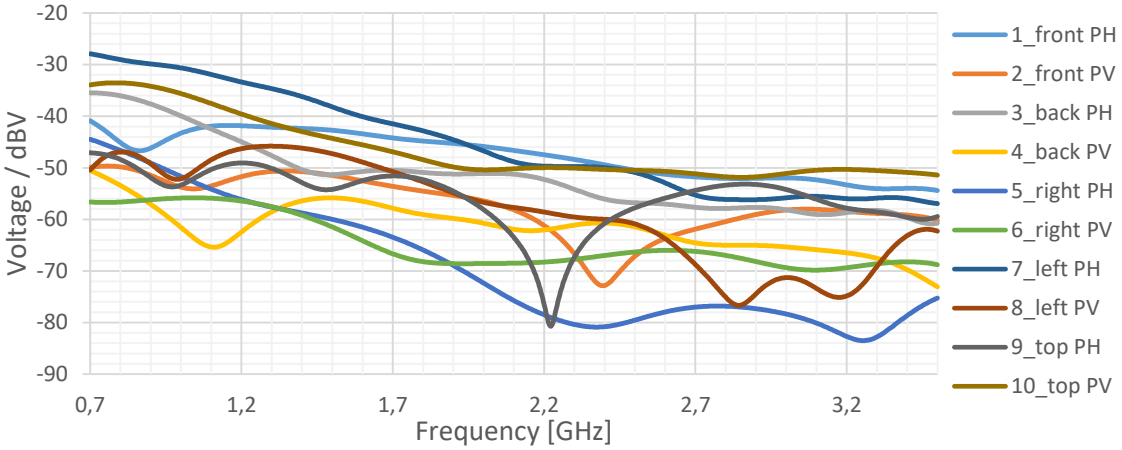

Figure C.7 - Voltage induced at each port for φ=180° and horizontal polarization

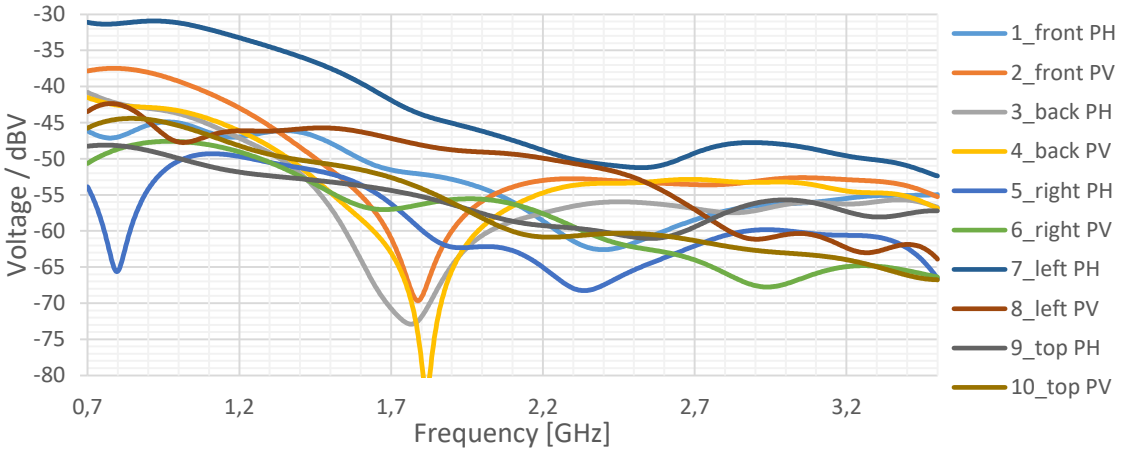

Figure C.8 - Voltage induced at each port for φ=225° and horizontal polarization

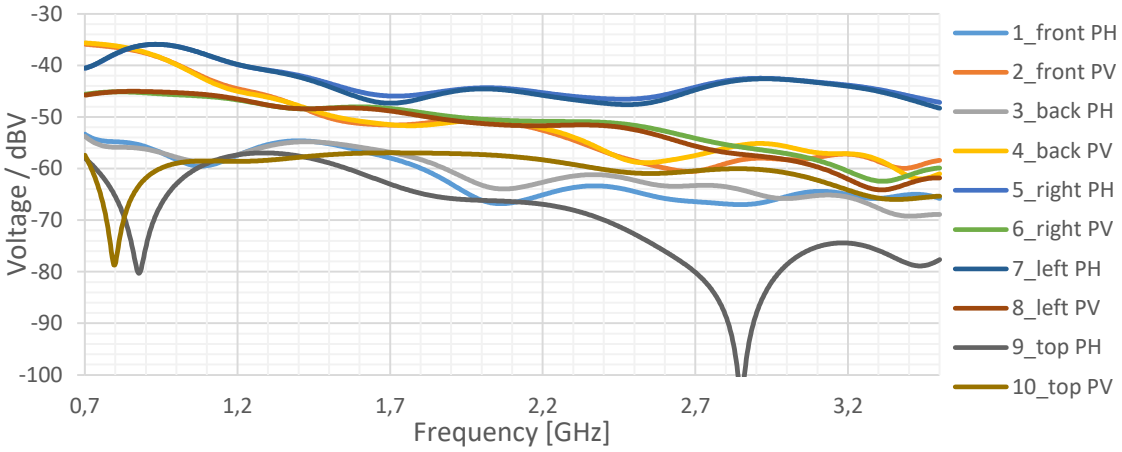

Figure C.9 - Voltage induced at each port for φ=270° and horizontal polarization

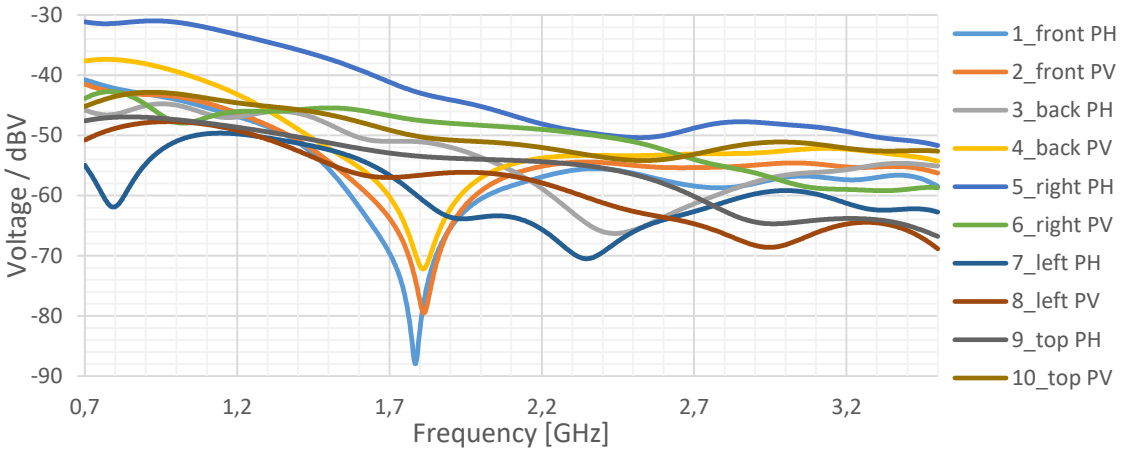

Figure C.10 - Voltage induced at each port for φ=315° and horizontal polarization

Finally, in the case of the incident wave has linear polarization at 45 degrees the results are as shown in figures C.11 to C.15.

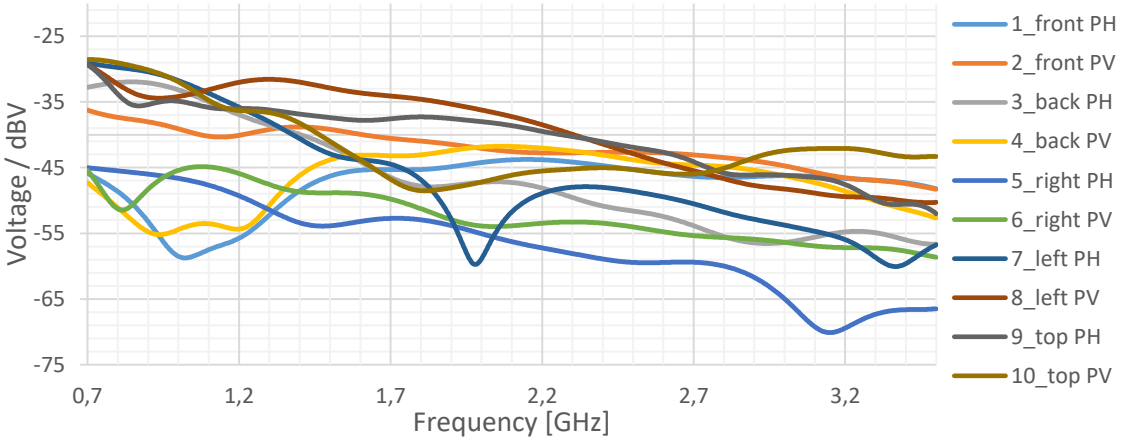

Figure C.11 - Voltage induced at each port for φ=135° and 45° linear polarization

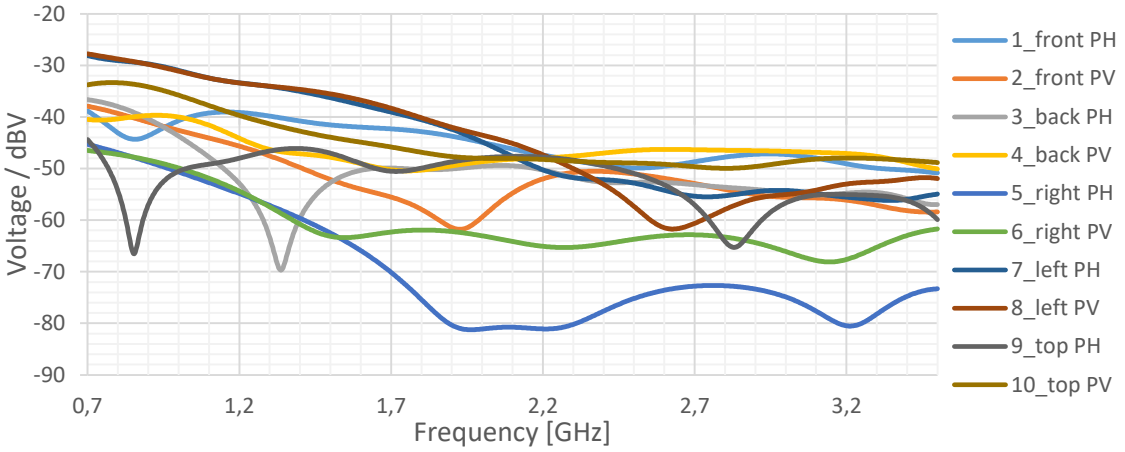

Figure C.12 - Voltage induced at each port for φ=180° and 45° linear polarization

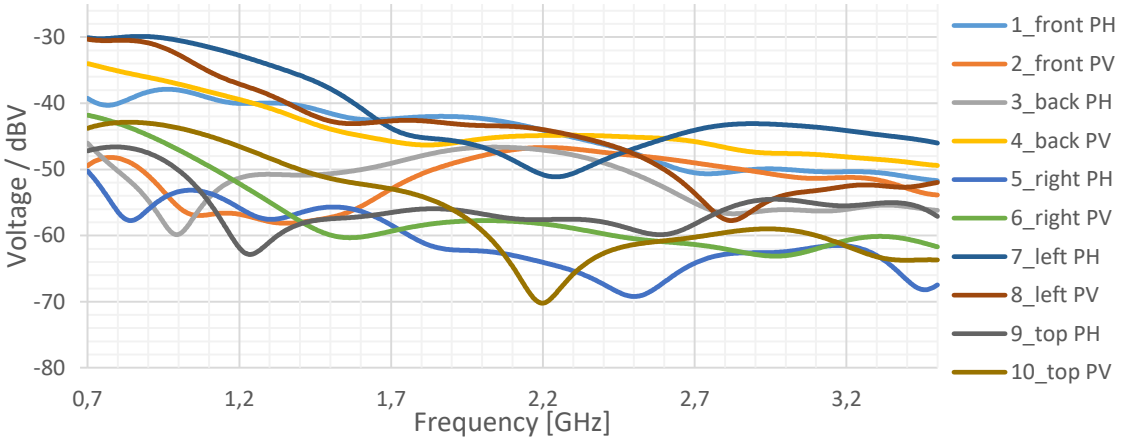

Figure C.13 - Voltage induced at each port for φ=225° and 45° linear polarization

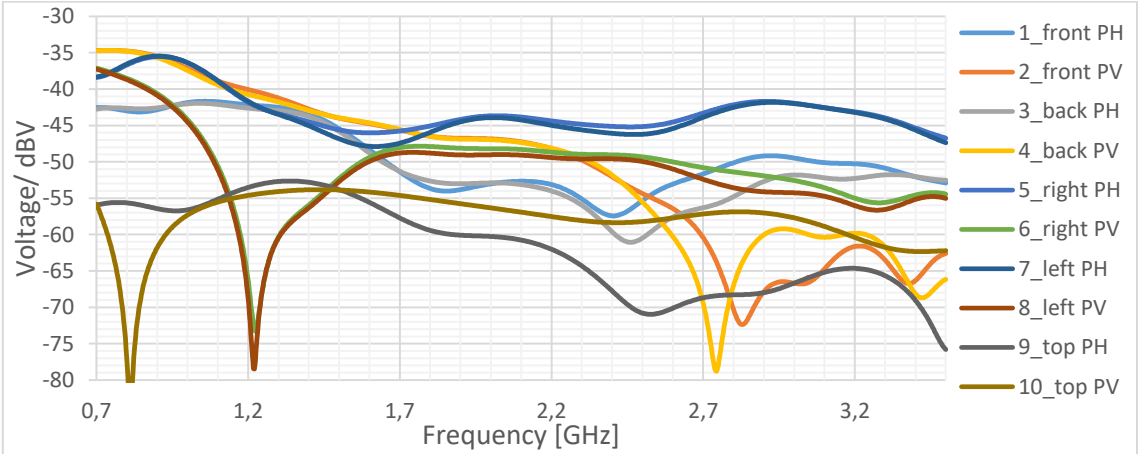

Figure C.14 - Voltage induced at each port for φ=270° and 45° linear polarization

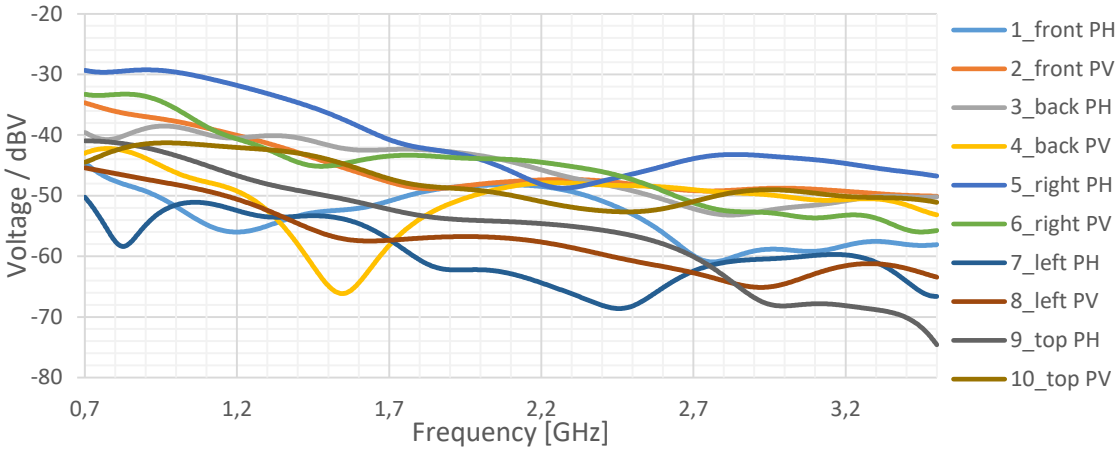

Figure C.15 - Voltage induced at each port for φ=315° and 45° linear polarization